

SOIL WATER CONTENT ESTIMATION FROM POINT SCALE TO PLOT SCALE

A THESIS SUBMITTED TO  
THE GRADUATE SCHOOL OF NATURAL AND APPLIED SCIENCES  
OF  
MIDDLE EAST TECHNICAL UNIVERSITY

BY

GÖKBEN DEMİR

IN PARTIAL FULFILLMENT OF THE REQUIREMENTS  
FOR  
THE DEGREE OF MASTER OF SCIENCE  
IN  
CIVIL ENGINEERING

FEBRUARY 2018



Approval of the thesis:

**SOIL WATER CONTENT ESTIMATION FROM POINT SCALE TO PLOT SCALE**

submitted by **GÖKBEN DEMİR** in partial fulfillment of the requirements for the degree of **Master of Science in Civil Engineering Department, Middle East Technical University** by,

Prof. Dr. Gülbin Dural Ünver  
Dean, Graduate School of **Natural and Applied Sciences**

\_\_\_\_\_

Prof. Dr. İsmail Özgür Yaman  
Head of Department, **Civil Engineering**

\_\_\_\_\_

Prof. Dr. Zuhall Akyürek  
Supervisor, **Civil Engineering Department, METU**

\_\_\_\_\_

**Examining Committee Members:**

Assoc. Prof. Dr. İsmail Yücel  
Civil Engineering Dept., METU

\_\_\_\_\_

Prof. Dr. Zuhall Akyürek  
Civil Engineering Dept., METU

\_\_\_\_\_

Prof. Dr. Andrew Binley  
Lancaster Environment Centre, Lancaster University

\_\_\_\_\_

Assoc. Prof. Dr. Koray K. Yılmaz  
Geological Engineering Dept., METU

\_\_\_\_\_

Asst. Prof. Dr. Onur Pekcan  
Civil Engineering Dept., METU

\_\_\_\_\_

**Date:** February 19, 2018

**I hereby declare that all information in this document has been obtained and presented in accordance with academic rules and ethical conduct. I also declare that, as required by these rules and conduct, I have fully cited and referenced all material and results that are not original to this work.**

Name, Last name: Gökben Demir

Signature :

## ABSTRACT

### SOIL WATER CONTENT ESTIMATION FROM POINT SCALE TO PLOT SCALE

Demir, Gökben

M.S., Department of Civil Engineering

Supervisor : Prof. Dr. Zuhal Akyürek

February 2018, 117 pages

Estimating soil moisture is crucial for understanding vadose zone and surface hydrology dynamics. In this study, soil moisture measurement is investigated by using a range of techniques spanning different spatial scales in a test basin in the south of Turkey. A cosmic ray sensor soil moisture probe (CRS) and a water content reflectometer (CS-616) have been installed for retrieving volumetric soil moisture data continuously. Lab analyses have been performed for calibrating the installed instruments and to obtain the pore water electrical conductivity range in the study area. The average pore water conductivity value is obtained as 933  $\mu\text{S}/\text{cm}$ , and it is observed that the variation of the pore water conductivity is not directly related to clay content. Electrical resistivity imaging (ERI) was used to map water content variation in a 2-D shallow unsaturated zone within the footprint of the CRS. Schlumberger and Wenner-Alpha electrode array with 0.50 m electrode spacing were used along 19.5 m resistivity profiles in the field surveys. Soil moisture measurements were done with CS-616 at these profile locations, concurrently. Archie's Law has been used to reveal the relationship between soil moisture and resistivity. Archie's cementation index ( $m$ ) and saturation index ( $n$ ) were calculated for the footprint as 1.57 and 1.152, respectively. This study reveals that ERI has limited sensitivity to the moisture content in the study area, whereas the CRS shows good agreement with the values obtained from the

installed CS-616 at point-scale, and rainfall amount observed at a nearby meteorological station.

Keywords: Cosmic Ray Sensor, Water Content Reflectometer, Electrical Resistivity Imaging, Pore Water Conductivity, Archie's Index

## ÖZ

### NOKTASAL ÖLÇEKTE ALANSAL ÖLÇEĞE TOPRAK SU İÇERİĞİNİN BELİRLENMESİ

Demir, Gökben

Yüksek Lisans, İnşaat Mühendisliği Bölümü

Tez Yöneticisi : Prof. Dr. Zuhâl Akyürek

Şubat 2018, 117 sayfa

Toprak suyu muhtevası, vadoz zonu ve yüzey hidrolojisi dinamikleri için oldukça önemlidir. Bu çalışmada, toprak nemi ölçümleri farklı mekansal ölçeklere sahip bir dizi teknik kullanılarak, Türkiye'nin güneyinde yer alan test havzasında gerçekleştirilmiştir. Kozmik ışın sensörü (CRS) ve su içeriği reflektometresi (CS-616) hacimsel toprak su içeriği verilerinin sürekli elde edilmesi için çalışma havzasına kurulmuştur. Kurulan istasyonların kalibrasyon işlemleri ve çalışma alanına ait boşluk suyu iletkenliğinin elde edilmesi için laboratuvar analizleri yapılmıştır. Ortalama boşluk suyu iletkenliği 933  $\mu\text{S}/\text{cm}$  olarak elde edilmiştir, ve boşluk suyu iletkenliği değişiminin, çalışma alanındaki kil yüzdesi ile doğrudan bağlantılı olmadığı belirlenmiştir. Elektriksel direnç görüntüleme (ERI) yöntemi, Schlumberger ve Wenner-Alpha elektrot dizilimleri ile 0.5 m elektrot aralığı kullanılarak 19.5 m direnç profilleri boyunca, CRS'nin ölçüm alanı içerisinde sığ doymamış zonalardaki toprak nemi değişiminin 2-B olarak haritalandırılması için kullanılmıştır. Direnç profilleri boyunca eş zamanlı olarak noktasal ölçekte harici toprak nemi ölçümleri CS-616 ile yapılmıştır. Toprak nemi ve direnç değişimi arasındaki ilişki Archie denklemi kullanılarak incelenmiştir. Archie sementasyon idenksi (m) ve Archie saturasyon indeksi (n) yinelemeli hesaplama yöntemi ile hesaplanarak; CRS ölçüm alanına ait değerleri 1.57 ve 1.152 olarak bulunmuştur. Bu çalışma, ERI'nın çalışma alanında toprak nemi değerlerinin elde edilmesinde sınırlı hassasiyete sahip olduğu, buna karşılık CRS'den ve kurulmuş CS-616'dan elde edilen noktasal ölçekteki değerlerinin,

uyumlu olduđu ortaya ıkarılmıřtır ve yađmur yađıř miktarları havza yakınında bulunan meteoroloji istasyonu ile gzlemlenmiřtir.

Anahtar Kelimeler: Kozmik Iřın Sensr, Su İeriđi Reflektometresi, Elektriksel Diren Grntleme, Bořluk Suyu İletkenliđi, Archie İndeksleri

*To My Mom and All Inspiring Women ...*

## ACKNOWLEDGEMENTS

First and foremost, I would like to express my sincere gratitude to my supervisor Prof. Dr. Zuhale Akyürek, for her continuous guidance, invaluable advice, care and insights throughout the research. She is one of the most special people in my life, meaning much more than a supervisor. I am really fascinated by not only her wide knowledge and experience in technical issues but also in life. She is not only a great academician but also an inspiring person. It is a great chance to meet her, to be a student of her. I sincerely believe that being a student of her is an important step for being a better researcher.

My sincere thanks also go to Prof. Dr. Andrew Binley, for his invaluable contributions to my thesis researches. It was a privilege having his support throughout my research since he is a pioneering academician in my field of interest.

I am forever in debt to Assoc. Prof. Dr. Nurünnisa Usul. She taught me hydrology is a touch to human life as well, and that is how I have found the courage in myself to study in the field of hydrology. I learned that a hydrologist should care about technique qualities beside social issues.

I appreciate the assistance offered by Ph.D. candidate Bizhan Abgarmi while carrying out resistivity survey in the field and the inversion procedure of the resistivity data. I also would like to thank Ph.D. candidate Mustafa Berk Duygu for his contribution to the CRS calibration procedure.

I would like to offer my special thanks to Adnan Başaran for his guidance to be familiar with the basin, and staff of DSI 4th Region Directorate for their endless help in the field studies.

I would like to acknowledge Ulaş Nacar and METU Civil Engineering Soil Mechanics Laboratory staff for their help during the lab analyses.

I am deeply grateful to my lovely friend Güncel Vara for his comments and correcting the use of English.

I wish to thank my dearest friends; Işıl Özge Işık, Medine Merve Olgun, Melis Deniz, Özer Gündüz. Their presence in my life and all the memories we share are really valuable and essential for me. I also would like to thank my friends; Başak Seyisoğlu, Barış Mert Pehlivan, Beyazıt Bestami Aydın, Hazal Güldür, İrem Ağaçoğlu, Korhan Kocamaz, Münci Tunç Kalaycıoğlu and Müge Özgenoğlu for all the support and enjoyable moments we have shared. They have made my stressful studying days bearable and fun.

I would like to thank my beloved mother Satı Demir, my father Tekin Demir and my brother Gökhan Demir for everything they have done for me so far. No word is enough to express my gratefulness to them. They have always been great role models and supporters of all my decisions in life. I owe almost everything to them.

Finally, this thesis study is supported by TÜBİTAK 1003 Primary Subjects R&D Funding Program (SU 0301) within the scope of 115Y041 numbered project titled Determination of Hydrologic Cycle Parameters Using Hydrologic Modeling; also, I would like to acknowledge for the scholar graduate studentship funded by the project budget during my master studies.

## TABLE OF CONTENTS

ABSTRACT .....	x
ÖZ.....	xkk
ACKNOWLEDGEMENTS .....	z
TABLE OF CONTENTS .....	zkk
LIST OF TABLES .....	zkk
LIST OF FIGURES.....	zx
LIST OF SYMBOLS AND ABBREVIATIONS.....	xviii
CHAPTERS	
1. INTRODUCTION.....	1
1.1 Motivation of the Study.....	3
1.2 Thesis Structure.....	4
2. LITERATURE REVIEW .....	7
2.1 Soil .....	7
2.2 Soil Moisture Measurement Techniques.....	8
2.2.1 Thermogravimetric Method .....	9
2.2.2 Remote Sensing Methods.....	9
2.2.3 Ground Penetrating Radar (GPR) .....	11
2.2.4 Time Domain Reflectometry (TDR) .....	13
2.2.5 Frequency Domain Sensors: Capacitance Probes and Frequency Domain Reflectometry (FDR).....	14
2.2.6 Neutron Scattering.....	16
2.2.7 Electrical Resistivity Method .....	18
3. STUDY AREA .....	23
3.1 Hydroclimatology of Çakıt Basin .....	24

3.1.1	Temperature .....	24
3.1.2	Rainfall.....	25
3.1.3	Wind and Humidity.....	26
3.2	Topographical Characteristics of Çakıt Basin .....	27
4.	SOIL MOISTURE MEASUREMENTS .....	35
4.1	Cosmic-ray Soil Moisture Sensor (CRS).....	35
4.1.1	Correction Procedure .....	36
4.1.2	Conversion of Corrected Neutron Flux to Soil Moisture.....	38
4.1.3	Field Calibration and Soil Properties .....	39
4.1.4	Volumetric Soil Moisture Data from CRS.....	43
4.2	Installed Water Content Reflectometry (CS-616).....	46
4.2.1	Laboratory Calibration Procedure of CS-616 .....	47
4.2.2	Volumetric Soil Moisture Data from the CS-616 .....	52
4.3	Electrical Resistivity Imaging (ERI) and Frequency Domain Reflectometry (FDR) Data Acquisition .....	54
4.3.1	Inversion Procedure and Interpretation of Inverted Resistivity Data.	59
4.3.2	Resistivity Data Conversion.....	63
5.	DISCUSSION OF THE RESULTS.....	77
5.1	Summary .....	77
5.2	Evaluation of the CRS and the Installed CS-616 Measurements.....	77
5.3	Evaluation of the Electrical Resistivity Imaging (ERI) Surveys .....	83
6.	CONCLUSIONS AND RECOMMENDATIONS.....	85
6.1	Conclusion .....	85
6.2	Recommendations .....	86
	REFERENCES.....	89
	APPENDICES	
A.	GROUND - BASED STATIONS .....	99
B.	INVERSION RESULTS OF ERI SURVEY PROFILES.....	101

## LIST OF TABLES

### TABLES

Table 3-1 Monthly averaged temperature values (°C) .....	24
Table 3-2 Long-term monthly averaged relative humidity values (%) .....	26
Table 4-1 CRS footprint soil properties .....	42
Table 4-2 Calibration values of the CS-616 .....	50
Table 4-3 Land use classification of profiles .....	56
Table 4-4 Clay content percentage classification of profiles .....	57
Table 4-5 Soil texture classification of the profiles .....	57
Table 4-6 FDR soil moisture measurements (%) along resistivity profiles .....	59
Table 4-7 Estimated pore water conductivity values and clay content information ..	70
Table 5-1 Rainfall event and the corresponding soil moisture change .....	80
Table A-1 Ground-based stations in Çakıt Basin .....	99

## LIST OF FIGURES

### FIGURES

Figure 1-1 Soil moisture sensors with respect to spatial extent (Vereecken et al. 2008) .....	3
Figure 2-1 Schematic soil component volumetric compositions at a theoretical conditions (Hillel 2004) .....	8
Figure 2-2 Active microwave and passive microwave approaches (Hassan 2014)...	10
Figure 2-3 The possible travel path of the electromagnetic wave in a soil involves two layers (Huisman et al. 2003) .....	11
Figure 2-4 GPR survey types; CMP (a), WARR (b), CO (c) (Galagedara et al. 2003) .....	12
Figure 2-5 TDR designs; three-rod probe, two-rod probe and parallel plate probe (Robinson et al. 2003) .....	13
Figure 2-6 Principle of four electrode measurement approach (Knödel et al. 2007).	19
Figure 2-7 Generally applied electrode geometry and their geometric factors (Loke et al. 2013) .....	21
Figure 3-1 Çakıt Basin and its location in Turkey .....	23
Figure 3-2 Yearly averaged temperature (°C) values.....	25
Figure 3-3 Annual total rainfall (mm) for the basin (1929-2017).....	25
Figure 3-4 General wind direction densities for Ulukışla Meteorological station.....	26
Figure 3-5 Wind directions and average speed (m/s) values for Ulukışla Meteorological Station .....	27
Figure 3-6 Hypsometric curve of Çakıt Basin .....	28
Figure 3-7 DEM and instrumentation of Çakıt Basin .....	29
Figure 3-8 Soil types in Çakıt Basin .....	30
Figure 3-9 Land use cover in Çakıt Basin.....	31
Figure 3-10 Geological map of Çakıt basin .....	32

Figure 3-11 Hydrogeological formation of Çakıt basin .....	33
Figure 4-1 Cosmic-ray soil moisture sensor system (CRS 2000/B) .....	36
Figure 4-2 Sample point locations (a) and soil sampling procedure (b, c) .....	40
Figure 4-3 Soil texture triangle, USDA .....	43
Figure 4-4 Rainfall, air temperature, the CRS soil moisture data .....	45
Figure 4-5 Installation scheme for water content reflectometer, soil temperature probes and heat flux installation scheme .....	46
Figure 4-6 Water content reflectometer, CS-616 .....	47
Figure 4-7 Homogeneously wetting (a), CS-616 measurement (b) .....	49
Figure 4-8 Calibration equation of the installed CS-616 .....	50
Figure 4-9 The site-specific calibration and the standard curves of the CS-616 .....	51
Figure 4-10 The CS-616 default data, corrected and calibrated data.....	53
Figure 4-11 Ares- Automatic Resistivity System and intelligent cable .....	54
Figure 4-12 Locations of sample points and ERI profiles (17 - 21 Aug 2017).....	55
Figure 4-13 ERI profiles; outside of the agricultural part (a), inside of the agricultural part (b).....	56
Figure 4-14 Sketch of the electrode and the CS-616 measurement locations in the resistivity survey line .....	59
Figure 4-15 ERI profile 1 (Aug 2017) inversion results; Wenner-alpha via Res2DInv (a), Wenner-Schlumberger via Res2DInv (b), combined electrode geometry via Profile R (c).....	61
Figure 4-16 Measured resistivity data with respect to FDR measurements.....	63
Figure 4-17 Disturbed soil sampling in August 2017 .....	66
Figure 4-18 Soil sample (a), consolidation cell with the sample (b), cure procedure (c) .....	68
Figure 4-19 Consolidation test setup.....	68
Figure 4-20 Pore water conductivity measurement by the EC probe .....	69
Figure 4-21 Estimated pore water conductivity with respect to clay content .....	70
Figure 4-22 Calculated water content in the lab by using soil phase relationships and conditions and CS-616 measurements .....	71

Figure 4-23 Expected Archie’s equation curve with random values (Lecture notes of Prof. Dr. Andrew Binley).....	73
Figure 4-24 Pore water conductivity range and FDR measurements .....	74
Figure 4-25 Saturation index (n) range and FDR measurements.....	75
Figure 4-26 Cementation index (m) and FDR measurements .....	76
Figure 5-1 Snow depth, air temperature data and the CRS soil moisture measurement .....	78
Figure 5-2 The CS-616 default measurement, calibrated measurement, calibrated and corrected measurement and soil temperature data .....	79
Figure 5-3 Soil moisture data retrieved from the installed instruments; CS-616 and CRS .....	81
Figure 5-4 Difference between soil moisture data retrieved from CRS and CS-616.	82
Figure B-6-1 ERI 1 (Aug 2017) inversion results; Wenner-alpha via Res2DInv (a), Schlumberger via Res2DInv (b), combined Wenner-alpha & Schlumberger geometry via ProfileR (c).....	102
Figure B-6-2 ERI 2 (Aug 2017) inversion results; Wenner-alpha via Res2DInv (a), Schlumberger via Res2DInv (b), combined Wenner-alpha & Schlumberger geometry via ProfileR (c).....	103
Figure B-6-3 ERI 3 (Aug 2017) inversion results; Wenner-alpha via Res2DInv (a), Schlumberger via Res2DInv (b), combined Wenner-alpha & Schlumberger geometry via ProfileR (c).....	104
Figure B-6-4 ERI 4 (Aug 2017) inversion results; Wenner-alpha via Res2DInv (a), Schlumberger via Res2DInv (b), combined Wenner-alpha & Schlumberger geometry via ProfileR (c).....	105
Figure B-6-5 ERI 5 (Aug 2017) inversion results; Wenner-alpha via Res2DInv (a), Schlumberger via Res2DInv (b), combined Wenner-alpha & Schlumberger geometry via ProfileR (c).....	106
Figure B-6-6 ERI 6 (Aug 2017) inversion results; Wenner-alpha via Res2DInv (a), Schlumberger via Res2DInv (b), combined Wenner-alpha & Schlumberger geometry via ProfileR (c).....	107

Figure B-6-7 ERI 7 (Aug 2017) inversion results; Wenner-alpha via Res2DInv (a), Schlumberger via Res2DInv (b), combined Wenner-alpha & Schlumberger geometry via ProfileR (c).....	108
Figure B-6-8 ERI 8 (Aug 2017) inversion results; Wenner-alpha via Res2DInv (a), Schlumberger via Res2DInv (b), combined Wenner-alpha & Schlumberger geometry via ProfileR (c).....	109
Figure B-6-9 ERI 9 (Aug 2017) inversion results; Wenner-alpha via Res2DInv (a), Schlumberger via Res2DInv (b), combined Wenner-alpha & Schlumberger geometry via ProfileR (c).....	110
Figure B-6-10 ERI 10 (Aug 2017) inversion results; Wenner-alpha via Res2DInv (a), Schlumberger via Res2DInv (b), combined Wenner-alpha & Schlumberger geometry via ProfileR (c).....	111
Figure B-6-11 ERI 11 (Aug 2017) inversion results; Wenner-alpha via Res2DInv (a), Schlumberger via Res2DInv (b), combined Wenner-alpha & Schlumberger geometry via ProfileR (c).....	112
Figure B-6-12 ERI 12 (Aug 2017) inversion results; Wenner-alpha via Res2DInv (a), Schlumberger via Res2DInv (b), combined Wenner-alpha & Schlumberger geometry via ProfileR (c).....	113
Figure B-6-13 ERI 13 (Aug 2017) inversion results; Wenner-alpha via Res2DInv (a), Schlumberger via Res2DInv (b), combined Wenner-alpha & Schlumberger geometry via ProfileR (c).....	114
Figure B-6-14 ERI 14 (Aug 2017) inversion results; Wenner-alpha via Res2DInv (a), Schlumberger via Res2DInv (b), combined Wenner-alpha & Schlumberger geometry via ProfileR (c).....	115
Figure B-6-15 ERI 15 (Aug 2017) inversion results; Wenner-alpha via Res2DInv (a), Schlumberger via Res2DInv (b), combined Wenner-alpha & Schlumberger geometry via ProfileR (c).....	116
Figure B-6-16 ERI 16 (Aug 2017) inversion results; Wenner-alpha via Res2DInv (a), Schlumberger via Res2DInv (b), combined Wenner-alpha & Schlumberger geometry via ProfileR (c).....	117

## LIST OF SYMBOLS AND ABBREVIATIONS

$\theta$	Volumetric water content
$w_n$	Gravimetric water content
$\rho_{\text{bulk}}$	Bulk density of soil
$\rho_{\text{bd}}, \rho_{\text{dry bulk}}$	Dry bulk density of soil
$G_s$	Specific gravity of soil
$e$	Void ratio of soil
$\phi$	Porosity
$\epsilon$	Bulk dielectric permittivity of soil
$\rho$	Bulk resistivity of soil
$\rho_w$	Resistivity of pore water
$\sigma$	Bulk conductivity of soil
$\sigma_w$	Conductivity of pore water
$S$	Saturation degree
$F$	Formation factor
$m$	Cementation index
$n$	Saturation index
$t, T$	Time
$\tau$	Time period of electromagnetic pulse
CL	Clay content
EC	Electrical conductivity
TDR	Time domain reflectometry
FDR	Frequency domain reflectometry
WCR	Water content reflectometer
CRP	Cosmic-ray probe
CRS	Cosmic-ray soil moisture sensor
ERI	Electrical resistivity imaging



## CHAPTER 1

### INTRODUCTION

Almost 75 % of the Earth's surface is covered with water in both liquid and solid form (NASA Earth Observatory n.d.), and it is requirement for life on the planet. However, only a small percentage of this amount of water is available as freshwater to meet human needs, particularly potable water and food production. Moreover, water resources have become the most dominant factor for economic and cultural improvements of humankind. As a result, management of fresh water resources has become a vital issue.

An endless movement of water throughout land, atmosphere, ocean; its storages, and its changes in physical state conditions are described by hydrological cycle. Evaporation, transpiration, precipitation, surface runoff, groundwater flow and infiltration are the elements of the cycle.

Soil moisture is 0.005% of the whole water storage in the Earth (Fetter 2001), albeit it has paramount influences on the cycle parameters. As soil moisture regulates the energy exchange between the land and the atmosphere, it affects evaporation besides transpiration (Seneviratne et al. 2010). Furthermore, it controls the portioning of rainfall into infiltration and runoff; hence, the amount of soil moisture present is important for understanding the relationship between rainfall and run-off for a basin. Dunne and Black (1970) showed that soil moisture conditions are the main control mechanism of the rainfall-runoff relationship of the basin, and more recent researches highlight how the antecedent soil moisture situation affects run-off amount (Brocca et al. 2008; Penna et al. 2011).

An understanding of hydrological processes, which are highly complicated, predictions for and forecasting of hydrologic quantities are essential for all kinds of water resources applications. Hydrologic models, which are simulations of certain parts of the hydrological cycle within a natural or a human-made system, have evolved in line with these fundamentals (Dingman 2002). The models might be physically or conceptually based. In both cases, the models can be operated successfully with sufficiently qualified and available data, since the GIGO principle i.e., Garbage In - Garbage Out, is valid for hydrological models as well.

Soil moisture data, which are temporally and spatially varied, should be retrieved in order to improve the understanding of hydrological processes and determine the conditions of hydrological states. This leads us to the fact that soil moisture data is critical for many types of hydrological modelling. Several studies revealed that the use of soil moisture data enhanced the prediction and forecasting of rainfall-runoff modeling besides flood modeling (Aubert et al. 2003; Bronstert et al. 2012; Goodrich et al. 1994).

Measurement of soil moisture can be carried out by using numerous different techniques for different scales from point to global-scale, and Figure 1-1 presents generally used methods. Some examples of point-scale measurement methods are thermogravimetric method, time domain reflectometry (TDR), frequency domain reflectometry (FDR); remote sensing tools provide soil moisture data for much larger areas (Lakshmi 2013). Geophysical methods, such as ground penetrating radar (GPR), electrical resistivity imaging (ERI) are promising techniques for obtaining soil moisture at the mesoscale (Huisman et al. 2003; Samouëlian et al. 2005). In addition, the cosmic-ray sensor (CRS) technique has been developed to meet the need for intermediate scale measurements by providing areal-average soil moisture data (Zreda et al. 2008).

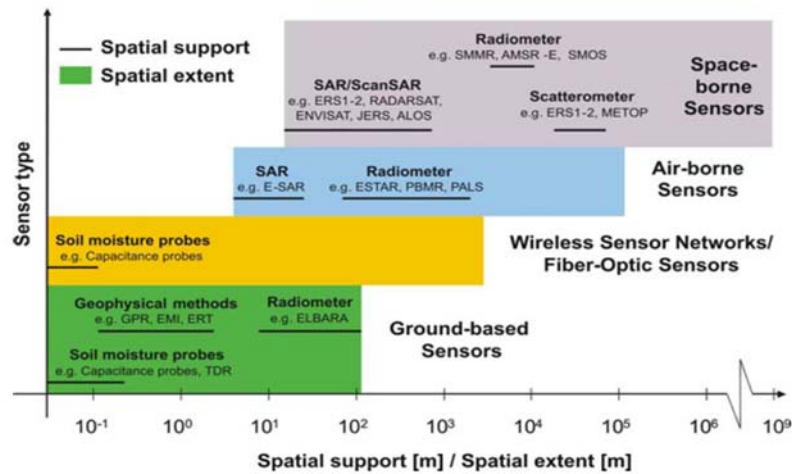


Figure 1-1 Soil moisture sensors with respect to spatial extent (Vereecken et al. 2008)

## 1.1 Motivation of the Study

Although soil moisture is assessed by using TDR and conventional gravimetric method within an acceptable accuracy, they are generally invasive. Additionally, these methods are not easily applicable to retrieve soil moisture data efficiently for large areas, due to their data acquisition scale. On the other hand, remote sensing is a beneficial method to estimate spatial soil moisture information; nevertheless, this method cannot provide sufficient depth of investigation for many hydrological modeling studies. Obviously, there is a gap between a point-scale and a global-scale soil moisture estimation (Robinson et al. 2008).

Unified multiscale soil moisture measurements for the characterization of near surface temporal and spatial soil moisture conditions is still a requirement for some hydrologic research. Multiscale soil moisture monitoring provides detailed soil water conditions, and the validation of basin-scale hydrological models depend on this information (Vereecken et al. 2008).

Requirement of unified multiscale soil water content measurement to supply sufficiently qualified data for a hydrological model have sparked the interest in

research which forms the basis of this thesis. The study aims to combine several soil moisture measurement techniques to obtain soil water content in a particular region and depth, and to meet this need through in point of view hydrology.

In this study, data from one cosmic-ray sensor (CRS) and a water content reflectometer (WCR), which is classified as a FDR instrument with soil temperature sensors, were used in order to monitor soil moisture continuously at the study area. Thermogravimetric sampling was done to calibrate these ground-based instruments. Furthermore, ERI method was performed to measure soil moisture at a scale that bridges that of the WCR and the CRS sensor, besides WCR measurements were carried out concurrently.

This study is a part of the project, Determination of Hydrological Cycle Parameters with a Conceptual Hydrological Model (Project number: 115Y041), aims to obtain hydrological cycle parameters by using data improved conceptual models.

## **1.2 Thesis Structure**

This thesis includes six chapters. Following the introductory part, in Chapter 2, some basic terms and soil moisture techniques are overviewed based on former research.

The study area is introduced in Chapter 3. Geographical information of the study area is provided in addition to hydro-climatologic, topographical, geological and hydrogeological properties. Additionally, the installed instruments are presented.

In Chapter 4, the methodology used in this study is explained. This chapter is divided into three sections. Calibration procedures for the data retrieved from the CRS and the WCR are clarified in detail in the first two sections. In August 2017, the ERI technique was applied to map 2-D resistivity variation in the CRS measurement area, and WCR was used to measure soil moisture along the resistivity survey lines in the study area. The relationship between these two different types of data and resistivity data interpretation are also detailed in this chapter.

The last two chapters, Chapter 5 and Chapter 6, discuss the results and conclude the study with further recommendations, respectively.



## **CHAPTER 2**

### **LITERATURE REVIEW**

#### **2.1 Soil**

Soil basically consists of three substances: solid particles, air and water. Solid particles have different chemical and mineralogical contents; also, they exhibit variety in size, shape and orientation. These textural attributes determine geometrical structure of the pore space. Organic matter, which sticks on solid particles, is also a component of the soil. The amount of air and water, which reside in pores, changes both in time and space. As the water generally includes dissolved minerals, it is defined as soil solution or pore water solution.

Hillel (2004) described the soil as a heterogeneous, polyphasic, particulate disperse and porous system, and schematic of natural situation of the soil is indicated in Figure 2-1.

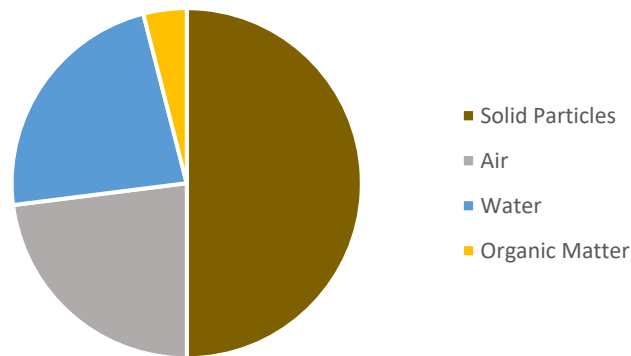


Figure 2-1 Schematic soil component volumetric compositions at a theoretical conditions (Hillel 2004)

## 2.2 Soil Moisture Measurement Techniques

Soil water content is the key variable for several issues in hydrological sciences, hence the estimation of soil water content value has become a critical task for water budget calculations, estimating actual evapotranspiration and surface water conditions. In literature, there are various techniques, and these techniques are being improved day by day.

Soil moisture measurement methods can be classified into two major groups: thermogravimetric method which is a direct method, and indirect methods that rely on conversion of the moisture content from obtained data by using empirical equations or models. In addition, these data depend on differences in physical and/or chemical properties of soil components such as dielectric permittivity, electrical resistivity, and neutron thermalization capacity.

The relative dielectric permittivity,  $\epsilon$ , which is described as the ratio of the permittivity of material to the permittivity of free space, is a dimensionless term, and it is often known as permittivity. Dielectric permittivity of water, which is around 80 is much greater than other soil components' dielectric permittivity values: which are 1 for air and around 5 for most of soil solid particles (Robinson et al. 2008). Therefore,

variation of the water content leads to remarkable changes in bulk dielectric permittivity of the soil. This incredible influence is used by remote sensing, ground penetrating radar, time domain reflectometry and frequency domain methods to retrieve soil moisture content.

### **2.2.1 Thermogravimetric Method**

The thermogravimetric method, which depends on the mass lost under rising temperature values, is used to obtain soil water content directly. The soil sample is oven-dried at  $105^{\circ}\text{C} \pm 5^{\circ}\text{C}$  for more than 12h, and the reduced mass amount is regarded as the amount of water in soil (ASTM D2216 2010). Even though the thermogravimetric method is regarded as the most accurate measuring technique, it is not conducted broadly in catchment-scale studies, because of its destructive nature and difficulties in its application. However, it is used (by converting gravimetric water content into volumetric) as a reference method to assess indirect method measurements.

### **2.2.2 Remote Sensing Methods**

Many remote sensing tools examine the Earth's land surface attributes by employing electromagnetic wave radiation at different spectrum – ultraviolet, visible, infrared and microwave sensors are placed in aircraft or satellite (Knödel et al. 2007). Soil moisture content regulates the electromagnetic reaction of the land surface since the water content influence dielectric permittivity of the soil significantly, but surface temperature, surface roughness and vegetation density affect the reaction, as well. In other words, scattering and emissivity properties mainly depend on soil moisture (Lakshmi 2013).

Although visible and thermal space-borne data have been used to determine surface soil moisture under non-cloudy day light conditions for more than forty years, microwave spectrum approaches using satellites has developed, and has become more

preferable both at regional and global-scale soil moisture measurements (Bittelli 2011). The microwave approach includes two methods: passive microwave and active microwave. These two methods are able to retrieve soil water content of the land surface over a depth of 0 to 5 cm, and their spatial resolutions are several meters to kilometers, for active and passive techniques respectively. In passive methods that are well equipped sensors based on measuring natural thermal radio emission, in active method microwave pulse is sent, and back scattered pulse is received (Figure 2-2). The comparison between sent and received wave power, back-scattering coefficient, indicates the land surface characteristics. Soil surface roughness, vegetation cover have significant influence on the inference of the relationship between data which are acquired from microwave approaches and soil water (Jackson et al. 1996).

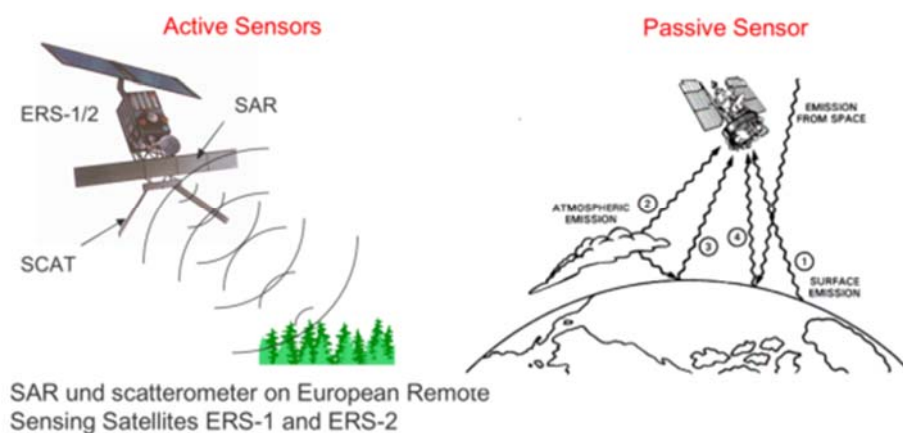


Figure 2-2 Active microwave and passive microwave approaches (Hassan 2014).

Remote sensing has been used to obtain soil moisture for catchment-scaled modelling studies in the literature (e.g. ; Brocca et al. 2010, Fang and Lakshmi 2014). However, due to the limitations in spatial resolution and the examination depth of the remote

sensing methods, these tools are generally adopted as more convenient for global-scale researches instead of the basin scale studies (Petropoulos et al. 2015).

### 2.2.3 Ground Penetrating Radar (GPR)

Ground Penetrating Radar (GPR) allows the scanning of alterations in the shallow subsurface formation along a survey line in ranges as narrow as a few centimeters or as large as a few kilometers. It is a geophysical method. GPR systems consist of two antennas, which are the transmitter and the receiver. High frequency electromagnetic waves relayed by the transmitter antenna penetrate the mapping region, and the receiver antenna measures the reflected wave. The reflection path of the electromagnetic wave is based on the differences between electric permittivity values of the heterogeneous layers in the soil (Huisman et al. 2003). The possible travel path of the wave is shown in Figure 2-3.

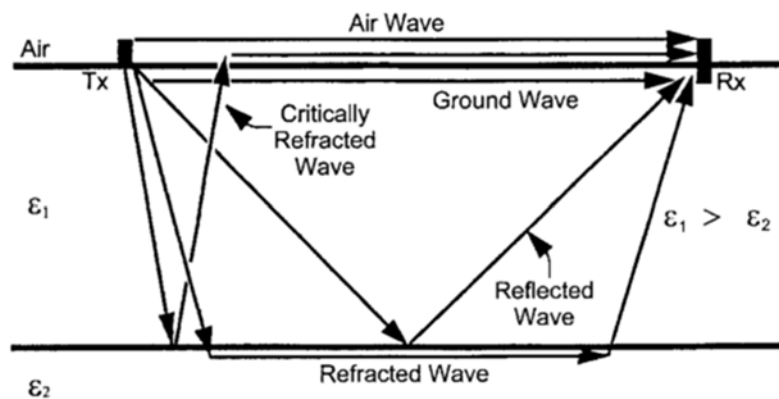


Figure 2-3 The possible travel path of the electromagnetic wave in a soil involves two layers (Huisman et al. 2003)

Data acquisition for obtaining soil water with GPR can be conducted in three different ways (Figure 2-4). These are identified according to the position of the antennas and movements of these with respect to each other. If the antennas are moved apart from each other with a specified distance incrementally, this is called common mid-point (CMP), which is the first of these survey types. In the second type; that is, wide angle reflection and refraction (WARR), the receiver antenna is shifted with a constant distance in small increments, whereas the transmitter is fixed at a point. In the third type of survey, common offset (CO), the distance between the antennas is fixed and, these are moved simultaneously along the survey line (Galagedara et al. 2003).

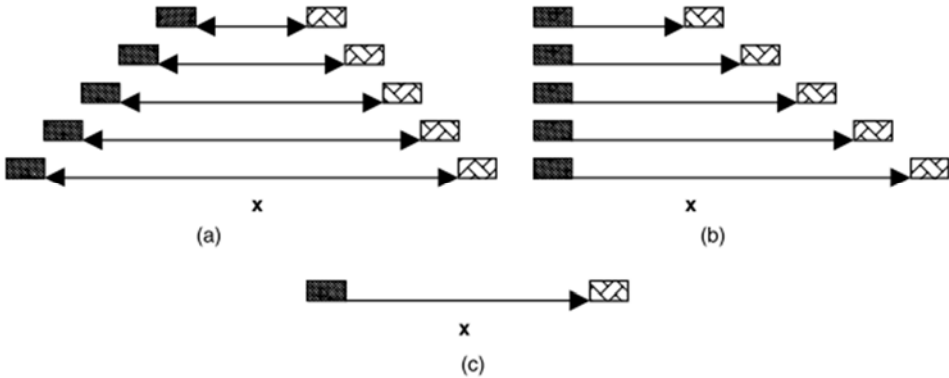


Figure 2-4 GPR survey types; CMP (a), WARR (b), CO (c) (Galagedara et al. 2003)

Data retrieved from GPR surveys are converted to soil water content by using empiric equations or mixing models; such as Topp’s equation, Equation 2-4, and complex refractive index model (CRIM) (Cassiani et al. 2006a).

#### 2.2.4 Time Domain Reflectometry (TDR)

The time domain reflectometry (TDR) method provides highly accurate soil moisture monitoring at the point-scale. A TDR instrument, presented in Figure 2-5, produces an electromagnetic wave with a bandwidth value in a range between 10 kHz and 1 GHz, and it is transmitted to the soil along probes. At the tip of the probe, the wave is reflected back along another inserted probe of the instrument. TDR measures the velocity of the guided electromagnetic wave which depends on the dielectric permittivity (Wraith et al. 2005).

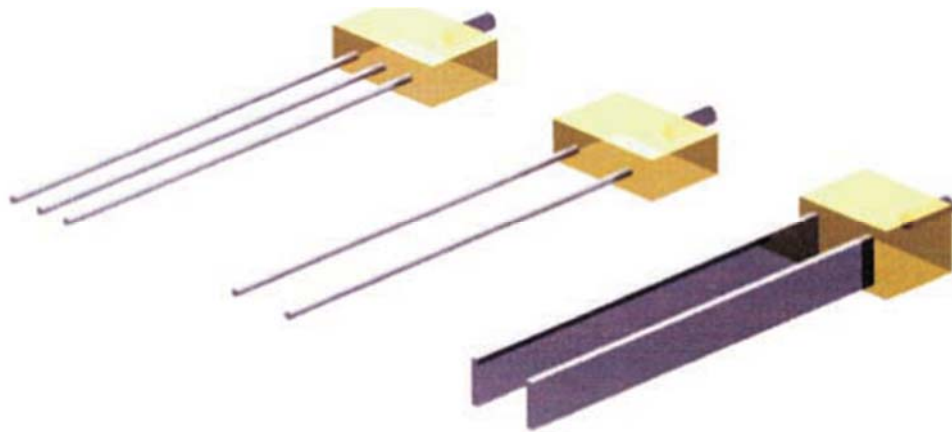


Figure 2-5 TDR designs; three-rod probe, two-rod probe and parallel plate probe (Robinson et al. 2003)

The velocity of the wave and the relationship between the velocity and the electric permittivity can be defined as follows:

$$v_p = 2L/t \quad (2.1)$$

$$v_p = c/\sqrt{\epsilon} \quad (2.2)$$

where  $v_p$  is the propagated wave velocity,  $L$  is probe length in m,  $t$  is the time for the round trip and  $c$  is the velocity of light in the free space, which is  $3 \times 10^8$  m/s.

Combination of Equation 2.1 and 2.2 is as follows:

$$t = \frac{2L\sqrt{\epsilon}}{c} \quad (2.3)$$

The empiric equation, Equation 2.4, which describes the interrelationship of volumetric water content and bulk dielectric permittivity of soil, was developed by Topp et al. (1980) at the end of experimental studies on different soil mineral types and textures, and the volumetric water content was estimated with an error of 1.3 %.

$$\theta = -5.3 \times 10^{-2} + 2.92 \times 10^{-2} \epsilon - 5.5 \times 10^{-4} \epsilon^2 + 4.3 \times 10^{-6} \epsilon^3 \quad (2.4)$$

Moreover, mixing model approaches have been improved to reveal the relationship between water content and dielectric constant. These approaches rely on taking into consideration of each soil component in the model individually (e.g. Chan and Knight 1999; Friedman 1998).

TDR is widely used in hydrological and agricultural studies, because it does not require calibration for many types of soil and it is considered a reliable method.

### **2.2.5 Frequency Domain Sensors: Capacitance Probes and Frequency Domain Reflectometry (FDR)**

Dean et al. (1987) developed a capacitance probe which was operated at 150 MHz to obtain soil water content, and described the relationships between capacitance, frequency, and dielectric constant as follows:

$$F = \frac{1}{2\pi\sqrt{L}} \sqrt{\left(\frac{1}{C} + \frac{1}{C_b} + \frac{1}{C_c}\right)} \quad (2.5)$$

$$C = g \varepsilon \quad (2.6)$$

where  $F$  is the frequency of oscillation,  $C_b$  is the total base capacitance,  $C_c$  is the collector capacitance, and  $C$  is the measured capacitance which is a function of dielectric permittivity,  $\varepsilon$  and here,  $g$  is geometrical probe design constant:

The probe, composed of a capacitance sensor element and an oscillator which was placed in the soil sample, and transmits an electromagnetic wave into the soil sample. The oscillation frequency values of the wave were recorded, the corresponding capacitance values were determined. This pioneering probe design and, the possibility of lower frequency electromagnetic waves being useful (Campbell 1990), have created an opportunity for manufacturing inexpensive soil moisture sensors.

Frequency domain reflectometry (FDR) operates according to the same working principle for the capacitance probes, but they operate at lower frequencies, which range between 10 MHz and 100 MHz, than those of the capacitance probes and TDR instruments (Western and Seyfried 2005).

Whereas TDR measures travel times, FDR and capacitance probes measure the oscillation frequency. FDR instruments are significantly cheaper than TDR sensors. These frequency domain instruments can be placed into the soil for a long time period (Veldkamp and O'Brien 2000).

TDR rarely requires calibration according to soil type; however, frequency domain sensors should be calibrated for site-specific soils, and for the soil temperature conditions to estimate soil water content accurately (Kizito et al. 2008; Mittelbach et al. 2012).

Soil water content - dielectric permittivity relationship has been already explained in empirical equations and mixing models (Topp et al. 1980; Whalley et al. 1992). The dielectric permittivity and the oscillation frequency are inversely proportional; hence,

frequency domain approaches have become an easily applicable soil water content measurement technique in the field.

The CS-616 (Campbell Scientific) water content reflectometer, which is the most commonly used FDR based sensor, was used in this study.

### **2.2.6 Neutron Scattering**

Neutron scattering method relies on the thermalization of the fast neutron which is at an energy level around a million electron volt or more by a hydrogen atom, and the fundamental principle was explained by Gardner and Kirkham (1952). Fast neutrons become slower and lose their energy when they elastically collide with the nuclei of atoms, and this is called thermalization. Collision with atoms with low atomic weights leads to much greater energy loss; as a result, hydrogen atoms slow down fast neutrons the most effectively. This principle is used by neutron moisture meters, neutron probes and neutron-scattering moisture meters. In these conventional instruments, fast neutrons are emitted by a suitable radioactive source artificially. For example, beryllium has been generally used owing to that it yields the highest neutron density compared to the other elements in the periodic table (Chanasyk and Naeth 1996).

Neutron scatter methods measure hydrogen density, which exists mostly in the form of water in soil, with the help of counting thermalized neutrons. The field application is as follows: the neutron probe is placed on the soil surface, and thermalized slow neutron intensity is accounted per unit time (Visvalingam and Tany 1972). The relationship between the resultant slow neutron density and soil moisture is revealed by calibration curves. Results of these applied conventional methods show that soil moisture content is obtained by the relationship between measured, and the calibrated neutron flux is consistent with the soil moisture data, which is measured by other techniques such as tensiometer, frequency domain reflectometer, and time domain reflectometer. All soil moisture sensors detect a similar trend in soil moisture variation (Leib et al. 2003).

Passive neutron sensors or cosmic ray probes (CRP), which do not need an artificial radioactive source for generation of fast neutrons, are promising instruments to obtain volumetric water content (VWC) at a field-scale (Zreda et al. 2008). The general working principle is similar to that of active neutron probes.

Cosmic rays are natural radiation sources, and they were discovered at the beginning of the 20th century by Hess (1912). The natural cosmic-ray radiation can be classified into two types: primary and secondary cosmic rays. Primary cosmic rays are radiated from the sun or space, and they penetrate the Earth atmosphere and collide with atoms in there. Secondary cosmic rays, which mainly consist of neutrons, are produced at the end of this collision (Bogena et al. 2013). Neutrons of these secondary cosmic-rays are at different energy levels, and they are described according to the energy level. These are namely, high energy neutrons; fast neutrons which are generated by the collision between high energy neutrons and terrestrial atomic nuclei in the air, vegetation, and soil; low energy thermal and epithermal neutrons which are formed by the moderation of fast neutrons through collisions with atomic nuclei (Zreda et al. 2012).

Fast neutrons can be absorbed and moderated most efficiently by hydrogen atoms, hence the neutron flux and plentitude of hydrogen atom density above the ground surface are inversely correlated. For example, while VWC typically varies between 0 to 40%, the cosmic ray neutron density declines to 60%, correspondingly. Therefore, this inverse correlation and measurement of neutron density are the main inputs for monitoring soil moisture at field-scale (Zreda et al. 2008).

Like active conventional neutron scattering methods, the relationship between soil moisture and the countered neutron intensity in the CRP measurements is deduced from calibration curves (Zreda et al. 2008). The CRP measurement needs not the only calibration but also the counted neutron intensity requires a range of corrections. There are several factors, which affect spatial cosmic-ray intensity. Atmospheric pressure, atmospheric vapor, spatial neutron flux density and cutoff rigidity are some of these factors. The cutoff rigidity is imposed by the geomagnetic field which is generally greater at low latitude (Desilets and Zreda 2001). CRP measurements can be converted to area-average soil water content with different methods. A site-specific method

(called the  $N_0$  method), a universal calibration method which is the hydrogen molar fraction method (hmf-method) and a Cosmic-ray Soil Moisture Interaction Code (COSMIC) method are parametrization approaches to develop site-specific neutron flux – soil moisture calibration curves. The  $N_0$  method is easily computable because it needs only one calibration parameter, but it relies on intensive soil sampling for determining this parameter accurately (Baatz et al. 2014).

The cosmic ray probe (CRP) provides soil moisture monitoring non-invasively besides it is a non-contact methods, insensitive to soil texture, bulk density, surface roughness or the physical state of water, and an environment-friendly method (Desilets et al. 2010). Moreover, it measures soil water content at an intermediate scale since it has a lateral measurement area with a diameter approximately 670 m at sea level, and it provides soil moisture monitoring at a depth, which changes in a range between 0.12 m to 0.76 m. While the measurement depth depends on only wetness conditions of the soil, the measurement area or its footprint is inversely proportional to the atmospheric pressure (Zreda et al. 2008). This useful technique has been used in many critical zone observatory studies (e.g. Baatz et al. 2015; Zreda et al. 2012).

### **2.2.7 Electrical Resistivity Method**

Electric resistivity imaging (ERI) is a geophysical technique frequently used for the characterization of shallow and deep subsoil structures. The working principles of this technique and improvements to the application advanced in the 1990s. ERI has become popular for solutions to environmental and engineering problems, such as, monitoring of subsurface flow (Daily et al. 2004).

The method is based on the inferring of vertical and/or lateral resistivity variation of the examined subsurface, and it is applied by injecting an artificial current, which is either an alternating current with a frequency less than 30 Hz or a direct current into the ground. The resistivity variation is expressed with the help of measuring the change in the electrical potential, which is a function of resistivity for a given applied current. Most of the resistivity methods are applied with four electrode measurement approach

(Figure 2-6). While two current electrodes - C1, C2 - transmit the current into the ground, the other two electrodes - P1, P2- measure the potential difference which is used to determine the apparent resistivity of the subsoil (Knödel et al. 2007).

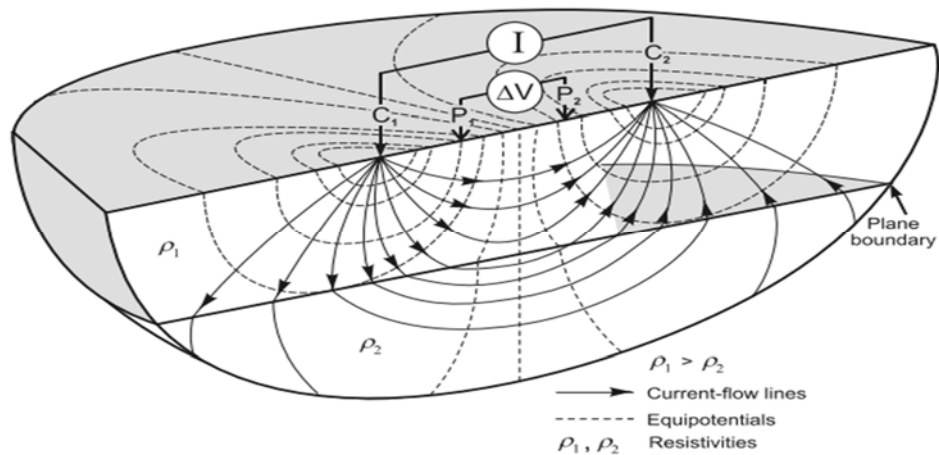


Figure 2-6 Principle of four electrode measurement approach (Knödel et al. 2007)

If a one-point electrical current source generates a direct current,  $I$ , the potential,  $V_r$ , which occurs at a distance  $r$  from the point, and the potential is expressed as follows:

$$V_r = \frac{\rho I}{2\pi r} \quad (2.7)$$

When a two-point source generates a current  $\mp I$ , the potential difference,  $\Delta V$ , occurs between the potential electrodes; i.e. four electrode geometry, and the potential difference is determined by using Equation 2.8:

$$\Delta V = \rho I \left[ \frac{1}{2\pi} \left( \frac{1}{r_1} - \frac{1}{r_2} - \frac{1}{r_3} + \frac{1}{r_4} \right) \right] \quad (2.8)$$

where  $r_1 = C_1P_1$ ,  $r_2 = C_1P_2$ ,  $r_3 = C_2P_1$ , and  $r_4 = C_2P_2$ .

If  $\left[ \frac{1}{2\pi} \left( \frac{1}{r_1} - \frac{1}{r_2} - \frac{1}{r_3} + \frac{1}{r_4} \right) \right]$  term can be defined as one parameter, it is called geometry factor or configuration factor, K. Therefore, the apparent resistivity can be calculated by using Equation 2.9 (Knödel et al. 2007):

$$\rho = K \frac{\Delta V}{I} \quad (2.9)$$

The electrodes are placed on the ground surface or in boreholes with different array combinations, some of which are shown in Figure 2-7, according to the desired precise resolution of the spatial resistivity variation and the aim of the implemented field analysis. Surface profiling, vertical sounding, azimuthal surveys and surface imaging are some of the operation types of the resistivity method (Binley and Kemna 2005).

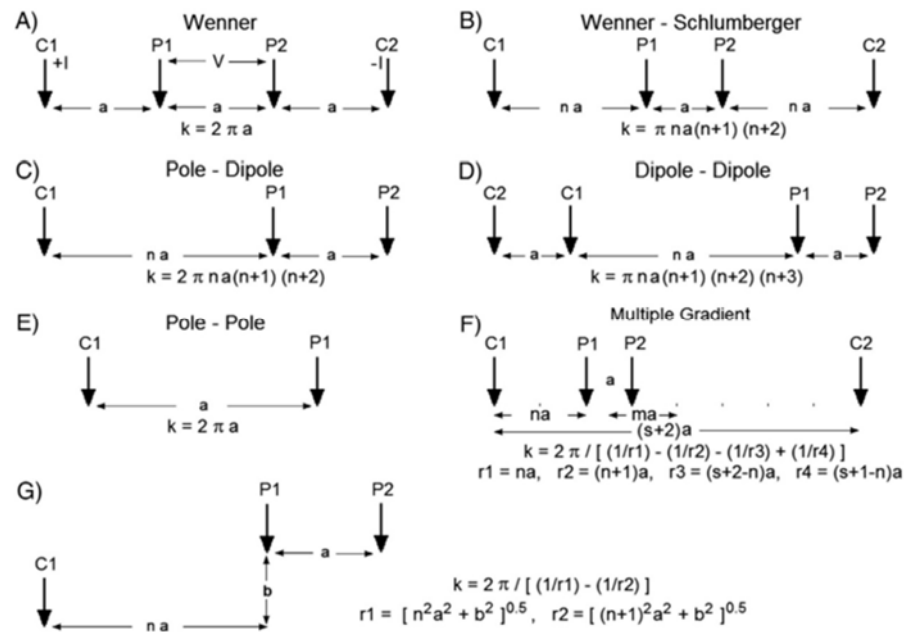


Figure 2-7 Generally applied electrode geometry and their geometric factors (Loke et al. 2013)

ERI allows the estimation of the bulk electrical conductivity, which is the reciprocal of the resistivity of the soil, at the mesoscale, and without disturbance. It is similar to other indirect methods in the respect that it employs empirical functions for the conversion of conductivity (or resistivity) data (Archie 1942; Waxman and Smits 1968). Proving to be advantageous in several respects, it has become a popular method for the estimation of soil water content and subsurface flow characterization (e.g; Binley et al. 2002; Garré et al. 2011; Kemna et al. 2002; Turesson 2006).



## CHAPTER 3

### STUDY AREA

Çakıt basin, having no water control structure in it, was selected as a study area for the TUBITAK project titled “Determination of Hydrological Cycle Parameters with a Conceptual Hydrological Model” (Project number: 115Y041). The basin is located at the south part of Turkey about 37° 22' - 37° 35' north and 34° 24' - 34°46' east. The surface area of the basin is 526 km<sup>2</sup>, and its location is given in Figure 3-1.

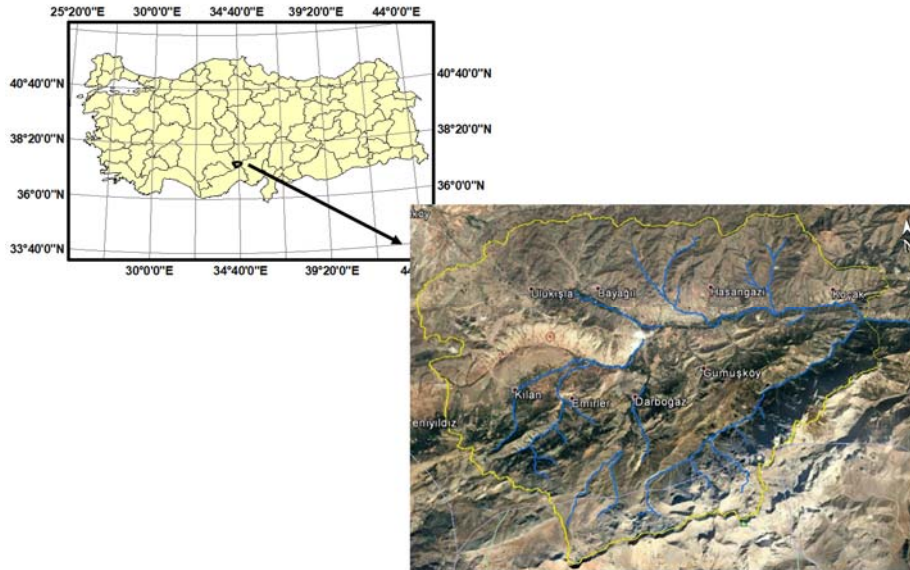


Figure 3-1 Çakıt Basin and its location in Turkey

### 3.1 Hydroclimatology of Çakıt Basin

There is a meteorological station, Ulukışla Meteorological Station, in the basin which has been operated for a long time by the General Directory of Meteorology (MGM). It is located at 37° 33' N and 34°29' E. Since it has long enough data records, the climatic features of the Çakıt catchment were obtained based on this meteorological station data.

#### 3.1.1 Temperature

According to long-term temperature data recorded between 1937 and 2017, the lowest temperature value is observed at the station as -8.3 °C, while the highest temperature value is 25.3 °C. Monthly based average temperature values are shown in Table 3-1. As seen in Table 3-1, January is the coldest month with an average temperature of -1.7 °C, July is the hottest period of the year with an average temperature of 21.6 °C. After 1990s, the temperature regime shows an increasing trend (Figure 3-2).

Table 3-1 Monthly averaged temperature values (°C)

<b>Jan</b>	<b>Feb</b>	<b>March</b>	<b>Apr</b>	<b>May</b>	<b>Jun</b>	<b>Jul</b>	<b>Aug</b>	<b>Sept</b>	<b>Oct</b>	<b>Nov</b>	<b>Dec</b>
-1.7	-0.3	3.5	8.9	13.5	18.1	21.6	21.3	16.7	10.9	5.0	0.4

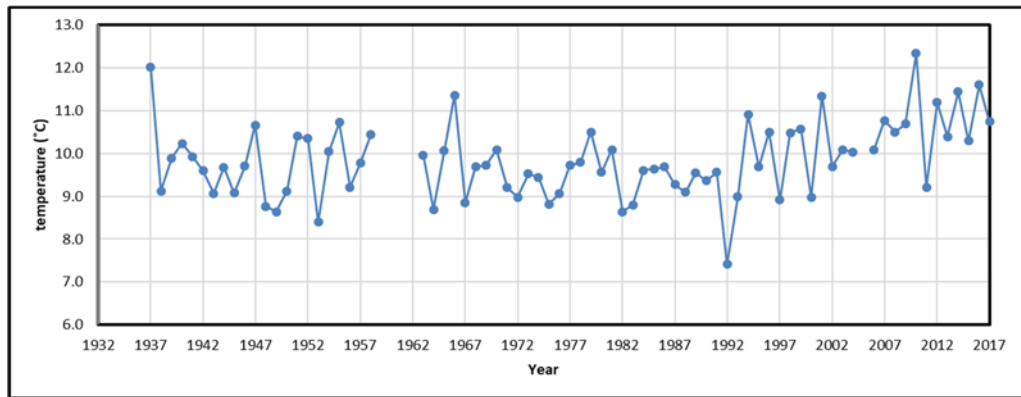


Figure 3-2 Yearly averaged temperature (°C) values

### 3.1.2 Rainfall

According to data collected between 1929 and 2017, the average annual rainfall in the basin is 332 mm which is less than average rainfall amount of Niğde, that is 341.1mm (“Meteoroloji Genel Müdürlüğü” n.d.). However, as Figure 3-3 shows there are lower values than average, especially for the last decade except for 2009, 2011 years.

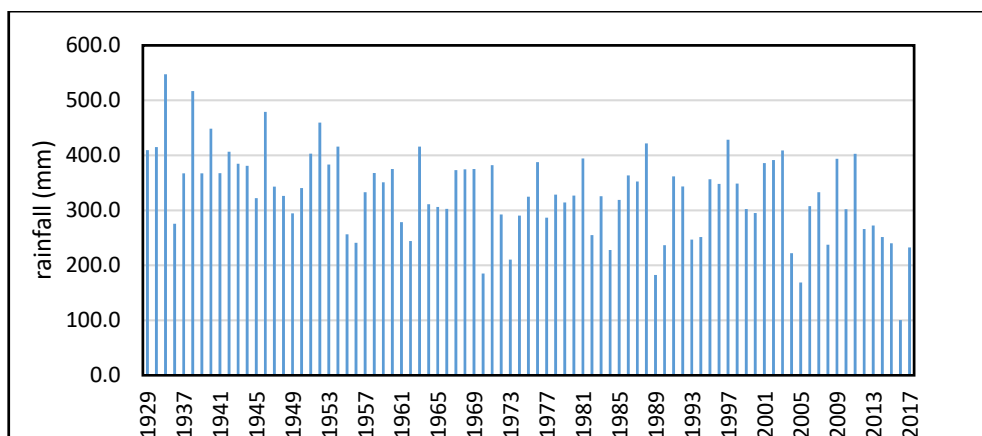


Figure 3-3 Annual total rainfall (mm) for the basin (1929-2017)

### 3.1.3 Wind and Humidity

Monthly averaged relative humidity values are summarized in Table 3-2, and these values are based on a long-term period (1975-2016).

Table 3-2 Long-term monthly averaged relative humidity values (%)

Jan	Feb	Mar	Apr	May	Jun	Jul	Aug	Sept	Oct	Nov	Dec
76.8	74.3	67.7	62.8	60.9	53.8	46.7	47.2	51.9	63.3	69.4	75.9

According to wind speed data obtained from the Ulukışla meteorological station between 1975 and 2005, the maximum wind speed was 6.1m/s and the minimum wind speed was 2.0 m/s. On the other hand, the average wind speed was 3.3 m/s. The dominant wind direction has been identified by analyzing wind direction and wind speed data: these are shown in Figure 3-4 and Figure 3-5, respectively. The analysis reveals that the dominant wind direction is East-South-East (ESE) with a wind speed of 21.1 m/s.

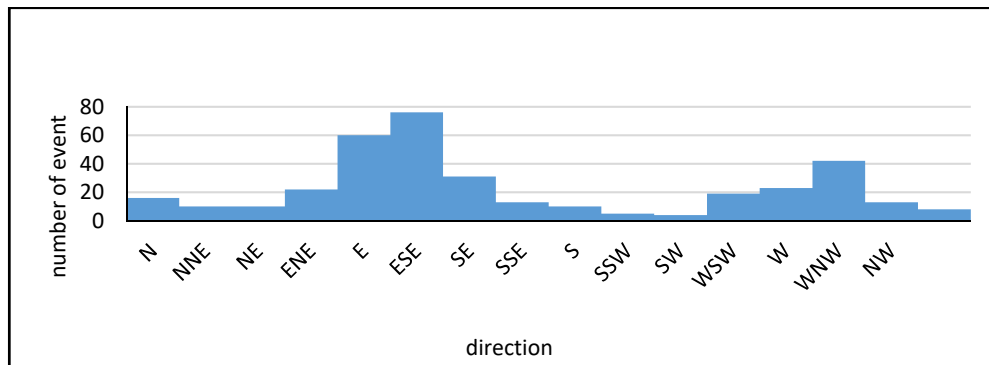


Figure 3-4 General wind direction densities for Ulukışla Meteorological station

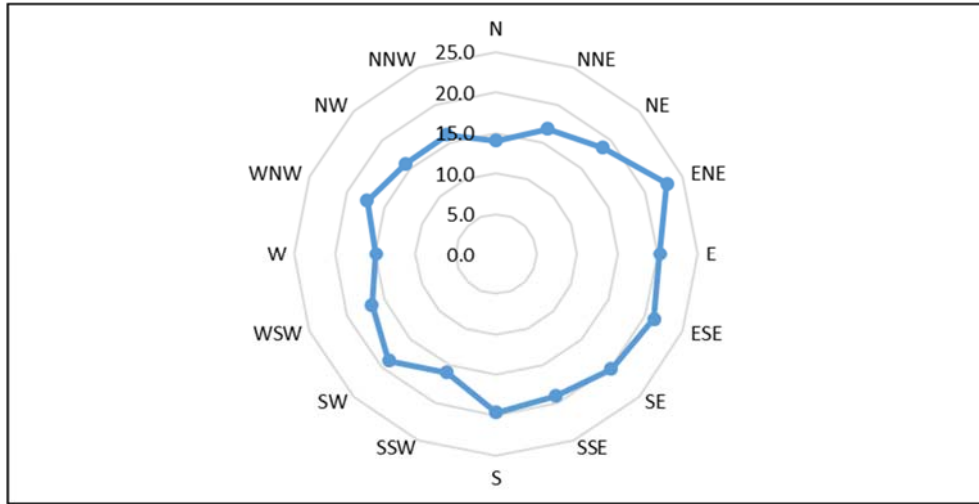


Figure 3-5 Wind directions and average speed (m/s) values for Ulukışla Meteorological Station

### 3.2 Topographical Characteristics of Çakıt Basin

Within the boundaries of the Çakıt Basin, the highest elevation is approximately 3450m, and the lowest elevation is 963 m. While the mean elevation is 1727 m, the median elevation value is 1600 m. These elevation values have been obtained from digital elevation model (DEM) of the Çakıt Basin. The hypsometric curve of the Çakıt catchment has been generated with the help of ArcGIS software (Figure 3-6): the DEM and instrumentation of the Çakıt Basin is shown in Figure 3-7.

A Cosmic Ray Sensor (CRS) and CS-616 water content reflectometer which is a part of an Eddy covariance open path system were installed at an elevation of 1459 m and 1464m, respectively. The CRS measurement area, the footprint, is around 0.28 km<sup>2</sup> (Figure 3-7).

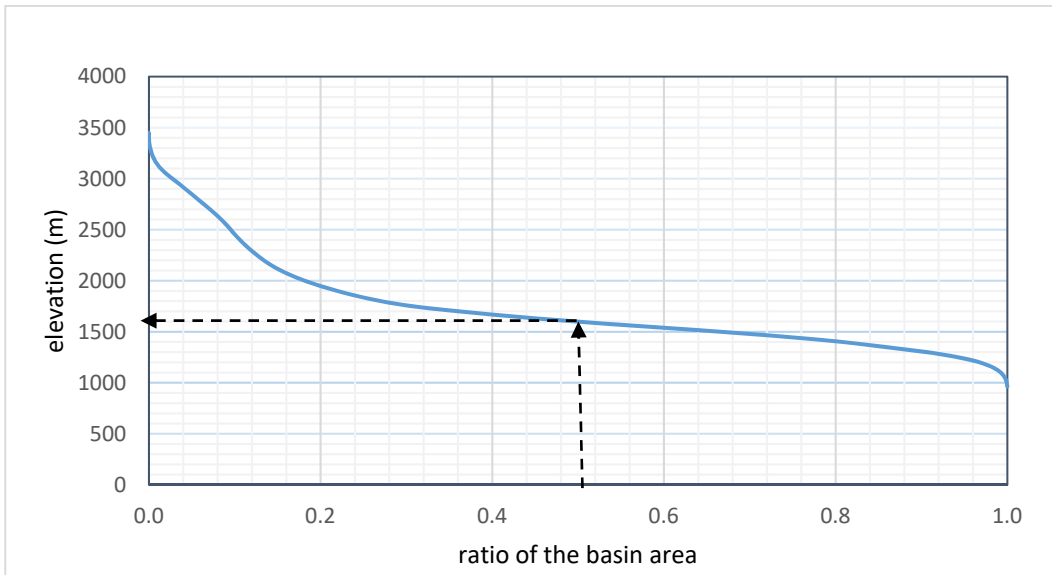


Figure 3-6 Hypsometric curve of Çakıt Basin

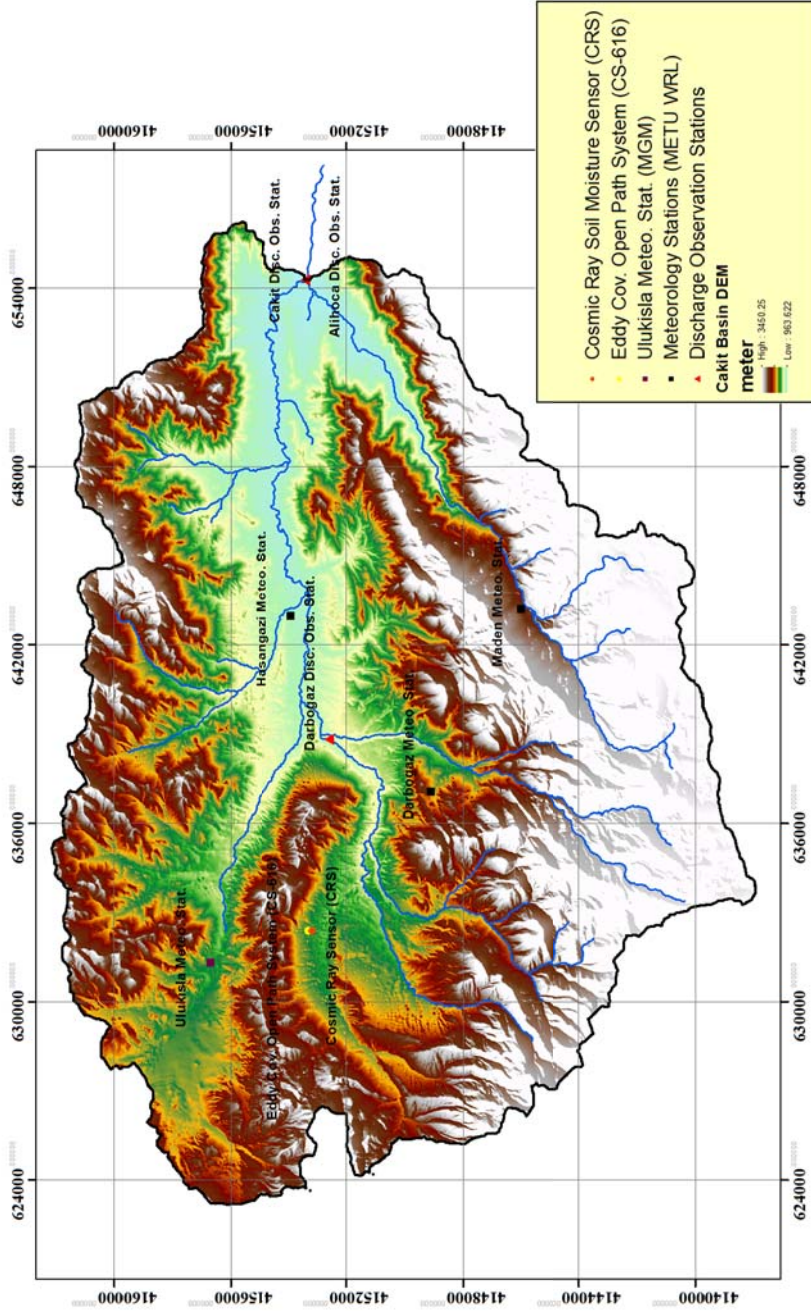


Figure 3-7 DEM and instrumentation of Çakıt Basin

Soil type data obtained from the State Hydraulic Works (DSI) indicates the common soil type in the Çakıt catchment is brown forest soil (Figure 3-8). However, the CRS footprint area has a colluvial soil type.

The CORINE database was used to retrieve land cover information. Natural vegetation covers the bulk of the Çakıt basin surface area and, the studied sub-area which is measurement area of the CRS. Moreover, agricultural lands and fruit trees have 3% of the whole surface area. Land use details are shown in Figure 3-9.

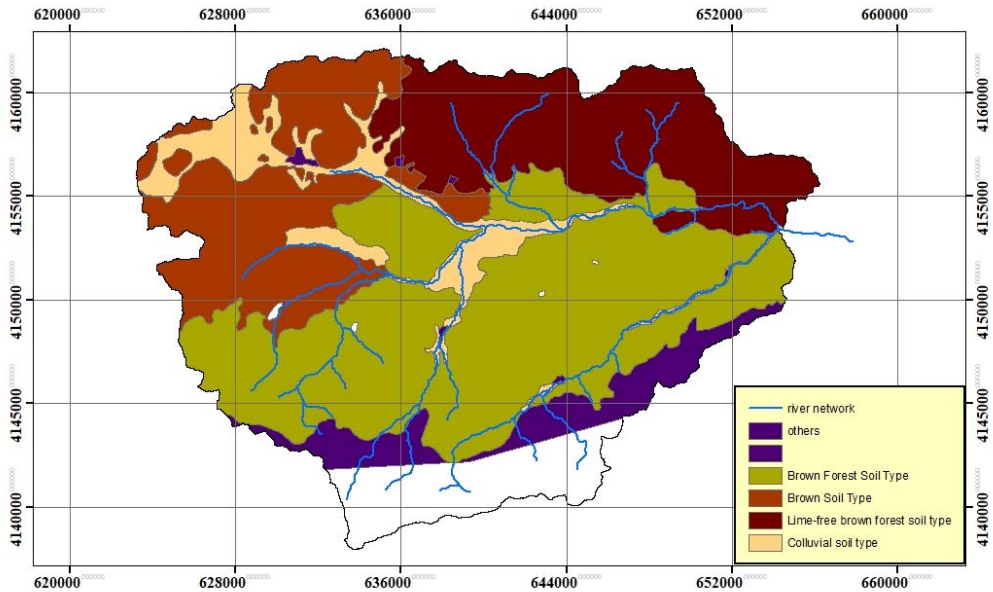


Figure 3-8 Soil types in Çakıt Basin

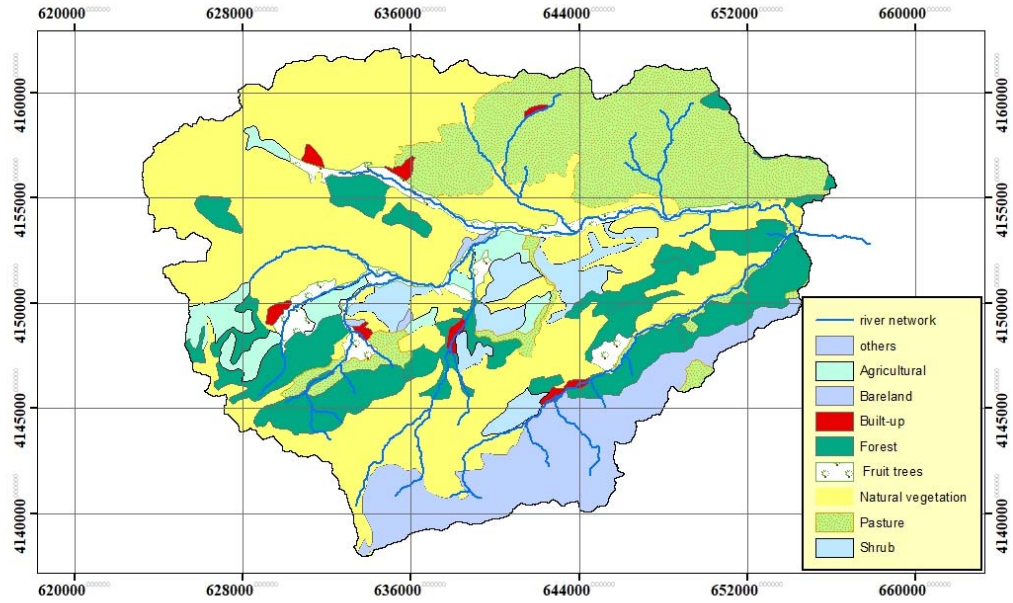


Figure 3-9 Land use cover in Çakıt Basin

The Çakıt Basin has a complex geological formation, since its soil structure contains many different formation types, but the CRS measurement area has mainly sandstone-chalk formation. The geological formation of the catchment is shown in Figure 3-10: this information was obtained from the General Directorate of Mineral Research and Explorations (MTA). Additionally, hydrogeological information of the basin (Figure 3-11) reveals larger aquifers in the basin (Seyhan Basin Master Plan report).

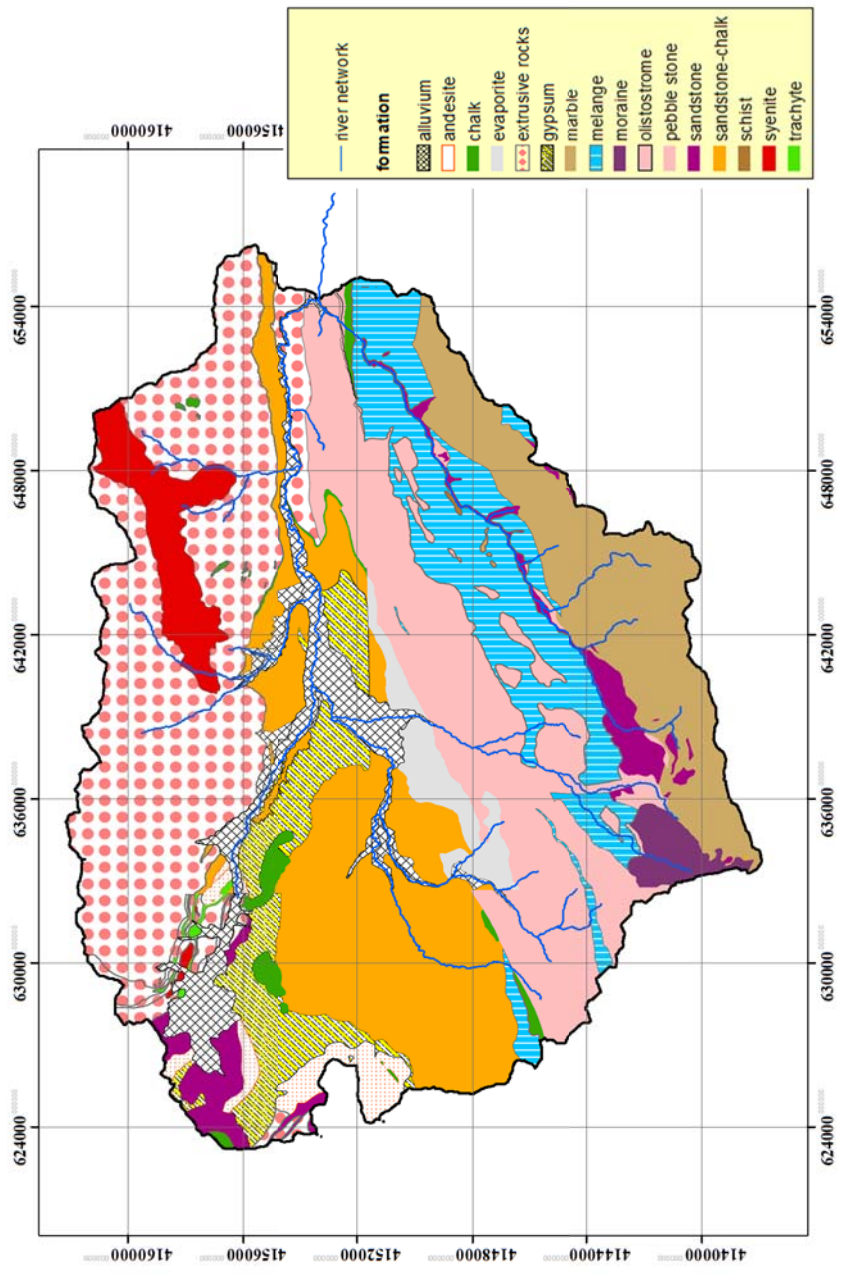


Figure 3-10 Geological map of Çakıt basin

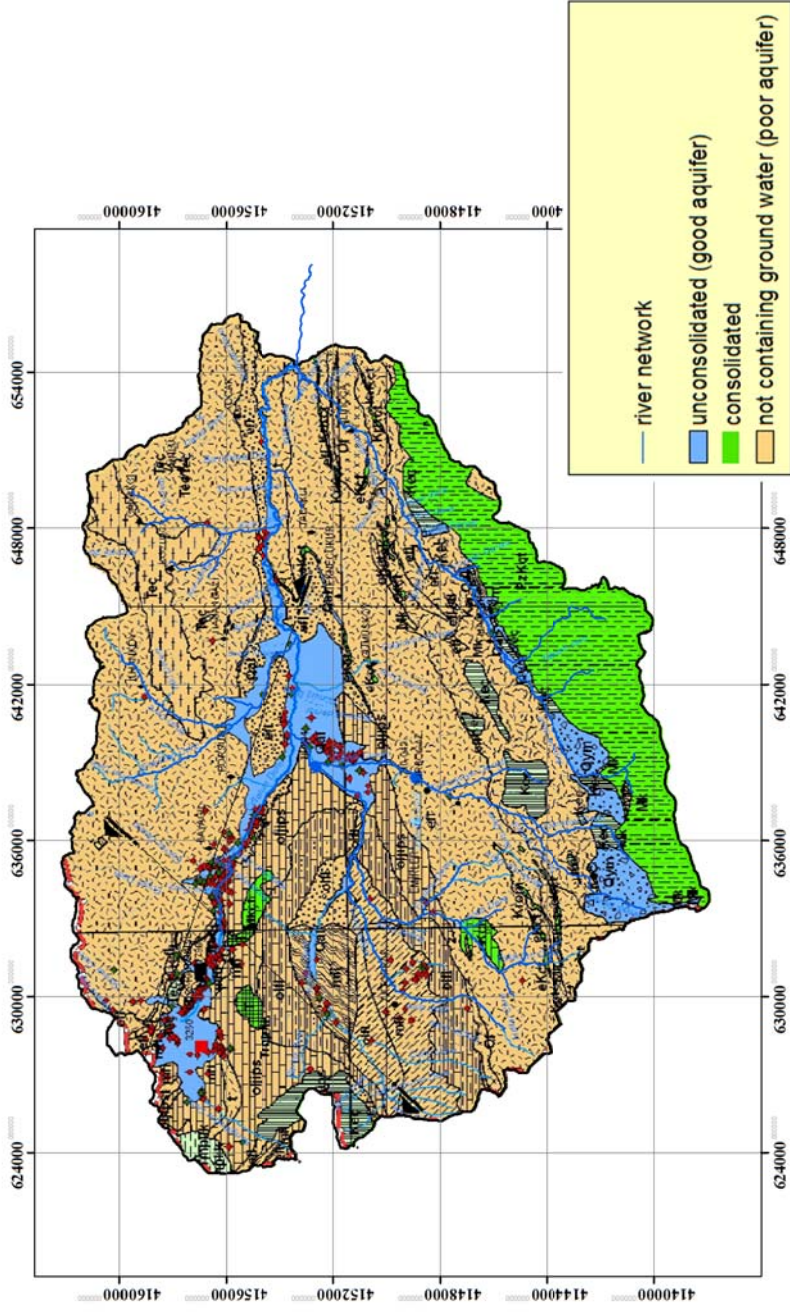


Figure 3-11 Hydrogeological formation of Çakıt basin



## CHAPTER 4

### SOIL MOISTURE MEASUREMENTS

In this study, soil moisture was measured by using a range of techniques spanning different spatial scales. The methods used are cosmic-ray soil moisture sensor (CRS), water content reflectometry and electrical resistivity imaging (ERI).

#### 4.1 Cosmic-ray Soil Moisture Sensor (CRS)

A Cosmic-ray soil moisture sensor (CRS) system was installed at the elevation of 1459 m in Çakıt basin. The system is passive, non-invasive and based on the indirect cosmic-ray method, and it using a natural radiation source, cosmic rays. The operation principle of the system is based on measuring neutron intensity, which is inversely proportional to the amount of the existing water near the land surface, and other hydrogen sources such as water in or on vegetation, and this is explained in Section 2.2.6 in detail. Therefore, due to the impact of hydrogen sources it was located far away from the river network and more densely vegetated part of the basin.

The installed system consists of one bare and one moderated neutron counter, and a relative humidity and a temperature sensor. It is a product of Hydroinnova LLC and has the product name CRS 2000/B (Figure 4-1). This system detects the neutron density within a footprint which has a lateral radius of around 300 m. In other words, the system measurement covers approximately 0.28 km<sup>2</sup> plan area, and the conversion of the measurement provides an area - averaged soil moisture value.



Figure 4-1 Cosmic-ray soil moisture sensor system (CRS 2000/B)

#### 4.1.1 Correction Procedure

Environmental factors affect the CRS neutron count measurements; hence, to obtain the relationship between soil moisture and site-specific neutron density data clearly, a correction procedure is a requirement for neutron counts. Atmospheric pressure, atmospheric water vapor and the incoming neutron flux are the main environmental factors, and measurements must be modified according to these factors.

Neutron counts can be corrected for changes in atmospheric pressure by using Equation 4.1 shown below:

$$f_p = \exp[\beta(P - P_{ref})] \quad (4.1)$$

where  $P$  is atmospheric pressure (mb), and  $P_{\text{ref}}$  is the reference atmospheric pressure (mb), which is 1013.25 hPa at the sea level,  $\beta$  is the atmospheric attenuation coefficient ( $\text{cm}^2/\text{g}$  or  $1/\text{mb}$ ) for neutron generating cosmic rays (Hawdon et al. 2014).  $\beta$  is taken as  $0.0077 \text{ hPa}^{-1}$  in this study.

Water vapor is another hydrogen reserve, so it is capable of thermalizing fast neutrons efficiently similar to the way soil water content does. Its effect should be accounted for and removed from the measurement. The water vapor correction factor can be calculated by using Equation 4.2, which is developed by Rosolem et al. (2013).

$$f_{\text{wv}} = 1 + 0.0054(p_{\text{v}0} - p_{\text{v}0}^{\text{ref}}) \quad (4.2)$$

where  $f_{\text{wv}}$  is the correction factor for water vapor pressure variation,  $p_{\text{v}0}^{\text{ref}}$  is the reference absolute humidity, and  $p_{\text{v}0}$  is absolute humidity at the surface.

Variation of solar activity leads to changes in the incoming neutron flux density. The solar activity is observed by cosmic ray neutron monitors, which only measure high-energy secondary neutrons, and are placed all around the world (Simpson 2000). This measurement is used for calculating the intensity correction factor. The correction factor can be described as shown in Equation 4.3 (Zreda et al. 2012).

$$f_i = \frac{I_m}{I_{\text{ref}}} \quad (4.3)$$

where  $f_i$  is the correction factor for the incoming neutron intensity,  $I_m$  is the selected neutron monitor measurement at any specific point in time, and  $I_{\text{ref}}$  is a reference counting rate for the same neutron monitor from an arbitrary fixed point in time.

Geomagnetic field variation, which changes spatially, influences the incoming neutron flux intensity, since geomagnetic field strength, expressed by vertical cutoff rigidity ( $R_c$ ), controls the minimum energy that a cosmic particle requires to penetrate the

Earth's magnetic field (Desilets and Zreda 2003). For that reason, the neutron flux intensity should be normalized with respect to the geographical location; in other words, it should be corrected with site-specific  $R_c$  values.

In this study, the neutron flux has been corrected according to the atmospheric pressure, atmospheric water vapor and the Neutron Monitor Data Base (NMDB). The monitor located in Athens, Greece was selected for the incoming neutron intensity correction procedures, due to it having the closest cutoff rigidity of the installed CRS, which is approximately 8.5 GV (Athanasios 2008).

#### 4.1.2 Conversion of Corrected Neutron Flux to Soil Moisture

The cosmic ray probe is an indirect sensor for obtaining soil moisture data, and the measured CRS data must be converted to soil moisture data by using calibration functions.

The site specific-shape defining function, i.e. the  $N_0$  method, was improved by Desilets et al. (2010) to obtain the soil moisture data from the counted neutron flux. This method describes the relationship between the locally calibrated and normalized fast neutron counts and soil water content. It has been calibrated with the Monte Carlo Neutron-Particle eXtended model (MCNPx). Volumetric water content is retrieved directly from the corrected neutron flux by using Equation 4.4 (Baatz et al. 2014).

$$\theta (N) = \frac{a_0 \times \rho_{bd}}{\left(\frac{N}{N_0}\right)^{-a_1}} - (a_2 \times \rho_{bd}) \quad (4.4)$$

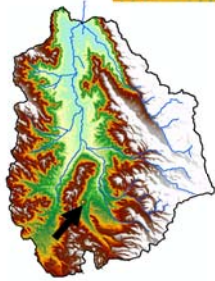
where  $\theta$  is volumetric water content,  $N$  is fast neutron intensity, which is corrected for changes in atmospheric pressure, atmospheric water vapor and incoming neutron intensity,  $N_0$  is the neutron intensity in the air above dry soil at the same reference conditions,  $\rho_{bd}$  is oven dry bulk density ( $\text{g}/\text{cm}^3$ ), and  $a_0, a_1, a_2$  are fitting parameters that characterize the shape of the calibration function. These dimensionless parameters

were determined as;  $a_0 = 0.0808$ ,  $a_1 = 0.372$ ,  $a_2 = 0.115$  from MCNPX calculations. It is assumed that these parameters are constant in time, and valid for soils with different chemical compositions (Desilets et al. 2010; Zreda et al. 2008).

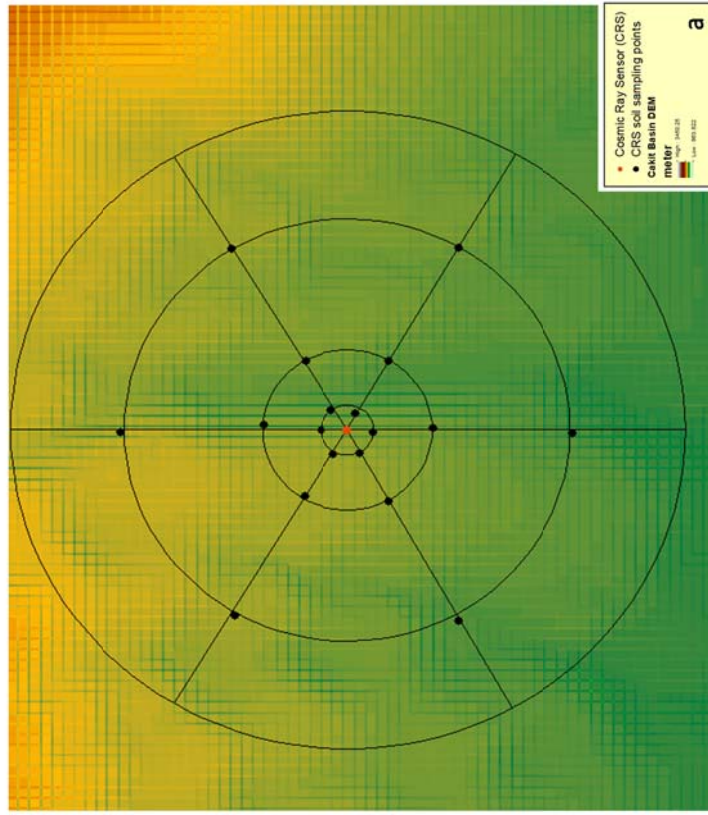
The  $N_0$  method is commonly used method due to its straight-forward applicability and simple computability (e.g.; Bogena et al. 2013; Franz et al. 2012). However,  $N_0$  method requires field calibration which demands intensive soil sampling from the field, since it is found out by using the weighted mean total gravimetric soil water content. Therefore, the method depends on the measurement area physical properties.

#### **4.1.3 Field Calibration and Soil Properties**

Undisturbed soil samples were collected from the CRS footprint on 2-4 December, 2016. This samplings was conducted in order to calibrate the CRS, and to obtain soil properties of the study area. The Cosmic-ray Soil Moisture Observing System, COSMOS (Zreda et al. 2012) soil sampling scheme was followed in this study. Even though this sampling needs extensive field work, it has been conducted by many researchers (e.g. Baatz et al. 2014; Bogena et al. 2013). Soil samples were taken from 18 different locations, and at six depths ranging from 0 to 30 cm with 5 cm increments, i.e. 108 total undisturbed soil samples. The sample points were located at six radial directions, and at distances 25, 75 and 200 m away from the CRS. Metal rings, 5 cm in height and 5 cm in diameter, were used to collect samples in the field (Figure 4-2).



Sample points locations



Soil sampling



Figure 4-2 Sample point locations (a) and soil sampling procedure (b, c)

These soil samples were analyzed in METU Civil Engineering Department, Soil Mechanics Laboratory with the method of sieving and hydrometer analysis to obtain soil particle size distribution and clay content as stated in ASTM D 6913/ D6913M-17 (2017) standard.

Table 4-1 shows the soil properties of the sampled locations. Moreover, water content ( $w_n$ ), bulk density ( $\rho_b$ ) and specific gravity ( $G_s$ ) values were estimated by gravimetric methods. Volumetric water content ( $\theta$ ), void ratio ( $e$ ) and porosity ( $\phi$ ) values were calculated by using soil phase relationships which are shown below:

$$\rho_{\text{bulk}} = \frac{\text{Total mass of the soil, } \Sigma M}{\text{Total volume of the soil, } \Sigma V} \quad (4.5)$$

$$w_n = \frac{\text{Mass of water, } M_w}{\text{Mass of solids, } M_s} \quad (4.6)$$

$$\rho_{\text{dry bulk}} = \frac{\rho_{\text{bulk}}}{1+w} \quad (4.7)$$

$$\theta = \frac{\text{volume of water}}{\text{total volume of soil}} = w_n \frac{\rho_{\text{dry bulk}}}{\rho_{\text{water}}} \quad (4.8)$$

$$G_s = \frac{\text{the solid particle density}}{\text{the water density, } \rho_w} \quad (4.9)$$

$$\phi = \frac{e}{1+e} \quad (4.10)$$

Soil texture classification was carried out according to a scheme developed by the U.S. Department of Agriculture, and it is shown in Figure 4-3.

Table 4-1 CRS footprint soil properties

Sample	$\rho_{\text{bulk}}$ (g/cm <sup>3</sup> )	$G_s$	$w_n$ (%)	$\rho_{\text{dry bulk}}$ (g/cm <sup>3</sup> )	$\theta$ (%)	$D_{50}$ (mm)	Clay content (%)	Soil Texture	$e$	$\phi$
1	1.49	2.69	18.04	1.26	22.7	0.006	34.5	SCL	1.13	0.53
2	1.55	2.7	15.39	1.34	20.6	0.006	36	SCL	1.02	0.5
3	1.48	2.71	13.16	1.31	17.2	0.013	22	SL	1.08	0.52
4	1.43	2.68	16.56	1.23	20.3	0.05	18.5	L	1.19	0.54
5	1.48	2.67	17.99	1.25	22.5	0.024	22	SL	1.13	0.53
6	1.44	2.69	16.09	1.24	19.9	0.015	23.5	SL	1.17	0.54
7	1.41	2.7	18.84	1.19	22.4	0.006	35.5	C	1.27	0.56
8	1.42	2.74	9.04	1.31	11.9	0.0525	6.5	SL	1.10	0.52
9	1.72	2.7	10.24	1.56	16	0.07	10	L	0.73	0.42
10	1.54	2.69	17.63	1.31	23.2	0.018	12	SL	1.05	0.51
11	1.39	2.58	11.37	1.25	14.2	0.256	20.5	SL	1.07	0.52
12	1.39	2.66	12.01	1.24	14.8	0.03	18.25	SL	1.14	0.53
13	1.49	2.69	20.24	1.24	25	0.0048	33	SCL	1.18	0.54
14	1.46	2.67	14.19	1.28	18.2	0.006	31	SCL	1.09	0.52
15	1.54	2.64	13.33	1.35	18.1	0.0178	24	SL	0.95	0.49
16	1.47	2.71	13.38	1.3	17.3	0.0108	32	C	1.09	0.52
17	1.59	2.71	12.97	1.41	18.3	0.013	23	SL	0.92	0.48
18	1.62	2.7	15.73	1.4	22.1	0.0037	39	SCL	0.92	0.48

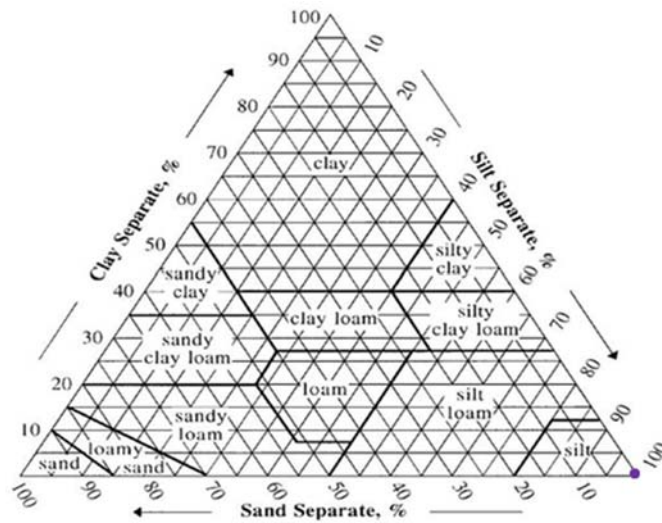


Figure 4-3 Soil texture triangle, USDA

The sampling shows that the average gravimetric water content of the footprint is 0.148 g/g at the specified dates, and the dry bulk density is 1.304 g/cm<sup>3</sup>; from Equation 4.4  $N_0$  is determined as 1440.6.

#### 4.1.4 Volumetric Soil Moisture Data from CRS

The COSMOS project research revealed that the previously mentioned field calibration of the CRS provides a long-term calibration stability of more than 4.5 years. Because vegetation includes a smaller amount of hydrogen, and the vegetation density changes seasonally, the effect of the vegetation in the retrieved data is not significant, and it already had been taken into consideration in the field calibration procedure (Zreda et al. 2012).

The installed CRS measures hourly neutron intensity values, and the real-time soil moisture data has been obtained since November 2016. In Çakıt basin, there are four meteorological stations (Figure 3-7) and rainfall data were used for indicating the variations in CRS measurements with respect to rainfall (Figure 4-4). Since the CRS measurement is sensitive to other hydrogen reserves, in winter times, the

measurements did not reflect the correct soil moisture distribution, due to snow cover in the area. Its influence was observed particularly for, the data obtained for dates between 30.12.2016 to 21.02.2017. The average air temperature was measured as  $-3.23\text{ }^{\circ}\text{C}$  and the average snow depth was recorded as 67.5 cm at the nearby meteorological station for this duration. It is obvious that this significant amount of the snow influence was noticeable in the CRS measurements; the deduced soil moisture data were abruptly increased to values which are higher than 60% at these dates. These moisture data were dominated by the snow cover are shown with the red circle in Figure 4-4.

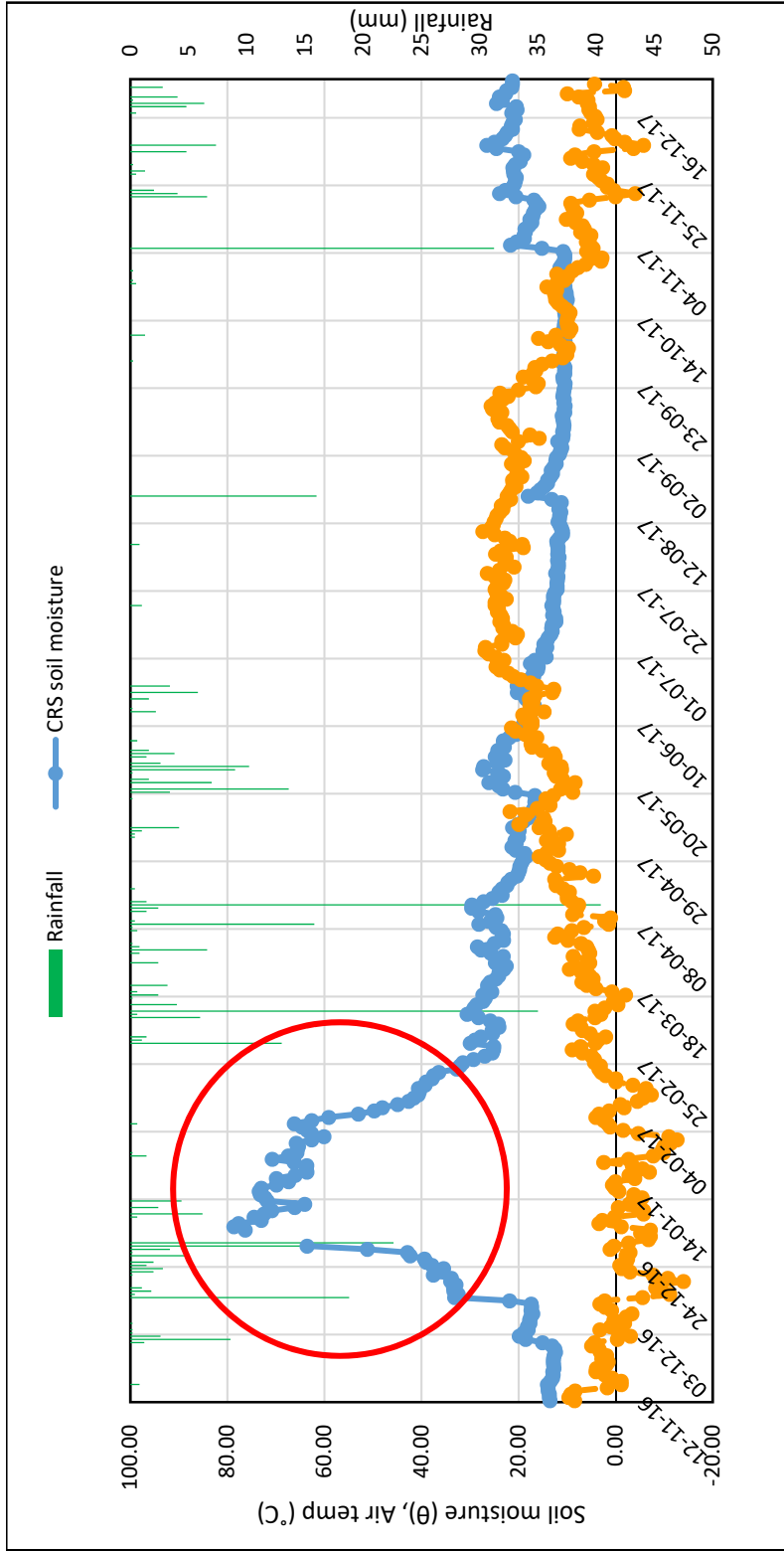


Figure 4-4 Rainfall, air temperature, the CRS soil moisture data

## 4.2 Installed Water Content Reflectometry (CS-616)

A water content reflectometer, four soil temperature probes and one heat flux plate (as a part of Eddy Covariance Open Path System, Figure 3-7) were installed at an elevation of 1464 m in the CRS measurement area for acquiring point-scaled soil moisture data, continuously. These devices are manufactured by Campbell Scientific, Inc., and their product names are CS-616, TCAV Averaging Soil Thermocouple Probe, and HFP01 Soil Heat Flux Plate, specifically. While CS-616 detects soil water fluxes for 2.5 cm depth, temperature probes provide average soil temperature data for 2 cm and 6 cm depth. Moreover, the heat flux plate was buried at a depth of 8 cm (Figure 4-5)

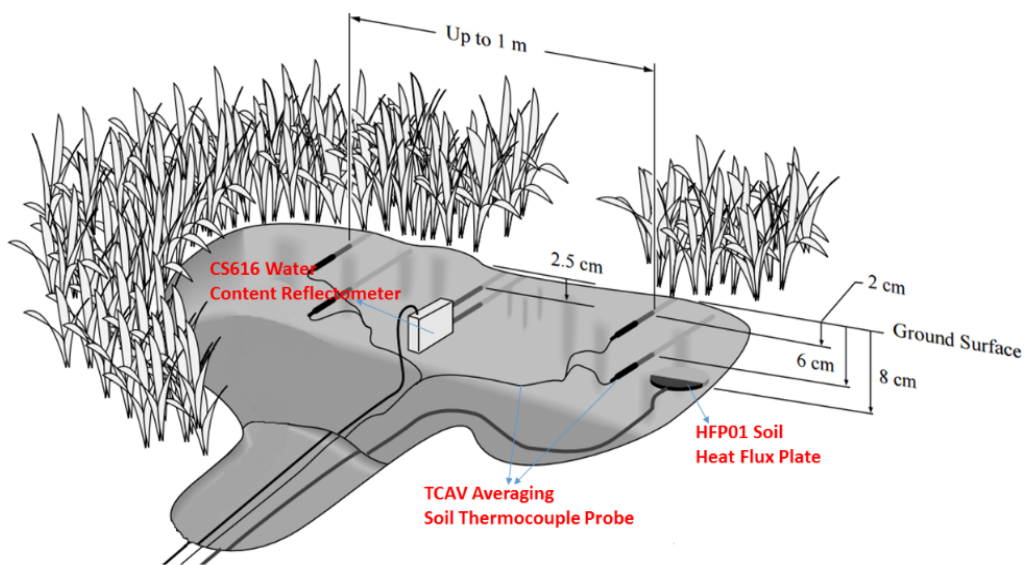


Figure 4-5 Installation scheme for water content reflectometer, soil temperature probes and heat flux installation scheme

The CS-616 consists of two stainless steel rods, which are placed with 3.2 cm spacing, and an epoxy encapsulated circuit board. These rods are 30 cm in length and 0.32 cm in diameter (Figure 4-6).

The main working principle of the soil moisture sensor is that an electromagnetic pulse is propagated along the steel rods, and the propagation velocity is dependent on dielectric permittivity details are explained in Section 2.2.5. As water has the highest dielectric permittivity among all soil components, the CS-616 is sensitive to changes in soil water content. The travel time of the electromagnetic pulse between two rods is the main measurement. In other words, this soil moisture sensor does not measure soil moisture directly; instead, it measures the travel time period, and the moisture value is calculated by the default standard second-degree calibration equation (Equation 4.11).

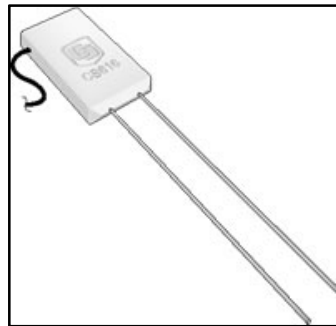


Figure 4-6 Water content reflectometer, CS-616

It is known that the soil moisture sensor should be calibrated specifically for the in-situ soil type of interest (Varble and Chávez 2011). In this study, laboratory calibration was performed to obtain more accurate point-scaled, continuous soil moisture data.

#### **4.2.1 Laboratory Calibration Procedure of CS-616**

The water content reflectometer was calibrated specifically for the soil type under investigation, and for the calibration, a disturbed soil sample was collected from the field.

#### **4.2.1.1 Materials Used in the Lab Calibration**

- Data logger connected to CS-616 to show the measured time period and default calculated volumetric water content
- No.4 Sieve
- PVC specimen container, with the dimensions of 10 cm diameter and 35 cm height
- Special sub-sample container
- Precision balances
- Oven at 105°C and 450 °C

#### **4.2.1.2 Calibration Procedure**

The collected soil samples were passed through a 4.75 mm sieve (No.4 sieve according to the ASTM D 6913/ D6913M-17 (2017) standard) and after that it was oven-dried at 105°C for 24 hours. This fully dried soil sample was mixed with water gradually until it reached its liquid limits. In other words, the sample was wetted with a certain amount of water and the application was stopped when the sample has reached to plastic behavior. At each wetting stage, water has been mixed homogenously, and a PVC specimen container has been filled with the unsaturated soil sample (Figure 4-7). This specimen has 1.3 g/cm<sup>3</sup>, which is less than the limit bulk density value for operating CS-616 successfully. The measurement of bulk density at each stage and the filling procedure was carried out with three compaction steps. In addition, at these stages, CS-616 measurements were conducted, and the sub-soil was taken, individually. These sub-samples were oven dried at 105°C for 24 hours, in this way wet and dried sub-sample mass is known. As a result, the gravimetric water content, and by using the specified bulk density volumetric water content values were calculated. Since the working principle of CS-616 is based on the return period of the electromagnetic wave, at each step, the duration of the time period of the measurement was obtained.



Figure 4-7 Homogeneously wetting (a), CS-616 measurement (b)

This laboratory procedure was conducted at nine stages. Table 4-2 summarizes the results from these nine stage. It is obvious that there is an oscillating difference between calculated and measured volumetric water content values.

Calculated water content values and measured return time period values were plotted together - see Figure 4-8. This plot was used to update the standard calibration equation, Equation 4.11, of the CS-616 with change in constants specifically, and the calibration equation was calculated and it is given in Equation 4.12. Figure 4-9 demonstrates standard and calibration equation curves.

$$\theta = +0.0007 \times \text{period}^2 - 0.0063 \times \text{period} - 0.0663 \quad (4.11)$$

$$\theta = -0.0016 \times \text{period}^2 + 0.1031 \times \text{period} - 1.2939 \quad (4.12)$$

Table 4-2 Calibration values of the CS-616

Sub-Sample	m <sub>oven-dry</sub> (gram)	m <sub>water</sub> (gram)	Volumetric Water Content (%)	Direct CS-616 Reading (%)
1	119.12	2.14	2.29	3.86
2	110.93	3.73	4.23	6.25
3	94.33	7.35	9.39	9.15
4	181.68	32.38	19.66	12.52
5	168.64	39.96	24.89	20.26
6	168.88	45.74	27.70	26.16
7	97.42	27.55	28.65	24.17
8	179.03	51.99	29.25	33.43
9	113.24	36.58	31.73	50.88

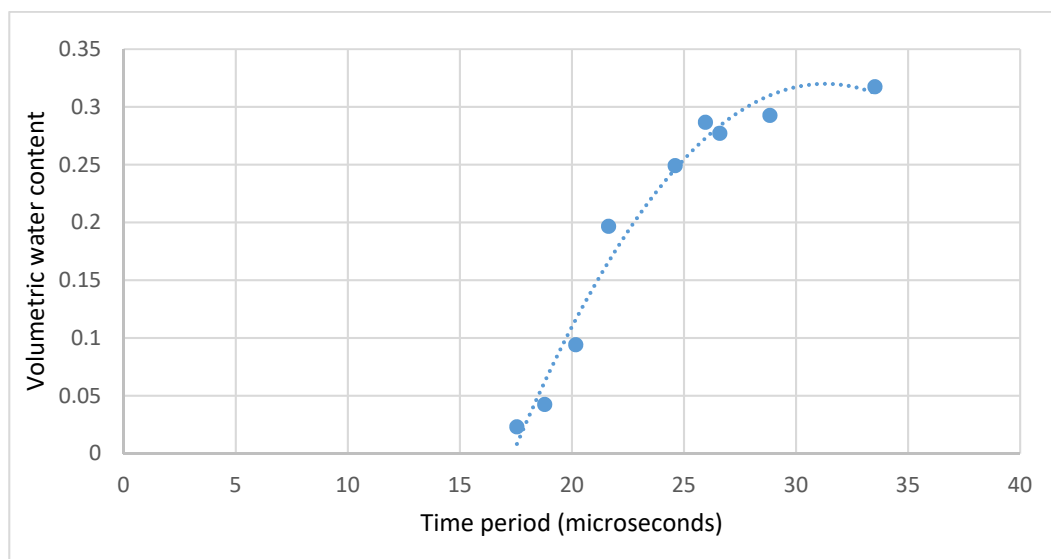


Figure 4-8 Calibration equation of the installed CS-616

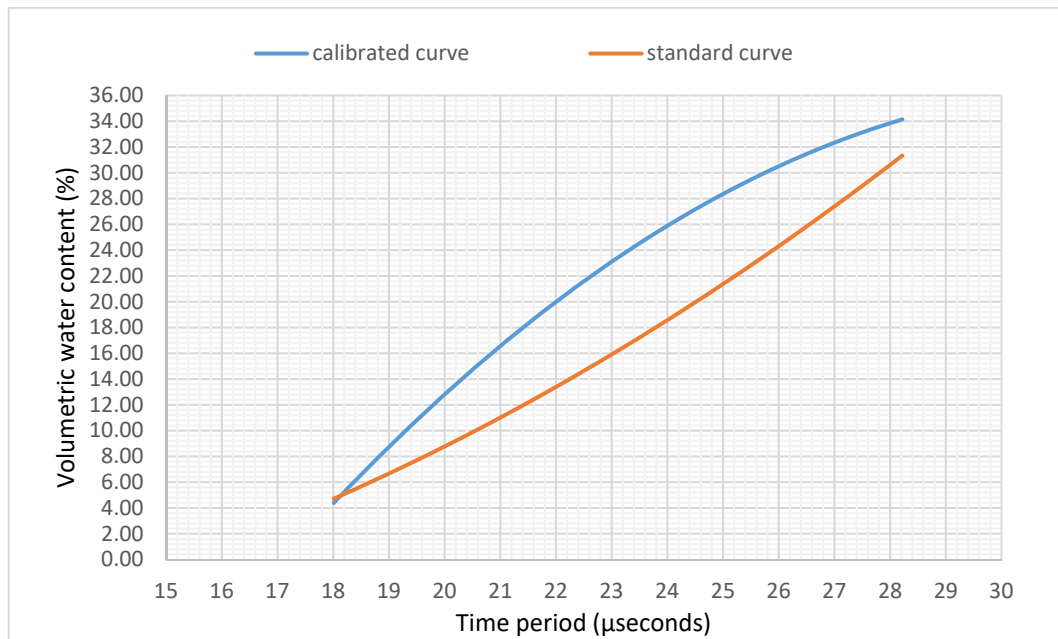


Figure 4-9 The site-specific calibration and the standard curves of the CS-616

Organic matter has an impact on the performance of CS-616 measurement due to the possibility that it might be highly polar. That means it affects travel time periods directly. In this study, gravimetric organic content was obtained. To do this, two sub-samples were oven-dried at 105°C for 24 hours, after that they were kept at 405 °C for more than one hour (ASTM D 2974 2014). Therefore, organic contents were calculated gravimetrically for each sub-sample, and their average was the organic content of the in-situ soil, that is 3.074%. The organic matter percentage is quite small, hence its effects can be ignored.

It is known that the CS-616 measurement is sensitive to changes in soil temperature, so it should be corrected according to the temperature (Varble and Chávez 2011). In this study, the water content reflectometer was installed with soil temperature probes which provide continuous, real time temperature data with the same measurement interval. The correction was carried out by using Equation 4.13.

$$\tau_c(T_{\text{soil}})=\tau_{\text{uc}}+(20-T_{\text{soil}})*(0.526-0.052*\tau_{\text{uc}}+0.00136*\tau_{\text{uc}}^2) \quad (4.13)$$

where  $T_{\text{soil}}$  is the soil temperature,  $\tau_{\text{uc}}$  is the standard time period and  $\tau_c$  is the corrected time period.

#### **4.2.2 Volumetric Soil Moisture Data from the CS-616**

When the corrected time period values are calculated by using Equation 4.13 and these values are inserted into the calibration equation (Equation 4.12), more reliable soil moisture data have been obtained from the CS-616. Retrieved data from the CS-616 for a year is shown in Figure 4-10. The default measurement data underestimates the soil moisture variation and the difference between the calibrated-corrected data and the uncalibrated measurements is more obvious at higher soil temperature values.

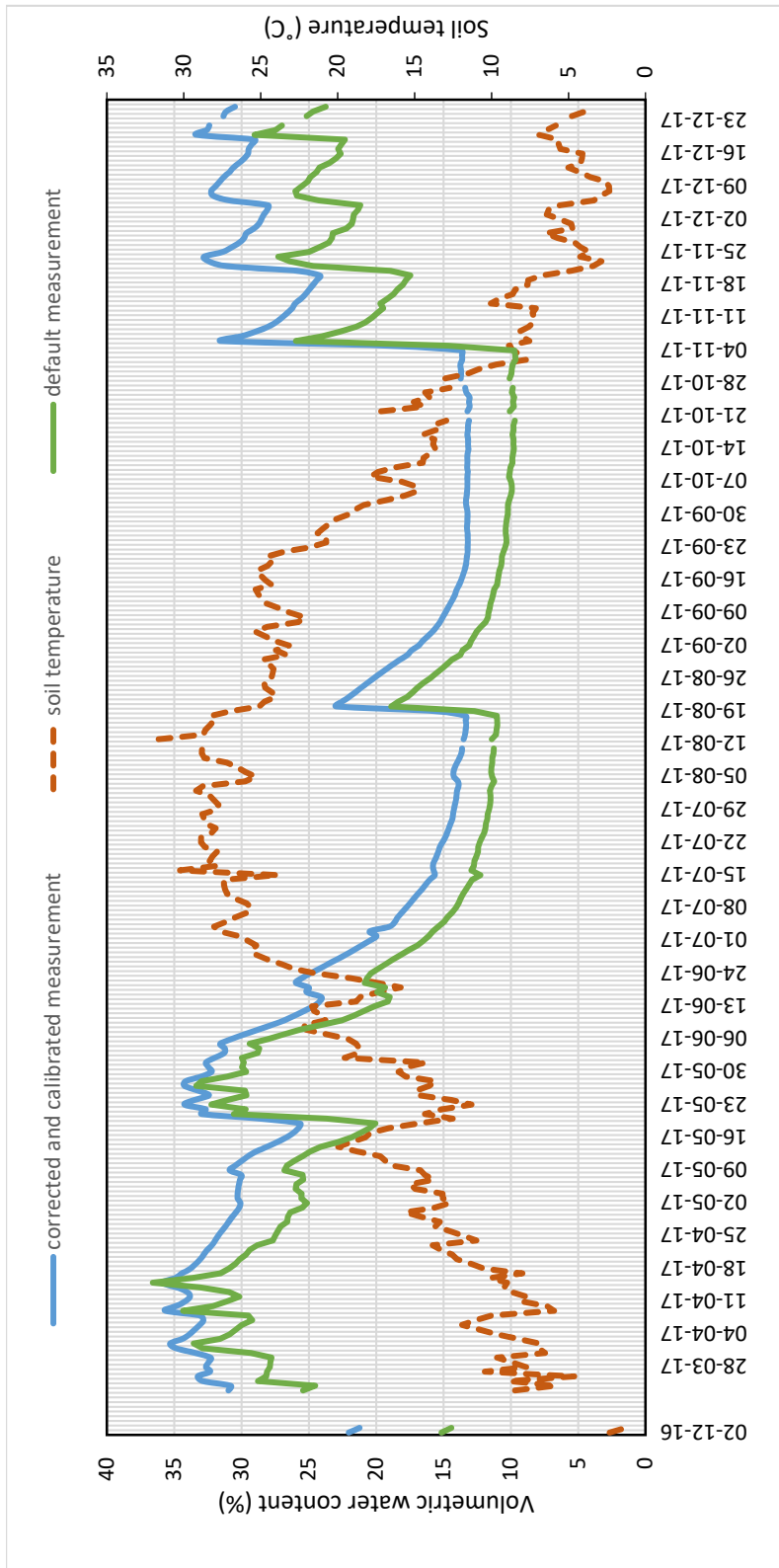


Figure 4-10 The CS-616 default data, corrected and calibrated data

### 4.3 Electrical Resistivity Imaging (ERI) and Frequency Domain Reflectometry (FDR) Data Acquisition

Electrical resistivity imaging (ERI) is a geophysical method commonly used for hydrological characterization of the subsurface, and its details are explained in Section 2.2.7. In this study, this technique was used for estimating water content variation in a 2-D shallow unsaturated zone within the footprint of the CRS, and to do this a field campaign was conducted in August 2017.

Ares – Automatic Resistivity System, which is the product of GF Instruments, and an intelligent cable with 40 stainless steel electrodes were used for resistivity surveys in the field (Figure 4-11). The system features provide 2D/3D multi-electrode resistivity with the current up to 5.0 A and 20M $\Omega$  input impedance.

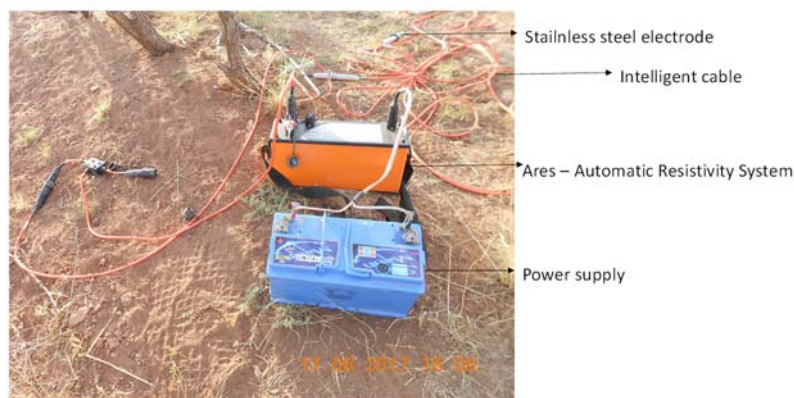


Figure 4-11 Ares- Automatic Resistivity System and intelligent cable

The resistivity method was conducted with 16 resistivity profiles for different locations in dates between 17-22 August, 2017. These locations have been selected according to the soil sampling points which had been analyzed earlier in order to calibrate the CRS. In that sampling, 108 undisturbed samples were collected at 18

locations from the top 30 cm of soil, and soil physical properties were revealed; such as soil texture and D<sub>50</sub> particle size (Section 4.1.3

Table 4-1). In other words, as shown in Figure 4-12, the midpoints of 15 of these resistivity profiles were located at the soil sampling points, but only one profile covered the two sampling locations, and one sampling point was not found proper to perform a resistivity survey for. It is assumed that soil physical properties are uniform through the profile length and for shallow depth, around 3 m.

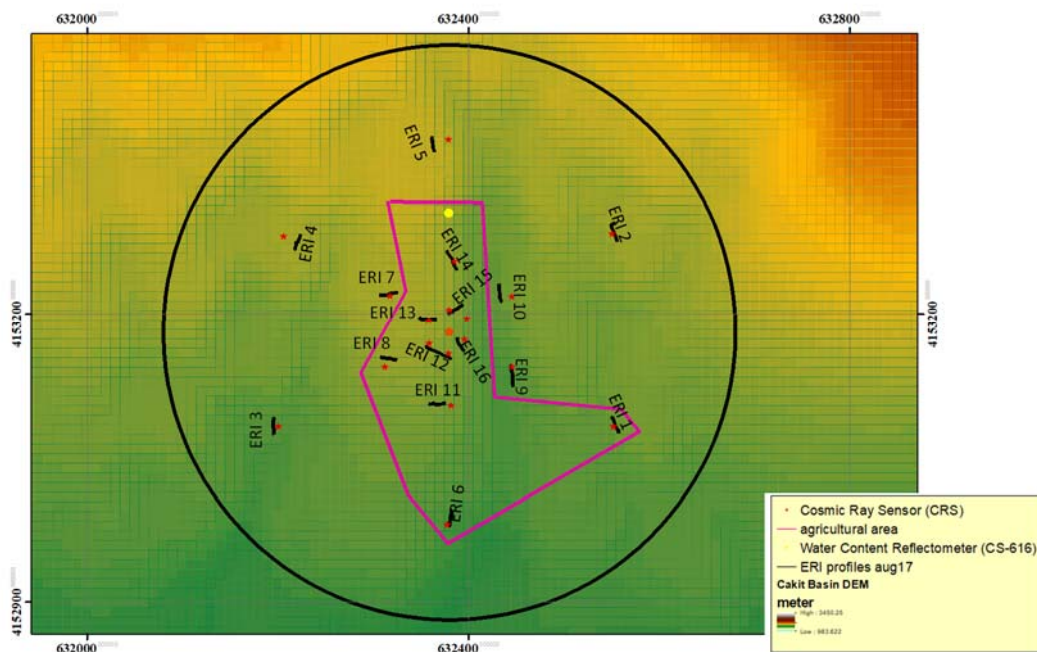


Figure 4-12 Locations of sample points and ERI profiles (17 - 21 Aug 2017)

During resistivity data acquisition in the field, ERI profiles were located both in and outside of the region of the footprint used for agricultural purposes (Figure 4-13). Generally, there are young cherry trees in these regions, and drip irrigation is used mostly in summer time period. In addition, soil texture and clay content vary profile

to profile. Table 4-3, Table 4-4 and Table 4-5 show classification of ERI profiles according to land use, soil texture, and clay content, respectively.

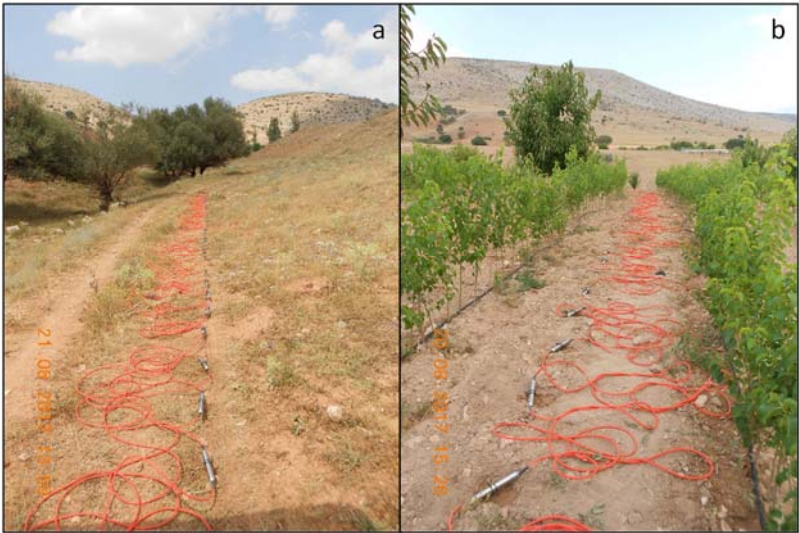


Figure 4-13 ERI profiles; outside of the agricultural part (a), inside of the agricultural part (b)

Table 4-3 Land use classification of profiles

Land use type	Profile name
<b>Natural vegetation</b>	ERI 2, ERI 3, ERI 4, ERI 5, ERI 7, ERI 9, ERI 10
<b>Agricultural</b>	ERI 1, ERI 8, ERI 6, ERI 12, ERI 13, ERI 14, ERI 15, ERI 16, ERI 11

Table 4-4 Clay content percentage classification of profiles

<b>Clay Content (CL) Percentage</b>	<b>Profile name</b>
<b>5% &lt; CL &lt; 20 %</b>	ERI 7, ERI 9, ERI 11
<b>20 % &lt; CL &lt; 30%</b>	ERI 1, ERI 3, ERI 8, ERI 12, ERI 13, ERI 16
<b>30% &lt; CL &lt;40%</b>	ERI 2, ERI 4, ERI 5, ERI 6, ERI 14, ERI 15

Table 4-5 Soil texture classification of the profiles

<b>Soil Texture</b>	<b>Profile name</b>
<b>Silt-Loam</b>	ERI 1, ERI 3, ERI 7, ERI 8, ERI 10, ERI 11, ERI 13, ERI 16, ERI 12
<b>Silt-Clay-Loam</b>	ERI 2, ERI 4, ERI 5, ERI 15
<b>Clay</b>	ERI 6, ERI 14
<b>Loam</b>	ERI 9, ERI 12

15 out of 16 resistivity profiles, covering one soil sampling point each, were surveyed with 0.50 m electrode spacing with Wenner-Schlumberger and Wenner-Alpha electrode geometry array (Knödel et al. 2007) along a length of 19.5 m; the other profile (ERI 12) survey was conducted for 39 m profile length with 1 m electrode spacing and the same electrode arrays were used. These electrode geometry configurations are commonly used for investigating water content in shallow unsaturated zones in field studies (Brunet et al. 2010; Cassiani et al. 2006b).

Schlumberger and Wenner-Alpha geometry arrays give a soil section coverage, which is around 1/5 and 1/6 of the maximum electrode distance between the first (C1) and the second (C2) current electrodes, respectively. Consequently, each of the 19.5 m resistivity profiles provide resistivity variation data for a maximum depth of 3 meters within an acceptable accuracy range. The longer profile provides resistivity characteristics to around 7 m depth.

During the survey, soil moisture data were collected concurrently by using a frequency domain reflectometry (FDR) instrument; this is CS-616 water content reflectometer (WCR), which is the product of Campbell Scientific Company, and the data logger of the probe provided simultaneous soil moisture data in the field. If a CS-616 probe, which is described in Section 4.2, is buried vertically into the soil, it gives an average soil water content value for 30 cm depth with  $\pm 2.5$  % accuracy for a soil medium which has a bulk density of lower than 1.55 g/cm<sup>3</sup>, and volumetric water content value between 0% and 50 % in the medium.

Point-scaled soil moisture data were collected along with the CS-616 at the beginning, at the end and at seven additional points with 2.5 m intervals along resistivity profiles. This measurement scheme is presented in Figure 4-14. Therefore, nine point-scaled soil moisture data were collected for resistivity profiles individually. However, owing to some problems in FDR measurements; such as highly compact soil, only six profiles could be surveyed with both these methods simultaneously. These are: ERI 1, ERI 2, ERI 6, ERI 8, ERI 11, ERI 12. Measured FDR values are summarized in Table 4-6. Based on these measurements, soil moisture data took values between 8.60 % and 29.53 %, the average value is 18.07 % for the dates 17-21 August, 2017. To qualify FDR measurements, water content values for the midpoints of ERI 1, ERI 2, ERI 6, ERI 8 and ERI 11 profiles were evaluated in the lab analysis (Section 4.3.2.1).

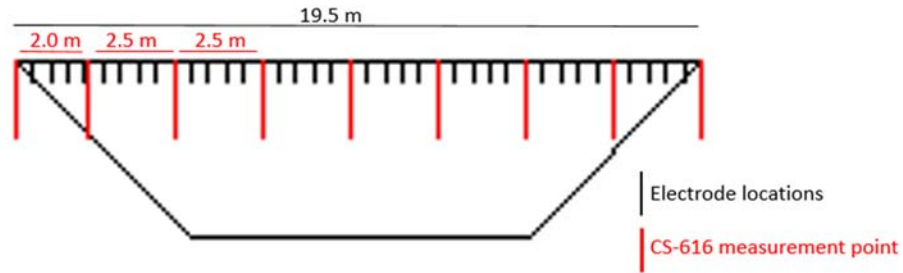


Figure 4-14 Sketch of the electrode and the CS-616 measurement locations in the resistivity survey line

Table 4-6 FDR soil moisture measurements (%) along resistivity profiles

# electrode	ERI 1	ERI 2	ERI 6	ERI 8	ERI 11	ERI 12
1	24.07	17.13	10.84	25.01	-	21.25
5	21.75	8.60	10.35	27.83	19.11	21.75
10	19.45	11.47	10.57	17.82	17.82	26.47
15	20.67	11.47	10.97	21.87	20.02	13.52
20	22.98	12.50	-	17.56	16.31	-
25	22.66	15.74	8.93	17.71	19.19	11.73
30	25.88	16.66	11.28	18.96	21.05	24.07
35	20.44	23.99	9.80	19.96	29.53	-
40	18.22	22.03	10.91	16.81	18.52	20.51

#### 4.3.1 Inversion Procedure and Interpretation of Inverted Resistivity Data

Measured resistivity values, i.e. apparent resistivity values, are interpolated to create a so-called pseudo section which is an arrangement of the resistivity variation in 2-D. Since soils do not have homogeneous structure, inversion of this pseudo-section is required for calculating the true electrical resistivity and the corresponding true depth values (Maillet et al. 2005).

In this study, Res2DInv was used for inverting the collected resistivity data for each profile and electrode geometry configuration individually. This software is widely used in resistivity surveys (e.g. Andrade 2011; Dannowski and Yaramanci 1999; Garambois et al. 2002; Groves et al. 2011; Maillet et al. 2005). Res2DInv was developed by Loke and Barker (1996), and it is based on the smoothness constrained least-square method (Sasaki 1992).

Each electrode array provides data with different sensitivity in terms of vertical and lateral resolutions and depth of investigation. Therefore, there are differences between data provided by Wenner-Schlumberger and Wenner-Alpha electrode configuration (Samouëlian et al. 2005). Two configurations were performed for each profile consecutively in this study. In addition, a combination of these electrode geometry data is helpful for mapping the resistivity variation by using all advantages of these configurations.

As Res2DInv is not capable of inverting the combination of different electrode geometry array data, another inversion software, ProfileR, was used. ProfileR was developed by Prof. Dr. Andrew Binley for electrical resistivity distribution imaging. Its inversion routine is built on a regularized objective function combined with weighted least squares (Binley 2003).

Resistivity data inverted by both these two different software were mapped for visualizing the true resistivity variation in 2-D. ProfileR inversion results are smoother and make it easier to follow the general trend in subsoil resistivity properties. For instance, Figure 4-15 shows inversion outputs produced by Res2DInv and ProfileR. All inversion results are shown in Appendix B.

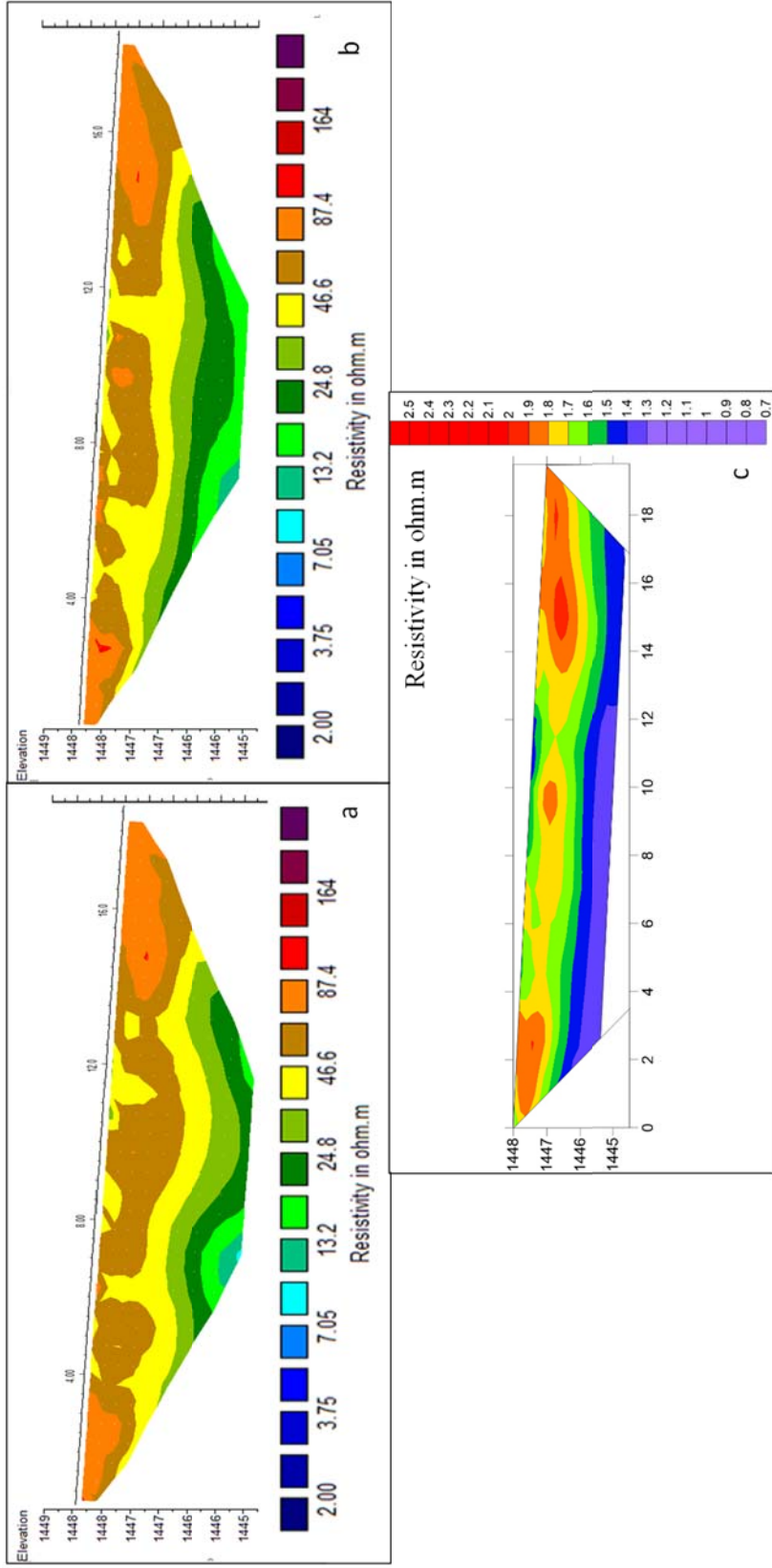


Figure 4-15 ERI profile 1 (Aug 2017) inversion results; Wenner-alpha via Res2DInv (a), Wenner-Schlumberger via Res2DInv (b), combined electrode geometry via Profile R (c)

As mentioned earlier, ERI profiles were located both in and outside of the cherry trees planted in a certain part of the CRS footprint. It is obvious that agricultural activities might lead to local minimal relative differences in resistivity variation. This can be observed easily in ERI 8, ERI 11 and ERI 13 (Appendix B). Moreover, the effect can be easily recognized from the comparison of ERI 10 and ERI 11 profiles. Their soil texture is the same; that is, silt-loam, and while ERI profile 10 has noticeable smooth horizontal layers with varying resistivity values, ERI profile 11 exhibits local anomalies in the upper part, since it is located in the cultivated area. On the other hand, in ERI 6, even though the upper part of the soil section shows high resistivity, it is quite thin. The deeper parts of the soil section of ERI 6 are more conductive, and also have the highest conductivity values among all profiles. The reason for this can be the soil texture, because the soil in that profile has the highest clay content. In ERI profile 14, the upper and the deeper parts are more resistive; thus, between the two resistive layers, there is a relatively conductive soil layer. It should be highlighted that the soil type of the profile is clay as well. Furthermore, the soil texture and the agricultural impacts have been observed in ERI 9, the soil type of which is loam, and it was located in area covered with natural vegetation. The variation of the resistivity of layers are more uniform than the profiles which were located in the agricultural part of the study area, and the conductivity differences in the layers can be identified easily.

In short, for all resistivity profiles, it was observed that the study area is typically conductive. There is also a general trend for all profiles such that the upper part of the soil is more resistive, and below that, the deeper layers have a more conductive nature.

While electrical resistivity imaging (ERI) is an indirect technique for deducing soil moisture values, frequency domain reflectometer (FDR) measurements provide simultaneous average water content values for the upper 30 cm of soil. There is an opportunity to compare measured water content values with corresponding measured resistivity data for the six resistivity profiles in this study.

As the Wenner-Schlumberger configuration is sensitive to vertical resistivity variation, it was used for the comparison of FDR measurements and bulk resistivity values. Since FDR provides point-scaled data, measured bulk resistivity values, which were inverted

by Res2DInv for depths of 13 and 38 cm, were used to see how FDR measurements are correlated with ERI surveys. Figure 4-16 shows that these two distinct types of data distribution in the study area. Although the relationship between soil moisture and bulk electrical resistivity of soil is should be negative, these data has positive trend.

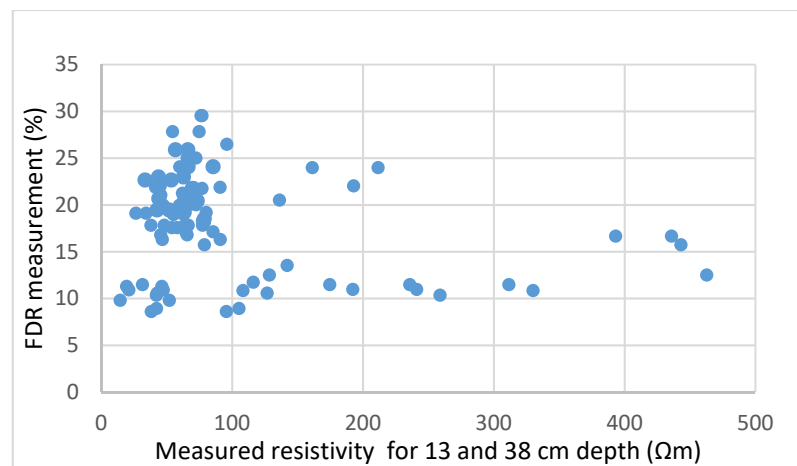


Figure 4-16 Measured resistivity data with respect to FDR measurements

### 4.3.2 Resistivity Data Conversion

Electrical properties of each soil component; namely air, water and solid particles, are different from each other. Therefore, the nature of each of these constituents directly influences electrical resistivity variation in the soil. Particle size, mineralogy, porosity, degree of saturation, solute concentration in pore water and temperature are the factors affecting the resistivity variation. However, water content and dissolved salt presence are the dominant ones among these factors, since electrical current is based on the movement of ions in pore water (Samouëlian et al. 2005). The relationship between electrical resistivity - or conductivity- of soil media and water content is typically investigated through empirical equations. One of these empirical equations is Archie's

Law, which has been implemented in many studies (e.g. Binley et al. 2002; Brunet et al. 2010; Turesson 2006).

In this study, Archie's Law was used for revealing the relationship between water content and measured resistivity data. Archie's Law is an empirical equation, and it was originally developed for the petroleum industry. It is widely used for relating the bulk electrical resistivity, pore fluid and the solved ion concentration; i.e. pore solution, and soil textural properties. It was enhanced for sandy soils (i.e. non-conducting matrix), and it was developed by Archie (1942) for two cases, which are fully filled pores (saturated state) and partly filled pores (unsaturated state).

– *Saturated state*

$$\rho_o = F\rho_w \quad (4.14)$$

where  $F$  is a formation factor which is mainly based on particle size and physical characteristics of the soil,  $\rho_o$  is the resistivity of saturated sand,  $\rho_w$  is the resistivity of pore solution. Archie's studies showed that Equation 4.14 can be written as:

$$\rho_o = \rho_w \phi^{-m} \quad (4.15)$$

where  $\phi$  is porosity, and  $m$  is an experimental parameter which is called cementation index.

– *Unsaturated state*

$$\rho = \rho_o S^{-n} \quad (4.16)$$

where  $\rho$  is the resulting resistivity of unsaturated sand,  $S$  is saturation degree, and  $n$  is saturation index.

Since conductivity is the reciprocal of resistivity, the relationship between saturation degree, porosity and water content can be expressed for unsaturated soil as follows, which is called as generalized Archie's Law :

$$\sigma = \sigma_w \phi^m S^n \quad (4.17)$$

In this study, pore water conductivity was assessed with laboratory analysis, and saturation and cementation index were calculated to implement Archie's Law for the study area. The ranges of these Archie's index and the pore water conductivity were analyzed to reveal the impacts of these parameters on the ERI data conversion procedure.

#### **4.3.2.1 Pore Water Conductivity Analysis**

Pore water conductivity is essential for the interpretation of soil resistivity, and it is a requirement for the application of Archie's Law. It can be measured in the field by drilling a borehole (e.g. Dannowski and Yaramanci 1999; Salem and Chilingarian 1999), but this procedure is invasive and expensive. In this study, pore water conductivity values of each resistivity profile was determined with the assistance of lab analyses.

##### **i. Pore Water Extraction Analysis**

In the literature, laboratory analyses have been resorted to by many researchers for obtaining pore water. For example, Shah and Singh (2005) obtained pore water solution with the help of prepared soil specimens. They mixed the soil with different amounts of distilled water, and stored in airtight glass containers for 24 h in the humidity- and temperature-controlled room. After that, they extracted pore water by applying one-dimensional pressure on the specimen.

In addition, there is a standard test method for pore water extraction and determination of the soluble salt content of soils by a refractometer (ASTM D4542-15 2015). This method is applicable only to fine-grained soils which have water content values equal to or greater than approximately 14%. Similarly, in this method, one-dimensional pressure is applied to the soil specimen for extracting pore water. However, an undisturbed soil sample must be collected to get the pore water conductivity, which is the representative in-situ pore water conductivity value, hence it is not easily applicable.

As stated before, between 17 – 22 August, 2017, electrical resistivity measurements were carried out in 16 different profiles, matching with the locations of 17 of the CRS soil sampling points. Disturbed soil samples from the top 5 cm (Figure 4-17) were collected from the midpoint of these resistivity survey profiles at the same dates. However, due to some difficulties; e.g. excessively-compacted soil or large vegetation root presence at the site, soil samples were collected at only 12 of the resistivity profiles. These samples were used for the preparation of test samples.



Figure 4-17 Disturbed soil sampling in August 2017

The assessment of the pore water conductivities for the resistivity profiles was carried out with the help of laboratory analysis, consisting of three main parts: preparation of

soil samples, curing, extraction and electrical conductivity (EC) measurement of the pore water. Soil samples were prepared according to in-situ bulk density values which were determined from the sampling done in December 2016. For each resistivity profile, five test specimens were prepared, and each specimen was 5 cm in height and 5 cm in radius, and five sheets of filter paper were placed to the bottom and the top of each specimen. The filter paper has 11 $\mu$ m pore size and 180  $\mu$ m thickness. These samples were fitted in consolidation test cells which were filled with distilled water, and the distilled water-filled glass tubes are connected to the test cells individually. After that, specimens were stored for 72 hours in a humidity- and temperature-controlled room (Figure 4-18). The samples were saturated with distilled water only by soaking the bottom and top surfaces at constant temperature and humidity conditions. Brunet et al. (2010) showed that if the soil is saturated with osmosed water; i.e. low mineralized water for more than 50 hours, the pore water resistivity value reaches to a constant value; and in this analysis, the cure time was selected as 72 hours. The cured samples were inserted in a consolidation set-up to apply one-dimensional pressure (Figure 4-19). After that, the pore water was extracted with the help of a syringe. For each resistivity profile, pore water values for more than three soil specimens were extracted, and electrical conductivity (EC) values were measured with Exstick II EC sensor, which is the product of EXTECH Instruments Company (Figure 4-20). Before the EC measurements, the sensor was calibrated with three different standard calibration solutions; 84  $\mu$ S/cm, 1413  $\mu$ S/cm, 12880  $\mu$ S/cm in the laboratory.

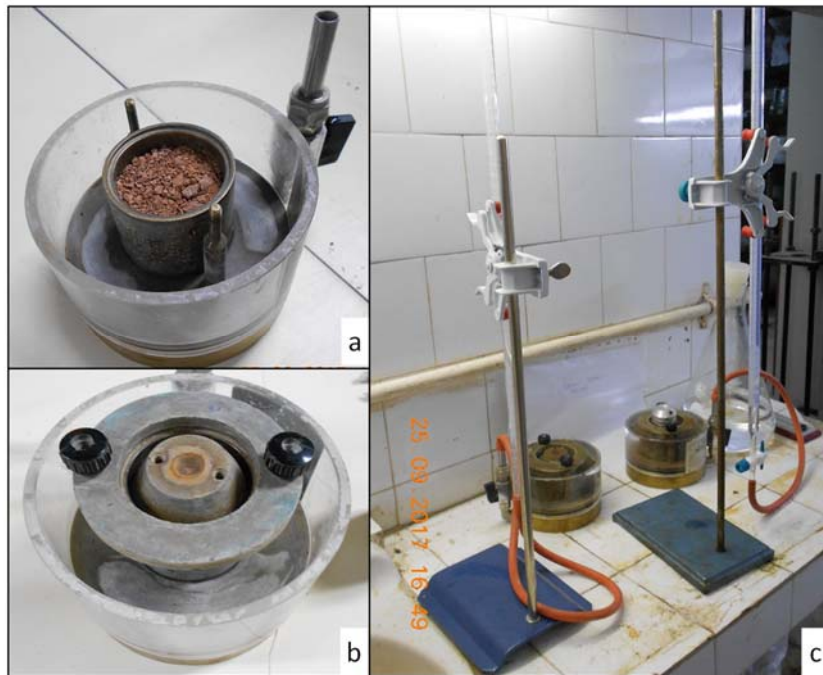


Figure 4-18 Soil sample (a), consolidation cell with the sample (b), cure procedure (c)



Figure 4-19 Consolidation test setup



Figure 4-20 Pore water conductivity measurement by the EC probe

The results of the extraction are summarized in Table 4-7. The pore water conductivity values changed between 654  $\mu\text{S}/\text{cm}$  and 2290  $\mu\text{S}/\text{cm}$ . Although most of these pore water conductivity values are less than 1200  $\mu\text{S}/\text{cm}$ , ERI 2 has pore water conductivity value much more greater than 1200  $\mu\text{S}/\text{cm}$ . One-point soil sampling might have caused this order of magnitude, so this value was not taken into consideration, as a result the most upper pore water conductivity value is selected as 1223  $\mu\text{S}/\text{cm}$  (ERI 14). The rest of these values are plotted with respect to clay content (Figure 4-21), and the plot shows that pore water conductivity is not directly related to clay content.

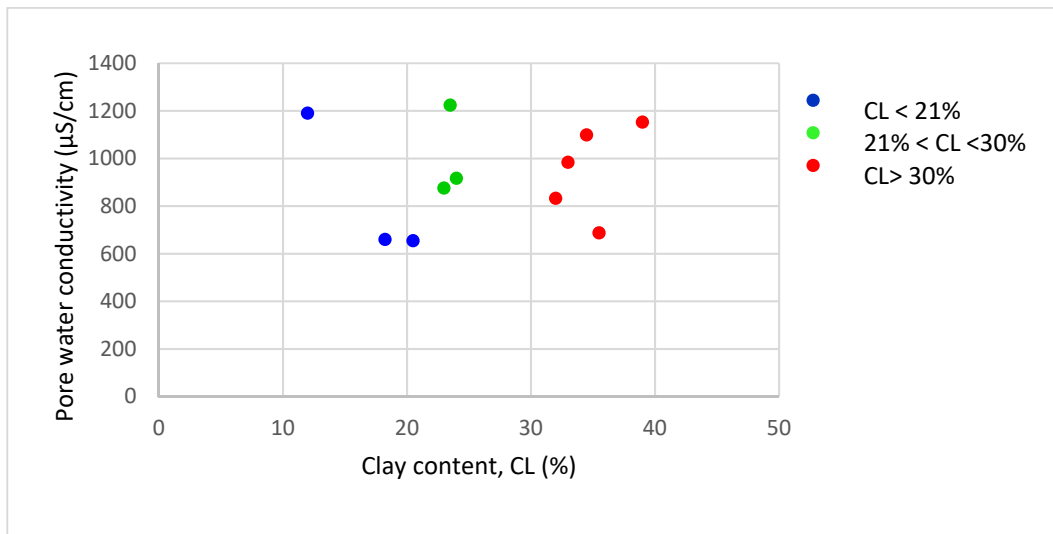


Figure 4-21 Estimated pore water conductivity with respect to clay content

Table 4-7 Estimated pore water conductivity values and clay content information

Resistivity Profile Name	EC ( $\mu\text{S}/\text{cm}$ )	$^{\circ}\text{C}$ (EC)	Clay Content, CL (%)
ERI 1	916	20.3	24
ERI 2	2290	19.8	31
ERI 3	875	19.7	23
ERI 4	1152	19	39
ERI 5	983	19.7	33
ERI 6	832	18.7	32
ERI 7	659	18.3	18.25
ERI 8	654	19.7	20.5
ERI 11	1190	18.6	12
ERI 14	1223	18.9	35.5
ERI 15	687	18.6	34.5
ERI 16	1098	19.1	22

During the lab analysis, not only pore water conductivity was determined, but also, gravimetric and volumetric water content of the disturbed samples were determined by using soil -phase relationships equations (Section 4.1.3). These calculations were used for checking the quality of CS-616 measurements which were conducted at the mid-points of the resistivity profiles for ERI 1, ERI 2, ERI 6, ERI 8 and ERI 11. There is a direct correlation between the measurements and lab calculations except one point (Figure 4 22).

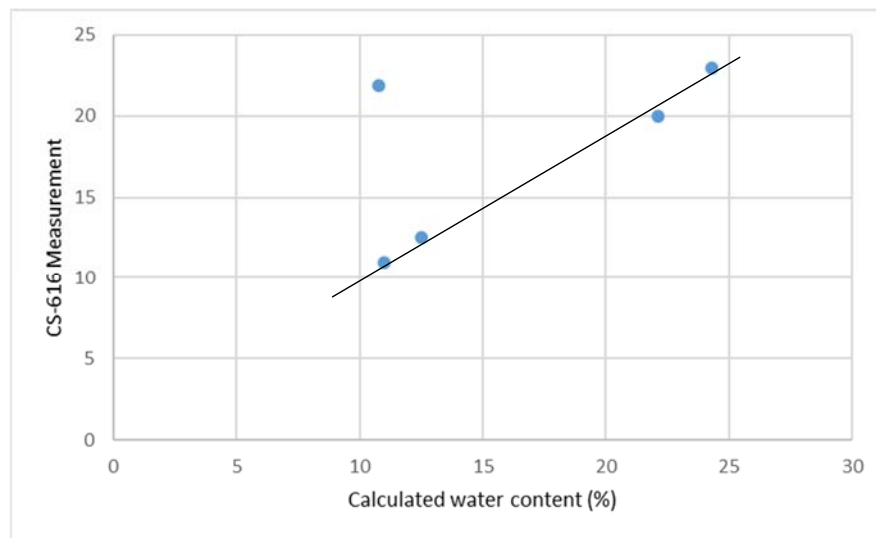


Figure 4-22 Calculated water content in the lab by using soil phase relationships and conditions and CS-616 measurements

## ii. Saturation Index (n) and Cementation Index (m) Calculations

Saturation index (n) values were very close to 2, cementation index (m) was calculated around 1.3 for clean unconsolidated sands in Archie's research. Furthermore, m has taken larger values ranging between 1.8 and 2.2 (Archie 1942). Saturation index (n) value has been adopted as 2 generally (Dannowski and Yaramanci 1999). However,

experimental studies of Ullrich and Slater (2004) showed that it can be a value in the range of 1.0 to 2.7.

Later studies showed that Archie's equation is applicable for various soils with the cementation index ranging from 1.2 to 4.0 (Friedman 2005). In addition, the typical range is between 1.5 and 2.5 for most sedimentary rocks, and for granular sediments, it is generally less than 1.5 (Garambois et al. 2002).

Even though typical ranges are defined for  $m$  and  $n$  parameters in literature, the cementation index varies widely from soil to soil or formation to formation, because  $m$  is affected by lithology, porosity, compaction degree, and cementation (Salem and Chilingarian 1999). Thus, it should be specified for the study area, and it has been estimated with least square fitting in some studies (e.g. Binley et al. 2002b; Wehrer et al. 2014).

In this study, representative  $m$  and  $n$  values for the footprint have been obtained. To fit  $m$  and  $n$  parameters to Archie's Law, six resistivity profile data with corresponding FDR soil moisture measurements have been used. For the profiles where FDR measurement could not be performed, the cosmic ray sensor soil moisture probe (CRS) data have been used. Equation 4.17 has been iteratively solved with 0.001 increments for  $m$  and  $n$  ranges, 1.3 to 3 and 1 to 2.7, respectively, to calculate the optimum  $m$  and  $n$  values, which has the minimum root mean square error for the calculated bulk conductivity. Soil properties; such as particle size, porosity, clay content and examined pore water conductivity in these six resistivity profiles have been compared to the average values for the footprint. The comparison shows that the profile which has the closest values to the average values could be used, since its soil properties are representative of the entire footprint. As a result,  $m$  has been selected as 1.57 among calculated values changing between 1.308 and 2.31. Also, calculated  $n$  values vary between 1.023 and 2.638, and the values obtained is 1.152 from the selected profile, which has the representative soil physical properties for the study area. In short, the most representative  $m$  and  $n$  values have been found for the cosmic ray sensor measurement area.

#### 4.3.2.2 Archie's Parameters and Pore Water Conductivity Range

Pore water conductivity values and representative Archie's indices for the study area were determined from lab analyses and mathematical operations. The ranges of these values were used to understand the relationship between soil moisture and bulk conductivity. By using Archie's Law, Equation 4.17, with the estimated  $m$  and  $n$  values, the lower and upper ranges of pore water conductivity were calculated.

It is observed that the determined values graph is different than an expected sample of Archie's curve (Figure 4-23). The soil moisture measured by FDR and corresponding conductive values are plotted on the same figure (Figure 4-24), and here,  $\mu\text{S}/\text{cm}$  as the unit of conductivity has been used. Moreover, the same equations by using the average pore water conductivity range of Archie's index were plotted with FDR measurements in Figure 4-25 and Figure 4-26. However, Figure 4-24 shows that there is no remarkable relationship between FDR measurements and bulk conductivity. In addition, the clay content does not show a significant impact on the scattering of the water content data. Furthermore, Archie's indices have a huge variation for the study area. These findings reveal that the ERI method has limited sensitivity in this study area.

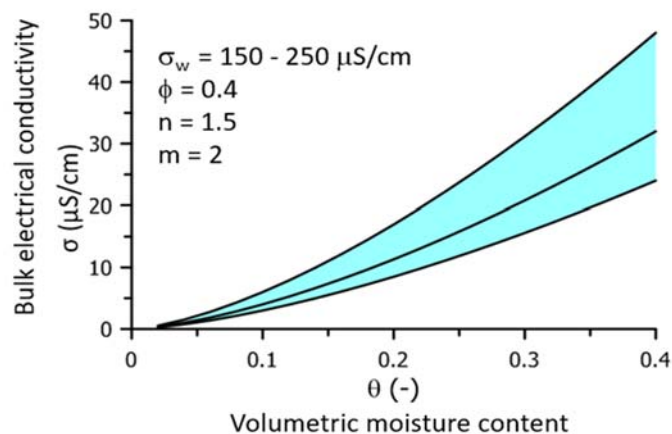


Figure 4-23 Expected Archie's equation curve with random values (Lecture notes of Prof. Dr. Andrew Binley)

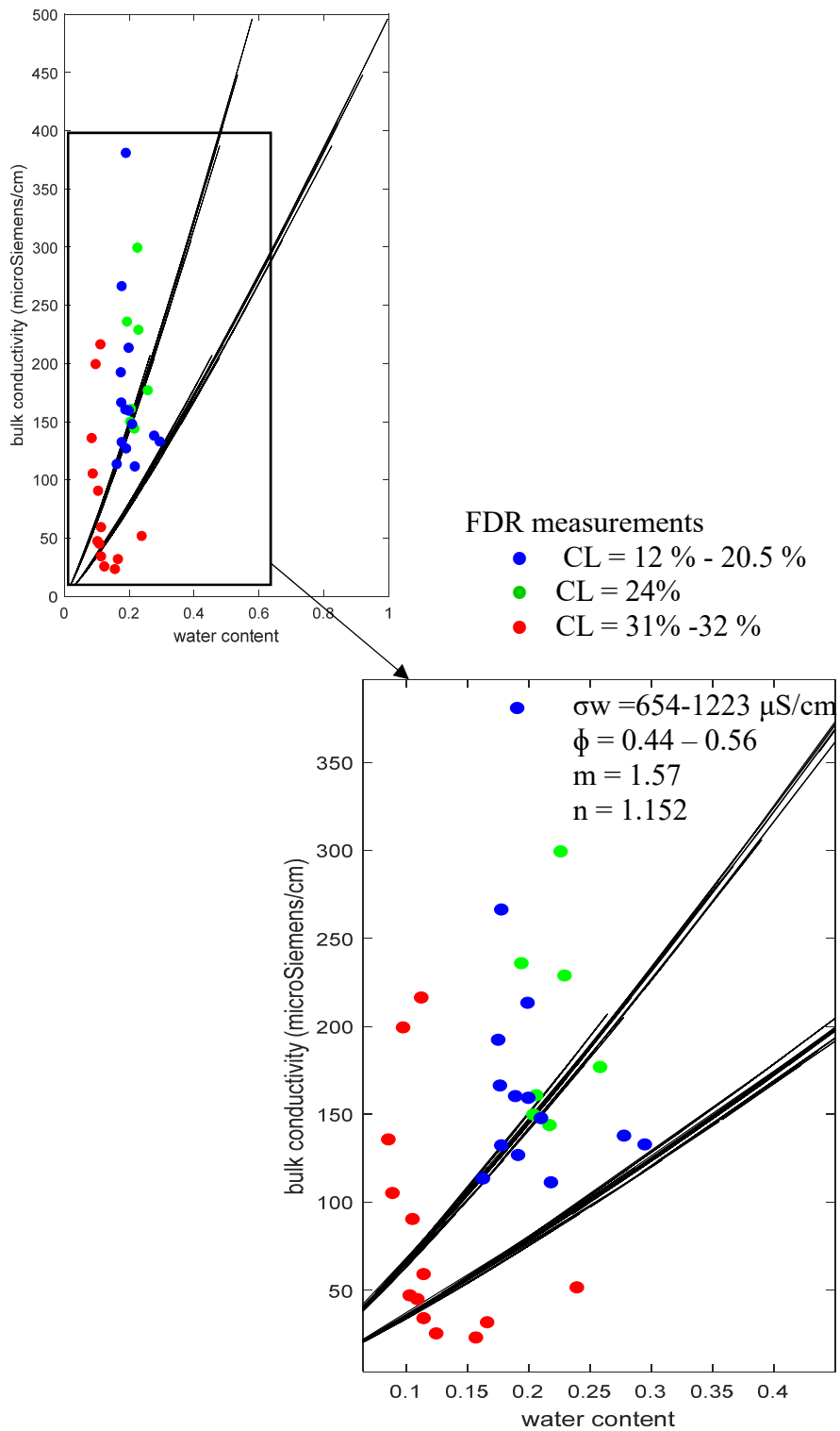


Figure 4-24 Pore water conductivity range and FDR measurements

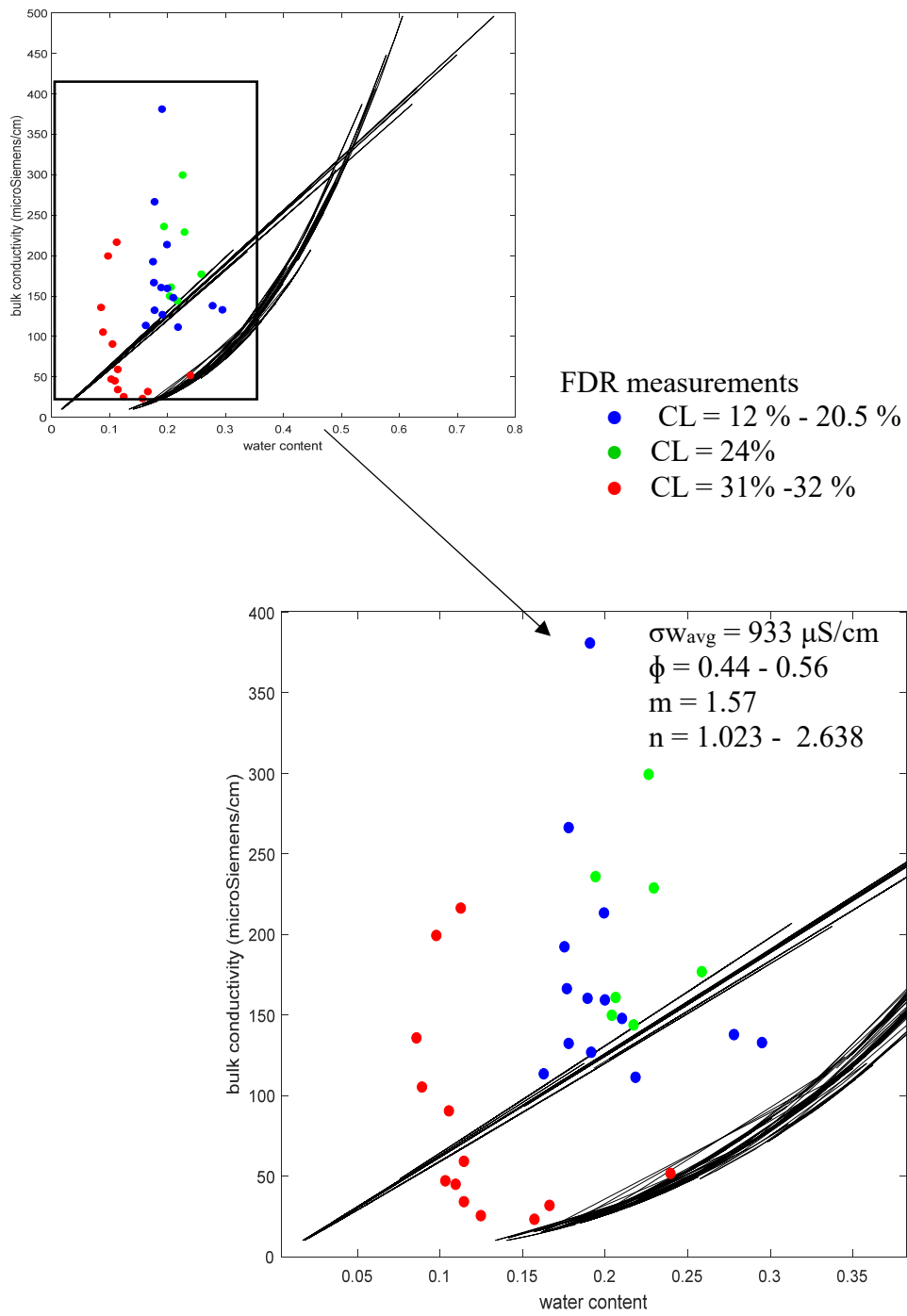


Figure 4-25 Saturation index (n) range and FDR measurements

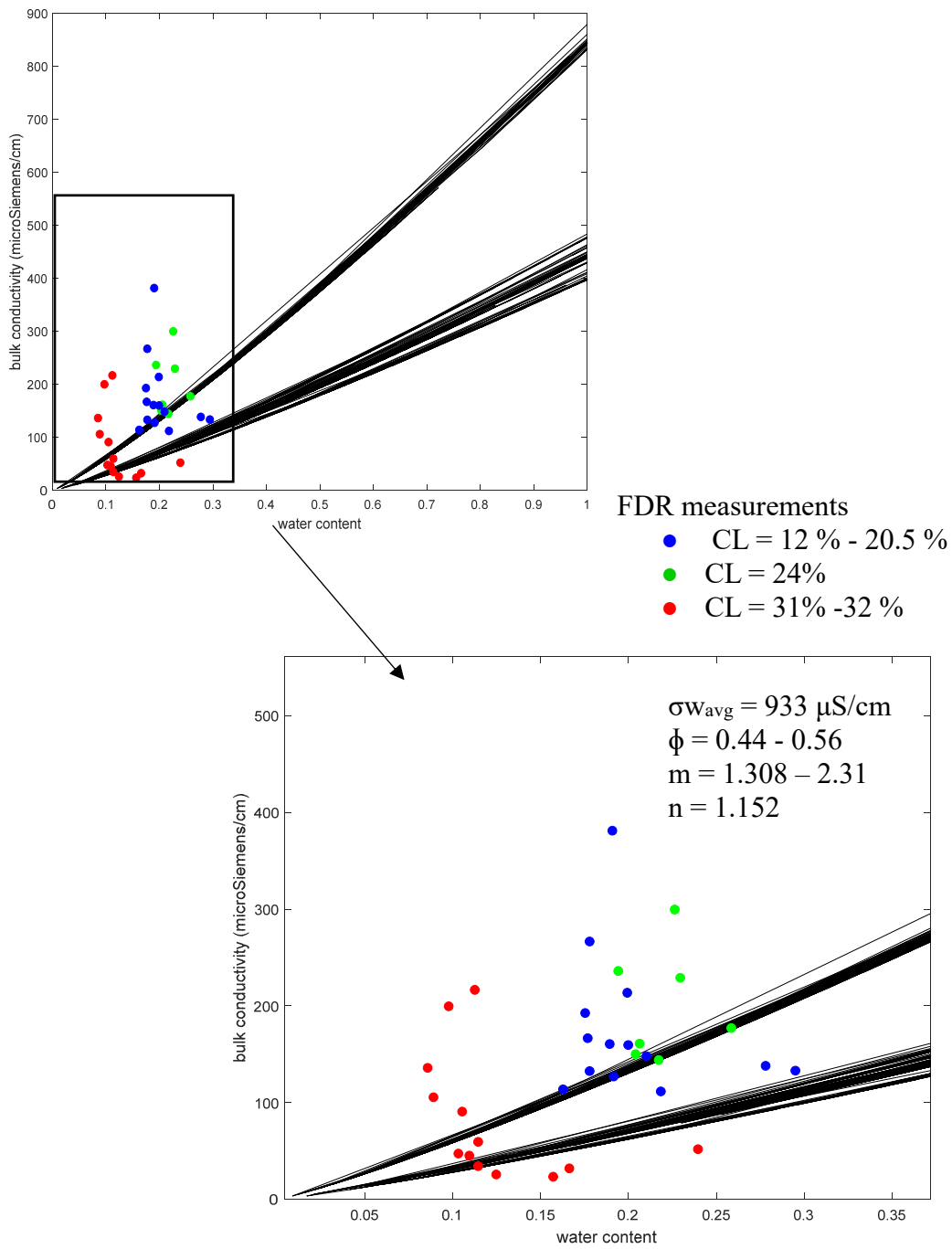


Figure 4-26 Cementation index (m) and FDR measurements

## CHAPTER 5

### DISCUSSION OF THE RESULTS

#### 5.1 Summary

This study aimed to estimate soil moisture by using a range of techniques spanning different spatial scales in Çakıt basin in the south of Turkey. Some complexities are observed in the geological formation of the test basin, considering the soil formation the common soil type is brown forest soil. The site properties; namely, average gravimetric water content and dry bulk density are 0.148 g/g and 1.304 g /m<sup>3</sup>, respectively, and they were used to determine the site-specific calibration parameter of the CRS probe,  $N_0$ , which is equal to 1440.6. Other attributes of the soil are; the average bulk density (1.495 g/cm<sup>3</sup>),  $D_{50}$  (0.033 mm), the average porosity (0.51) and the dominant soil texture is silt-loam. Two ground-based instruments provided continuous soil moisture data in point-scale and plot-scale separately, and electrical resistivity surveys, which provide the intermediate-scale measurements, were conducted in order to characterize the unsaturated shallow zone with respect to soil water content variation.

#### 5.2 Evaluation of the CRS and the Installed CS-616 Measurements

Cosmic ray sensor (CRS) and water content reflectometry (WCR) - CS-616 - were employed to retrieve continuous soil moisture data. While the CRS has a footprint of approximately 0.3 km<sup>2</sup> in area, and measurement is sensible to a depth of 12 cm for

saturated soils and 76 cm for dry soils, the installed CS-616 measured water flux for 2.5 cm in depth at point-scale.

Data obtained from the CRS were corrected according to changes in atmospheric pressure, atmospheric water vapour and the intensity of incoming neutron flux. No method was performed to calibrate the neutron counts site-specifically. Since CRS measurement principle bases on the thermalization of fast neutrons by hydrogen atoms, which are generally exist as water form in soil, it is affected by other hydrogen sources. In this study, it was observed that in winter times, particularly when the average snow depth is more than 65 cm, the CRS measured the soil moisture content unrealistically. For example on 12.02.2016, the volumetric water content and the snow depth were recorded as 17.34 % and 0.4 cm respectively. After the snow depth has increased to 80.7 cm, the obtained soil moisture value from the CRS was 76.29 %. This influence continued up to mid of the February when the average air temperature has started to increase above 0°C. Figure 5-1 presents snow depth amounts and snow depth influence on the CRS measurement.

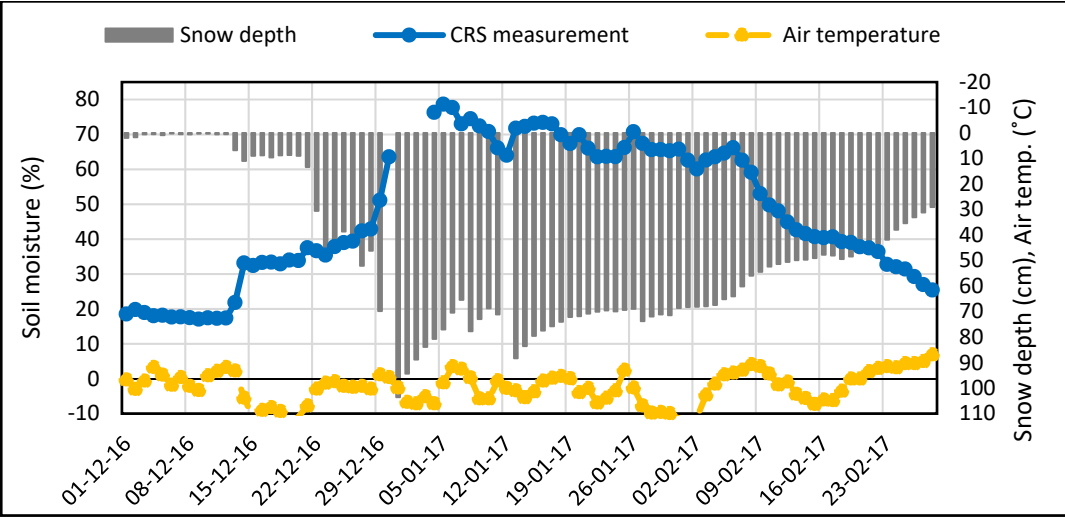


Figure 5-1 Snow depth, air temperature data and the CRS soil moisture measurement

The CS-616 was calibrated and corrected with respect to site-specific soil properties and soil temperature; as a result, the unique calibration equation was determined for the in-situ soil type of interest. It is known that CS-616 is sensitive to the changes in temperature, hence the correction procedure helped to minimize the sensitivity. The correction equation (Equation 4.13) is provided by the manufacturer (Campbell Scientific 2012). The equation counts the evaporation effect when the soil temperature is higher than 20°C. During summer times, the soil temperature values rise to 30 °C in the study area, for example the daily values for August 2017, the calibrated measurements overestimate the moisture content, but the correction procedure reduces the soil water content with taking into the evaporation account (Figure 5-2). Furthermore, the high amount of organic content can affect the operation efficiency of the dielectric permittivity based methods. In this study, the gravimetric organic content was determined as 3.074 %, the effect of which can be neglected.

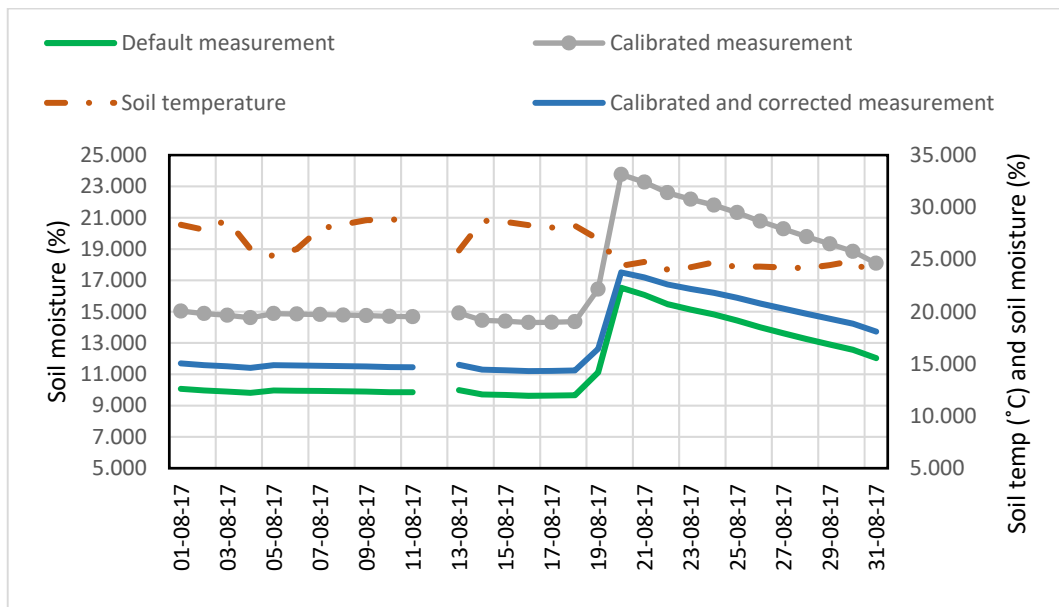


Figure 5-2 The CS-616 default measurement, calibrated measurement, calibrated and corrected measurement and soil temperature data

The continuous soil moisture data deduced from these two installed instruments and the rainfall data are presented in Figure 5-3. The increment pattern in soil moisture during the rainfall events that have occurred in the basin have been recorded similarly. On 05.11.2017, 31.24 mm rainfall was recorded, and this event led to an immediate increase of volumetric water content (VWC) by around 4.4 %, 4.28% and 5.41% for the CRS, CS-616 default, calibrated and corrected CS-616 measurements respectively. The comparison of the values for the day before the event and after the event is summarized in Table 5-1. The default measured soil moisture data by the CS-616 were closer to the CRS data, and the corrected and calibrated CS-616 measurements overestimated the soil moisture content. However, it is highlighted that since the CS-616 measures at more shallower depth - 2.5cm- than the CRS - 12 cm to 76cm- the response to the rainfall event can be expected to be more. Additionally, while CRS provided the area-average data, the CS-616 measured at point-scale; hence the differences in soil moisture values obtained from these two instruments are acceptable.

Table 5-1 Rainfall event and the corresponding soil moisture change

Date	Rainfall (mm)	VWC (CRS) (%)	VWC (Default CS-616) (%)	VWC (CS-616) (%)
04.11.2017	0	10.76	8.52	13.67
05.11.2017	31.24	15.16	12.8	19.08
06.11.2017	0	21.62	22.71	31.46

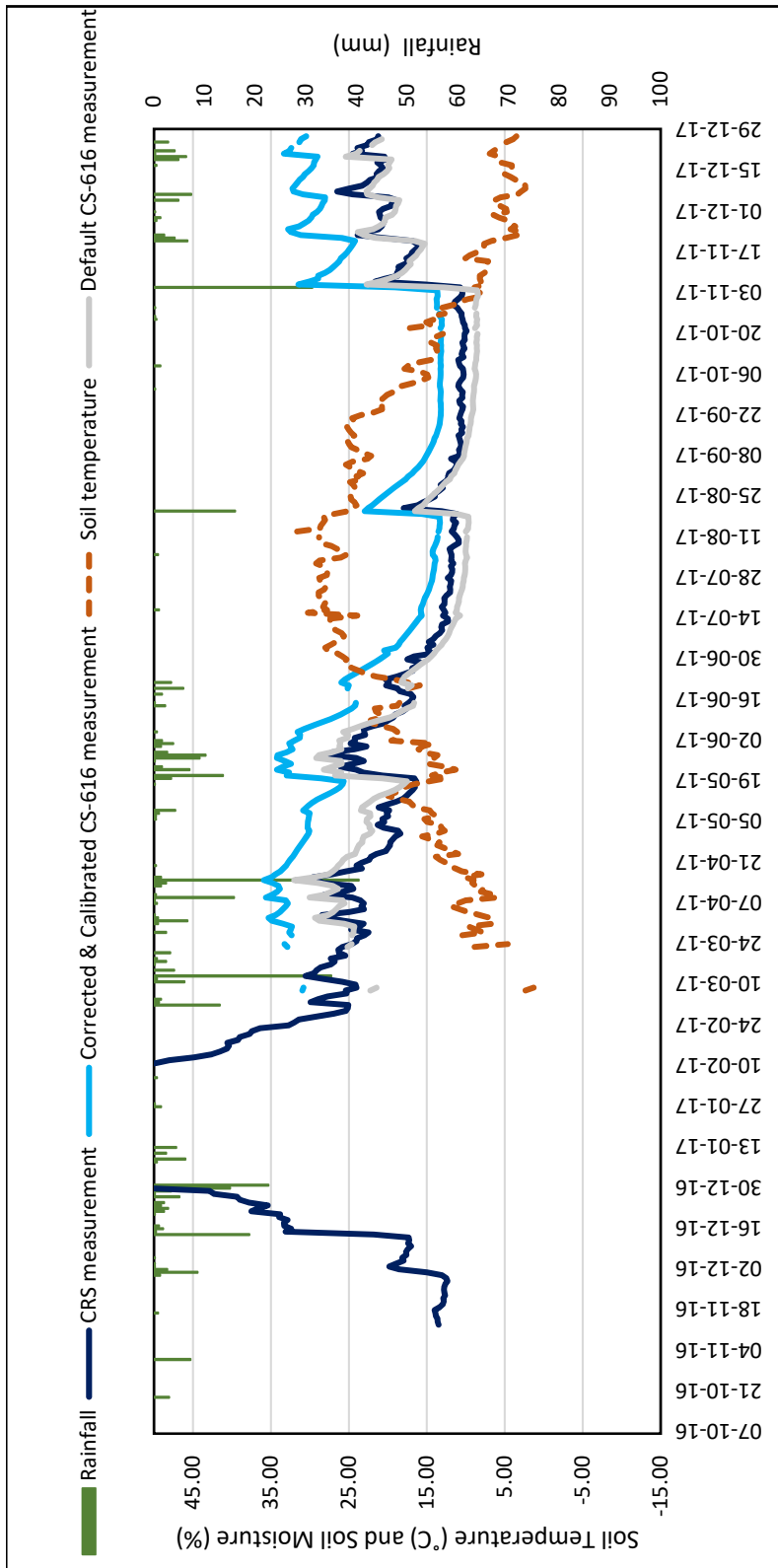


Figure 5-3 Soil moisture data retrieved from the installed instruments; CS-616 and CRS

It is known that; even though CS-616 is calibrated and corrected with respect to soil temperature, it cannot provide highly precise data, due to the low frequency of the operational electromagnetic wave of this instrument. Lower frequencies lead to measurement capabilities with less sensitivity for WCR instruments (Kelleners et al. 2005). In comparison with the soil moisture data obtained from the CRS, the CS-616 (calibrated and corrected) overestimates the soil moisture and the amount of rainfall influence the changes between the measured soil moisture values. However, the difference is not larger than 12% (5-3 and 5-4).

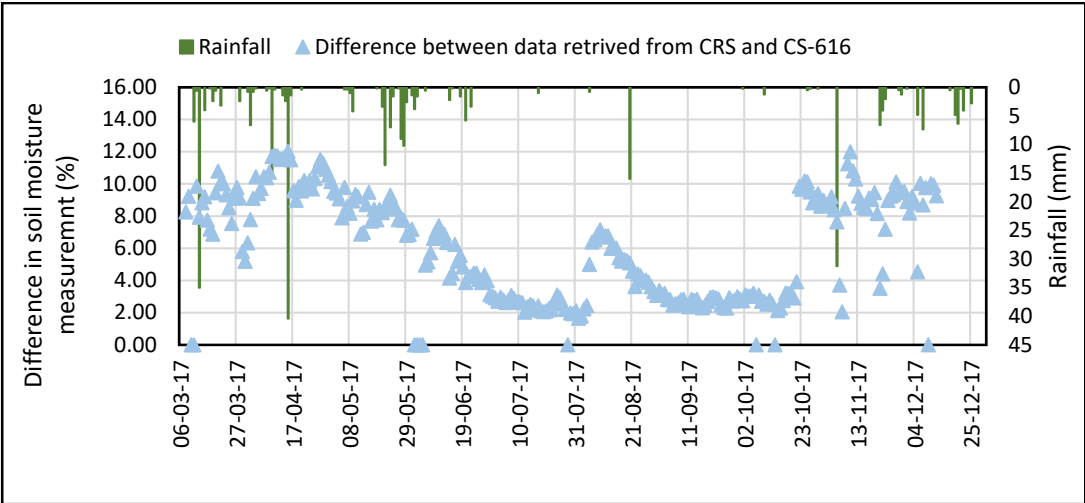


Figure 5-4 Difference between soil moisture data retrieved from CRS and CS-616

### 5.3 Evaluation of the Electrical Resistivity Imaging (ERI) Surveys

Electrical resistivity surveys were carried out to acquire the variation of the water content in 3 m depth along 19.5 m profiles, within the CRS footprint; in this way, the soil moisture condition was investigated with three different spatial scales.

Soil moisture was measured by CS-616 concurrently. The simultaneous point-scaled measurements were evaluated in the laboratory studies to ensure good data quality. These CS-616 measurement values were found out to be generally within the data set provided by the installed instruments at the specified dates. Also, the average bulk density of the study area is less than  $1.55 \text{ g/cm}^3$ , which is a constraint for the WCR data accuracy prescribed by the default standard calibration equation. However, the CS-616 data were taken into consideration cautiously, because of data accuracy limitations. Besides, the instrument is not easily applicable to stiff and hard soil. When the instrument put into the soil, it cannot be inserted easily, and the parallel rods can become misshaped. This means that, the usage of CS-616 at the field studies is not convenient for all soil types. On the other hand, if the instrument is buried horizontally in the soil, and the position of rods with respect to each other is conserved, it provides more reliable VWC data.

Archie's Law was implemented to investigate how bulk resistivity of the soil and water content are interconnected to each other. Pore water conductivity values were determined at the end of the laboratory procedure for each resistivity survey line location. The pore water conductivity values were attained without being directly influenced by the clay content distribution in the field, and it changes between 654 and 1223  $\mu\text{S/cm}$  for the samples analyzed. Although exact pore water conductivity value cannot be determined easily, this laboratory analysis provided a range for the pore water conductivity value.

There are generally adopted values of the Archie's indices according to soil type in the literature (for instance Friedman (2005) summarized the values of the indices ). However, these indices are site-specific values, and they change from soil to soil. Particularly the lithology, porosity, the compaction degree influence the cementation index. For this reason, the determination of the indices specifically is critical for the

Archie's Law implementation. In this study, Archie's cementation index,  $m$ , and Archie's saturation index,  $n$ , were iteratively calculated; and these parameters were determined as 1.57 and 1.152, respectively. It should be highlighted that, all physical properties of the soil such as porosity, soil texture, and the pore water conductivity values, were adjusted for deeper layers of soil than sampling depth, 30 cm. Therefore, the average porosity value, which was found as 0.51, is higher than that for the deeper soils; and it can limit the efficiency of the empirical equation which was originally developed for deeper zone investigations in oil industry. Additionally, Archie's Law based on non-conducting soil, i.e. neglecting soil surface conductivity, however, the nature of the solid particles of the study area contains clay, hence, neglecting surface conductivity is the main reason having the limitations of application of ERI by using Archie's Law.

Archie's Law was utilized individually for the highest and lowest values of the pore water conductivity, the cementation and the saturation indices. As a result, the solution boundary of possible result combinations of the empirical equation was assessed. Nevertheless, most of the simultaneous point-scaled soil moisture measurements do not fall into the possible solution set of the implementation; only 24% of the FDR measurements were in agreement with the results of the empirical equation.

Since clay content influences the bulk electrical conductivity of the soil, the VWC measurements were classified according to the clay content of the corresponding survey line. For this study area, no significant relationship between the clay content value and the VWC measurements was revealed.

It is obvious that, not only water content and clay content but also soil texture, particle size, porosity, salinity, pore water conductivity and temperature control the bulk electrical conductivity of the soil; and for this study area, the water content cannot be identified as a major factor for the electrical resistivity variation.

## CHAPTER 6

### CONCLUSIONS AND RECOMMENDATIONS

Soil moisture measurements are important for determining particular hydrological state conditions, soil hydraulic parameters and soil water fluxes. Each soil moisture measurement technique has its own drawbacks and advantages; for that reason, a combination of these techniques offers advantages for the determination of soil moisture conditions. In this study, three different techniques were combined, particularly cosmic ray sensor probe (CRS), water content reflectometer (CS-616) and electrical resistivity imaging (ERI) to estimate soil moisture at multi-scale both in time and space.

In this chapter, the conclusion of this study is drawn under Section 6.1, and recommendations are provided in Section 6.2.

#### 6.1 Conclusion

Indirect soil water content estimation methods require calibration. For this reason, different approaches must be combined. In this study, the laboratory calibration of the installed soil moisture sensors, laboratory analysis of the site-specific properties and the field work were jointly conducted.

Comparison of the inverted resistivity data and the concurrent CS-616 measurements revealed that the ERI has limited sensitivity in obtaining soil water content for the study area. Although the bulk resistivity of soil is predominantly controlled by water content, it is also modulated by the ion concentration in pore water and the textural

properties of the soil. ERI as a geophysical method helps to characterize the subsurface ground and give information to understand the soil structure.

Soil moisture data deduced from the CRS and the CS-616 instruments indicate that these two different techniques can be used for supplementing each other for inferring soil moisture changes in the near-surface. Differences between the data provided by the CRS and CS-616 were not greater than 12%. Since the instruments have different depth of investigation and measurement scale, this difference is acceptable. It is observed that soil moisture changing trend was recorded by these two sensors similarly. This study reports results from the first implementation of CRS in Turkey. The results show great promise for using this sensor in monitoring soil water content, including drought conditions.

Understanding the hydrological processes is still challenging. Data is needed but there are still limitations of data collection methods in space and time scale to understand the processes in detail. New techniques, good instrumentation at the field scale, supported lab studies and modelling are needed to answer the research question of “why” rather than “what”.

## **6.2 Recommendations**

When the findings of this study are taken into account, the following suggestions can be made, especially for the study area:

- New ERI measurements can be conducted at the same locations to observe the resistivity variation in time. This may help to eliminate the current limitation of the technique, because the reason of the time dependent resistivity changes can be more useful to identify main driving force of the resistivity variation.
- Another soil moisture measurement method, which provides a scale range similar to that of the ERI, can be used to understand influencing factors of the resistivity variations.
- The applicability of ERI method to retrieve 2-D soil moisture at plot scale must be tested in a resistive site.

- CS-616 sensors can be deployed at different depths to monitor the soil moisture changes in a profile. Hence the movement of the water in the soil can be understood much better.
- As CRS measurements cover approximately 0.3 km<sup>2</sup>, the data can be used in validation of remote sensing soil moisture products.



## REFERENCES

- Andrade, R. (2011). "Intervention of Electrical Resistance Tomography (ERT) in resolving hydrological problems of a semi arid granite terrain of Southern India." *Journal of the Geological Society of India*, 78(4), 337–344.
- Archie, G. E. (1942). "The Electrical Resistivity Log as an Aid in Determining Some Reservoir Characteristics." *Petroleum Technology*, (October), 54–62.
- ASTM International. (2010). *ASTM D2216-10 - Standard Test Methods for Laboratory Determination of Water (Moisture) Content of Soil and Rock by Mass*. ASTM International, 1–7.
- ASTM International. (2014). *ASTM D 2974 - Standard test methods for moisture, ash, and organic matter of peat and other organic soils*. ASTM International, 1–4.
- ASTM Standard D4542-15. (2015). *Standard Test Methods for Pore Water Extraction and Determination of the Soluble Salt Content of Soils by Refractometer 1*. ASTM International.
- Athanasios, P. (2008). "Athens NM, Greece (ATHN)." <<http://www.nmdb.eu/?q=node/44>> (Sep. 25, 2017).
- Aubert, D., Loumagne, C., and Oudin, L. (2003). "Sequential assimilation of soil moisture and streamflow data in a conceptual rainfall - Runoff model." *Journal of Hydrology*, 280(1–4), 145–161.
- Baatz, R., Bogena, H. R., Franssen, H. H.-J., Huisman, J. A., Montzka, C., and Vereecken, H. (2015). "An empirical vegetation correction for soil water content quantification using cosmic ray probes." *Water Resources Research*, 51, 2030–2046.
- Baatz, R., Bogena, H. R., Hendricks Franssen, H. J., Huisman, J. A., Qu, W., Montzka, C., and Vereecken, H. (2014). "Calibration of a catchment scale cosmic-ray probe

- network: A comparison of three parameterization methods.” *Journal of Hydrology*, 516, 231–244.
- Binley, A. (2003). “ProfileR version 2.5.” <<http://www.es.lancs.ac.uk/people/amb/Freeware/Profiler/ProfileR.pdf>> (Sep. 2, 2017).
- Binley, A., Cassiani, G., Middleton, R., and Winship, P. (2002a). “Vadose zone flow model parameterisation using cross-borehole radar and resistivity imaging.” *Journal of Hydrology*, 267(3–4), 147–159.
- Binley, A., and Kemna, A. (2005). “DC Resistivity and Induced Polarization Methods.” *Hydrogeophysics*, Y. Rubin and S. S. Hubbard, eds., Springer, Dordrecht, 129–156.
- Binley, A., Winship, P., West, L. J., Pokar, M., and Middleton, R. (2002b). “Seasonal variation of moisture content in unsaturated sandstone inferred from borehole radar and resistivity profiles.” *Journal of Hydrology*, 267(3–4), 160–172.
- Bittelli, M. (2011). “Measuring soil water content: A review.” *HortTechnology*, 21(3), 293–300.
- Bogena, H. R., Huisman, J. A., Baatz, R., Hendricks Franssen, H. J., and Vereecken, H. (2013). “Accuracy of the cosmic-ray soil water content probe in humid forest ecosystems: The worst case scenario.” *Water Resources Research*, 49(9), 5778–5791.
- Brocca, L., Melone, F., and Moramarco, T. (2008). “On the Estimation of Antecedent Wetness conditions in Rainfall-Runoff Modelling.” *Hydrological Processes*, 22, 629–642.
- Brocca, L., Melone, F., Moramarco, T., and Morbidelli, R. (2010). “Spatial-temporal variability of soil moisture and its estimation across scales.” *Water Resources Research*, 46(2), 1–14.
- Bronstert, A., Creutzfeldt, B., Graeff, T., Hajnsek, I., Heistermann, M., Itzerott, S., Jagdhuber, T., Kneis, D., Lück, E., Reusser, D., and Zehe, E. (2012). “Potentials and constraints of different types of soil moisture observations for flood

- simulations in headwater catchments.” *Natural Hazards*, 60(3), 879–914.
- Brunet, P., Clément, R., and Bouvier, C. (2010). “Monitoring soil water content and deficit using Electrical Resistivity Tomography (ERT) - A case study in the Cevennes area, France.” *Journal of Hydrology*, Elsevier B.V., 380(1–2), 146–153.
- Campbell, J. E. (1990). “Dielectric Properties and Influence of Conductivity in Soils at One to Fifty Megahertz.” *Soil Science Society of America Journal*, 54(2), 332.
- Campbell Scientific. (2012). “CS616 and CS625 water content reflectometers.” *Instruction manual*, 50.
- Cassiani, G., Binley, A., and Ferre, T. P. A. (2006a). “Unsaturated zone processes.” *Applied Hydrogeophysics*, H. Vereecken, A. Binley, G. Cassiani, A. Revil, and K. Titov, eds., Springer, 75–116.
- Cassiani, G., Bruno, V., Villa, A., Fusi, N., and Binley, A. M. (2006b). “A saline trace test monitored via time-lapse surface electrical resistivity tomography.” *Journal of Applied Geophysics*, 59(3), 244–259.
- Chan, C. Y., and Knight, R. J. (1999). “Determining water content and saturation from dielectric measurements in layered materials commonly made to determine water and in turn to determine accuracy with which water content or saturation information can be obtained from dielectric homogeneous mi.” *Water Resources Research*, 35(1), 85–93.
- Chanasyk, D. S., and Naeth, M. A. (1996). “Field measurement of soil moisture using neutron probes.” *Canadian Journal of Soil Science*, 76(3), 317–323.
- Daily, W., Ramirez, A., Binley, A., and LeBrecque, D. (2004). “Electrical resistance tomography.” *The Leading Edge*, 23(5), 438–442.
- Dannowski, G., and Yaramanci, U. (1999). “Estimation of water content and porosity using combined radar and geoelectrical measurements.” *European Journal of Environmental and Engineering Geophysics*, 4, 1–15.
- Dean, T. J., Bell, J. P., and Baty, A. J. B. (1987). “Soil moisture measurement by an

- improved capacitance technique, Part I. Sensor design and performance.” *Journal of Hydrology*, 93(1–2), 67–78.
- Desilets, D., and Zreda, M. (2001). “On scaling cosmogenic nuclide production rates for altitude and latitude using cosmic-ray measurements.” *Earth and Planetary Science Letters*, 193(1–2), 213–225.
- Desilets, D., and Zreda, M. (2003). “Spatial and temporal distribution of secondary cosmic-ray nucleon intensities and applications to in situ cosmogenic dating.” *Earth and Planetary Science Letters*, 206(1–2), 21–42.
- Desilets, D., Zreda, M., and Ferre, T. P. A. (2010). “Nature’s neutron probe: Land surface hydrology at an elusive scale with cosmic rays.” *Water Resources Research*, 46(11), 1–7.
- Dingman, L. S. (2002). *Physical Hydrology*. Waveland Press, Inc.
- Dunne, T., and Black, R. D. (1970). “An Experimental Investigation of Runoff Production in Permeable Soils.” *Water Resources Research*, 6(2), 478–490.
- Fang, B., and Lakshmi, V. (2014). “Soil moisture at watershed scale: Remote sensing techniques.” *Journal of Hydrology*, Elsevier B.V., 516, 258–272.
- Fetter, C. W. (2001). *Applied Hydrogeology*. Upper Saddle River, New Jersey Prentice Hall.
- Franz, T. E., Zreda, M., Ferre, T. P. A., Rosolem, R., Zweck, C., Stillman, S., Zeng, X., and Shuttleworth, W. J. (2012). “Measurement depth of the cosmic ray soil moisture probe affected by hydrogen from various sources.” *Water Resources Research*, 1–9.
- Friedman, S. P. (1998). “A saturation degree-dependent composite spheres model for describing the effective dielectric constant of unsaturated porous media.” *Water Resources Research*, 34(11), 2949–2961.
- Friedman, S. P. (2005). “Soil properties influencing apparent electrical conductivity: A review.” *Computers and Electronics in Agriculture*, 46(1–3 SPEC. ISS.), 45–70.

- Galagedara, L. W., Parkin, G. W., and Redman, J. D. (2003). “An analysis of the ground-penetrating radar direct ground wave method for soil water content measurement.” *Hydrological Processes*, 17(18), 3615–3628.
- Garambois, S., Sénéchal, P., and Perroud, H. (2002). “On the use of combined geophysical methods to assess water content and water conductivity of near-surface formations.” *Journal of Hydrology*, 259(1–4), 32–48.
- Gardner, W., and Kirkham, D. (1952). “Determination of Soil Moisture by Neutron Scattering.” *Soil Science*, 73, 391–401.
- Garré, S., Javaux, M., Vanderborght, J., Pagès, L., and Vereecken, H. (2011). “Three-Dimensional Electrical Resistivity Tomography to Monitor Root Zone Water Dynamics.” *Vadose Zone Journal*, 10(1), 412.
- Goodrich, D. C., Schmugge, T. J., Jackson, T. J., Unkrich, C. L., Keefer, T. O., Parry, R., Bach, L. B., and Amer, S. A. (1994). “Runoff Simulation Sensitivity to Remotely-Sensed Initial Soil-Water Content.” *Water Resources Research*, 30(5), 1393–1405.
- Groves, P., Cascante, G., Dundas, D., and Chatterji, P. K. (2011). “Use of geophysical methods for soil profile evaluation.” *Canadian Geotechnical Journal*, 48(9), 1364–1377.
- Hassan, A. A. (2014). “Electrical Resistivity Method for Water Content Characterisation of Unsaturated Clay Soil.” Durham University.
- Hawdon, A., McJannet, D., and Wallace, J. (2014). “Calibration and correction procedures for cosmic-ray neutron soil moisture probes located across Australia.” *Water Resources Research*, 5029–5043.
- Hess, V. F. (1912). “Über Beobachtungen der durchdringenden Strahlung bei sieben Freiballonfahrten.” *Physik. Zeitschr.*, XIII, 1084–1091.
- Hillel, D. (2004). *Introduction to Environmental Soil Physics*. Elsevier Academic Press.
- Huisman, J. A., Hubbard, S. S., Redman, J. D., and Annan, A. P. (2003). “Measuring Soil Water Content with Ground Penetrating Radar: A Review.” *Vadose Zone*

- Journal*, 2, 476–491.
- Jackson, T. J., Schmugge, J., and Engman, E. T. (1996). “Remote sensing applications to hydrology: soil moisture.” *Hydrological Sciences Journal*, 41(4), 517–530.
- Kelleners, T. J., Seyfried, M. S., Blonquist, J. M., Bilskie, J., and Chandler, D. G. (2005). “Improved Interpretation of Water Content Reflectometer Measurements in Soils.” *Soil Science Society of America Journal*, 69(6), 1684.
- Kemna, A., Kulesa, B., and Vereecken, H. (2002). “Imaging and characterisation of subsurface solute transport using electrical resistivity tomography (ERT) and equivalent transport models.” *Journal of Hydrology*, 267(3–4), 125–146.
- Kizito, F., Campbell, C. S., Campbell, G. S., Cobos, D. R., Teare, B. L., Carter, B., and Hopmans, J. W. (2008). “Frequency, electrical conductivity and temperature analysis of a low-cost capacitance soil moisture sensor.” *Journal of Hydrology*, 352(3–4), 367–378.
- Knödel, K., Lange, G., and Voigt, H.-J. (2007). *Environmental Geology Handbook of Field Methods and Case Studies*. Springer.
- Lakshmi, V. (2013). “Remote Sensing of Soil Moisture.” *ISRN Soil Science*, 2013, 1–33.
- Leib, B. G., Jabro, J. D., and Matthews, G. R. (2003). “Field Evaluation and Performance Comparison of Soil Moisture Sensors.” *Soil Science*, 168(6), 396–408.
- Logsdon, S. D. (2009). “CS616 Calibration: Field versus Laboratory.” *Soil Science Society of America Journal*, 73(1), 1.
- Loke, M. H., and Barker, R. D. (1996). “Rapid least-squares inversion of apparent resistivity pseudosections by a quasi-Newton method.” *Geophysical Prospecting*, 44, 131–152.
- Loke, M. H., Chambers, J. E., Rucker, D. F., Kuras, O., and Wilkinson, P. B. (2013). “Recent developments in the direct-current geoelectrical imaging method.” *Journal of Applied Geophysics*, Elsevier B.V., 95, 135–156.

- Maillet, G. M., Rizzo, E., Revil, A., and Vella, C. (2005). “High resolution Electrical Resistivity Tomography (ERT) in a transition zone environment: Application for detailed internal architecture and infilling processes study of a Rhône River paleo-channel.” *Marine Geophysical Researches*, 26(2–4), 317–328.
- “Meteoroloji Genel Müdürlüğü.” (n.d.). <<https://www.mgm.gov.tr/veridegerlendirme/il-ve-ilceler-istatistik.aspx?m=NIGDE>> (Sep. 20, 2017).
- Mittelbach, H., Lehner, I., and Seneviratne, S. I. (2012). “Comparison of four soil moisture sensor types under field conditions in Switzerland.” *Journal of Hydrology*, Elsevier B.V., 430–431, 39–49.
- NASA Earth Observatory. (n.d.). “Earth Observatory Water Cycle Overview | Precipitation Education.” <<https://pmm.nasa.gov/education/articles/earth-observatory-water-cycle-overview>> (Jan. 8, 2018).
- Penna, D., Tromp-Van Meerveld, H. J., Gobbi, A., Borga, M., and Dalla Fontana, G. (2011). “The influence of soil moisture on threshold runoff generation processes in an alpine headwater catchment.” *Hydrology and Earth System Sciences*, 15(3), 689–702.
- Petropoulos, G. P., Ireland, G., and Barrett, B. (2015). “Surface soil moisture retrievals from remote sensing: Current status, products & future trends.” *Physics and Chemistry of the Earth*, Elsevier Ltd, 83–84, 36–56.
- Robinson, D. A., Campbell, C. S., Hopmans, J. W., Hornbuckle, B. K., Jones, S. B., Knight, R., Ogden, F., Selker, J., and Wendroth, O. (2008). “Soil Moisture Measurement for Ecological and Hydrological Watershed-Scale Observatories: A Review.” *Vadose Zone Journal*, 7(1), 358.
- Robinson, D. A., Jones, S. B., Wraith, J. M., Or, D., and Friedman, S. P. (2003). “A review of advances in dielectric and electrical conductivity measurement in soils using time domain reflectometry.” *Vadose Zone Journal*, 2(4), 444–475.
- Rosolem, R., Shuttleworth, W. J., Zreda, M., Franz, T. E., Zeng, X., and Kurc, S. A. (2013). “The Effect of Atmospheric Water Vapor on Neutron Count in the

- Cosmic-Ray Soil Moisture Observing System.” *Journal of Hydrometeorology*, 14(5), 1659–1671.
- Salem, H. S., and Chilingarian, G. V. (1999). “The cementation factor of Archie’s equation for shaly sandstone reservoirs.” *Journal of Petroleum Science and Engineering*, 23(2), 83–93.
- Samouëlian, A., Cousin, I., Tabbagh, A., Bruand, A., and Richard, G. (2005). “Electrical resistivity survey in soil science: A review.” *Soil and Tillage Research*, 83(2), 173–193.
- Sasaki, Y. (1992). “Resolution of Resistivity Tomography Inferred From Numerical Simulation.” *Geophysical Prospecting*, 40(4), 453–463.
- Seneviratne, S. I., Corti, T., Davin, E. L., Hirschi, M., Jaeger, E. B., Lehner, I., Orlowsky, B., and Teuling, A. J. (2010). “Investigating soil moisture-climate interactions in a changing climate: A review.” *Earth-Science Reviews*, 99(3–4), 125–161.
- Shah, P. H., and Singh, D. N. (2005). “Generalized Archie’s Law for Estimation of Soil Electrical Conductivity.” *Journal of ASTM International Paper ID JA113087*, 245(21), 31–2016.
- Simpson, J. A. (2000). “The cosmic ray nucleonic component: the invention and scientific uses of the neutron monitor.” (1947), 11–32.
- Topp, G. C., Davis, J. L., and Annan, A. P. (1980). “Electromagnetic Determination of Soil Water Content:” *Water Resources Research*, 16(3), 574–582.
- Turesson, A. (2006). “Water content and porosity estimated from ground-penetrating radar and resistivity.” *Journal of Applied Geophysics*, 58(2), 99–111.
- Ullrich, C., and Slater, L. D. (2004). “Induced polarization measurements on unsaturated, unconsolidated sand.” *Geophysics*, 69(3), 762–771.
- Varble, J. L., and Chávez, J. L. (2011). “Performance evaluation and calibration of soil water content and potential sensors for agricultural soils in eastern Colorado.” *Agricultural Water Management*, Elsevier B.V., 101(1), 93–106.

- Veldkamp, E., and O'Brien, J. J. (2000). "Calibration of a Frequency Domain Reflectometry Sensor for Humid Tropical Soils of Volcanic Origin." *Soil Science Society of America Journal*, 64(5), 1549.
- Vereecken, H., Huisman, J. A., Bogaen, H., Vanderborght, J., Vrugt, J. A., and Hopmans, J. W. (2008). "On the value of soil moisture measurements in vadose zone hydrology: A review." *Water Resources Research*, 44(W00D06), 1–21.
- Visvalingam, M., and Tandy, J. D. (1972). "The Neutron Method For Measuring Soil Moisture - A Review." *Journal of Soil Science*, 2(4), 499–511.
- Waxman, M. H., and Smits, L. J. M. (1968). "Electrical conductivities in oil-bearing shaly sands." *Society of Petroleum Engineers Journal*, 243, 107–122.
- Wehrer, M., Lissner, H., Bloem, E., French, H., and Totsche, K. U. (2014). "Electrical resistivity tomography as monitoring tool for unsaturated zone transport: An example of preferential transport of deicing chemicals." *Environmental Science and Pollution Research*, 21(15), 8964–8980.
- Western, A. W., and Seyfried, M. S. (2005). "A calibration and temperature correction procedure for the water-content reflectometer." *Hydrological Processes*.
- Whalley, W. R., Dean, T. J., and Izzard, P. (1992). "Evaluation of the capacitance technique as a method for dynamically measuring soil water content." *Journal of Agricultural Engineering Research*, 52(C), 147–155.
- Wraith, J. M., Robinson, D. A., Jones, S. B., and Long, D. S. (2005). "Spatially characterizing apparent electrical conductivity and water content of surface soils with time domain reflectometry." *Computers and Electronics in Agriculture*, 46(1–3 SPEC. ISS.), 239–261.
- Zreda, M., Desilets, D., Ferré, T. P. A., and Scott, R. L. (2008). "Measuring soil moisture content non-invasively at intermediate spatial scale using cosmic-ray neutrons." *Geophysical Research Letters*, 35(21), 1–5.
- Zreda, M., Shuttleworth, W. J., Zeng, X., Zweck, C., Desilets, D., Franz, T., and Rosolem, R. (2012). "COSMOS: The cosmic-ray soil moisture observing system." *Hydrology and Earth System Sciences*, 16(11), 4079–4099.



## APPENDIX A

### GROUND- BASED STATIONS

Ground-based stations in Çakıt Basin is presented in Table A-1.

Table A-1 Ground-based stations in Çakıt Basin

<b>Stat. name</b>	<b>Duration</b>	<b>Easting (UTM 36)</b>	<b>Northing (UTM 36)</b>	<b>Elevation(m)</b>
Darboğaz Meteo Stat.	Jul 2016-	637073	4149103	1580
Maden Meteo Stat.	Jul 2016-	643208	4145985	1790
Hasangazi Meteo Stat.	Jul 2016-	642985	4153899	1246
Ulukışla Meteo Stat	1929-	631337	4156702	1453
Eddy Cov. Open Path System	Oct 2016-	632379	4153306	1464
Cosmic Ray Sensor (CRS)	Oct 2016-	632380	4153181	1459

Table A-1 Ground-based stations in Çakıt Basin (cont'd)

<b>Stat. name</b>	<b>Duration</b>	<b>Easting (UTM 36)</b>	<b>Northing (UTM 36)</b>	<b>Elevation(m)</b>
Darboğaz Discharge Observ. Stat.	Oct 2016-	638836	4152598	1286
Alihoca Discharge Observ. Stat.	Oct 2016-	654275	4153322	983
Çakıt Discharge Observ. Stat.	Oct 2016-	654265	4153354	974

## **APPENDIX B**

### **INVERSION RESULTS OF ERI SURVEY PROFILES**

In this study ERI data were inverted by using Res2DInv and ProfileR program. All inversion results were mapped into 2-D and these are as follows:

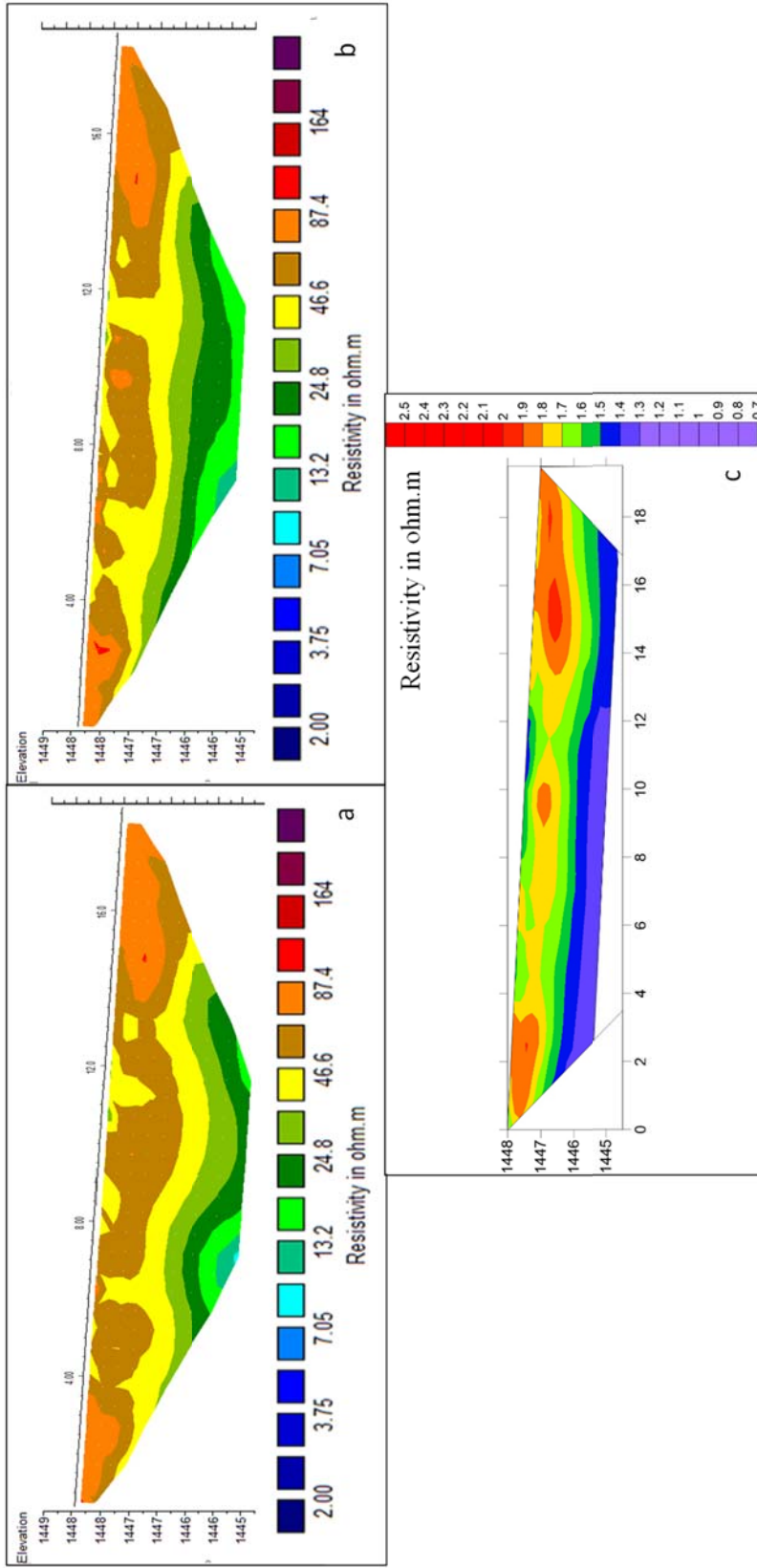


Figure B-6-1 ERI 1 (Aug 2017) inversion results; Wenner-alpha via Res2DInv (a), Schlumberger via Res2DInv (b), combined Wenner-alpha & Schlumberger geometry via ProfileR (c)



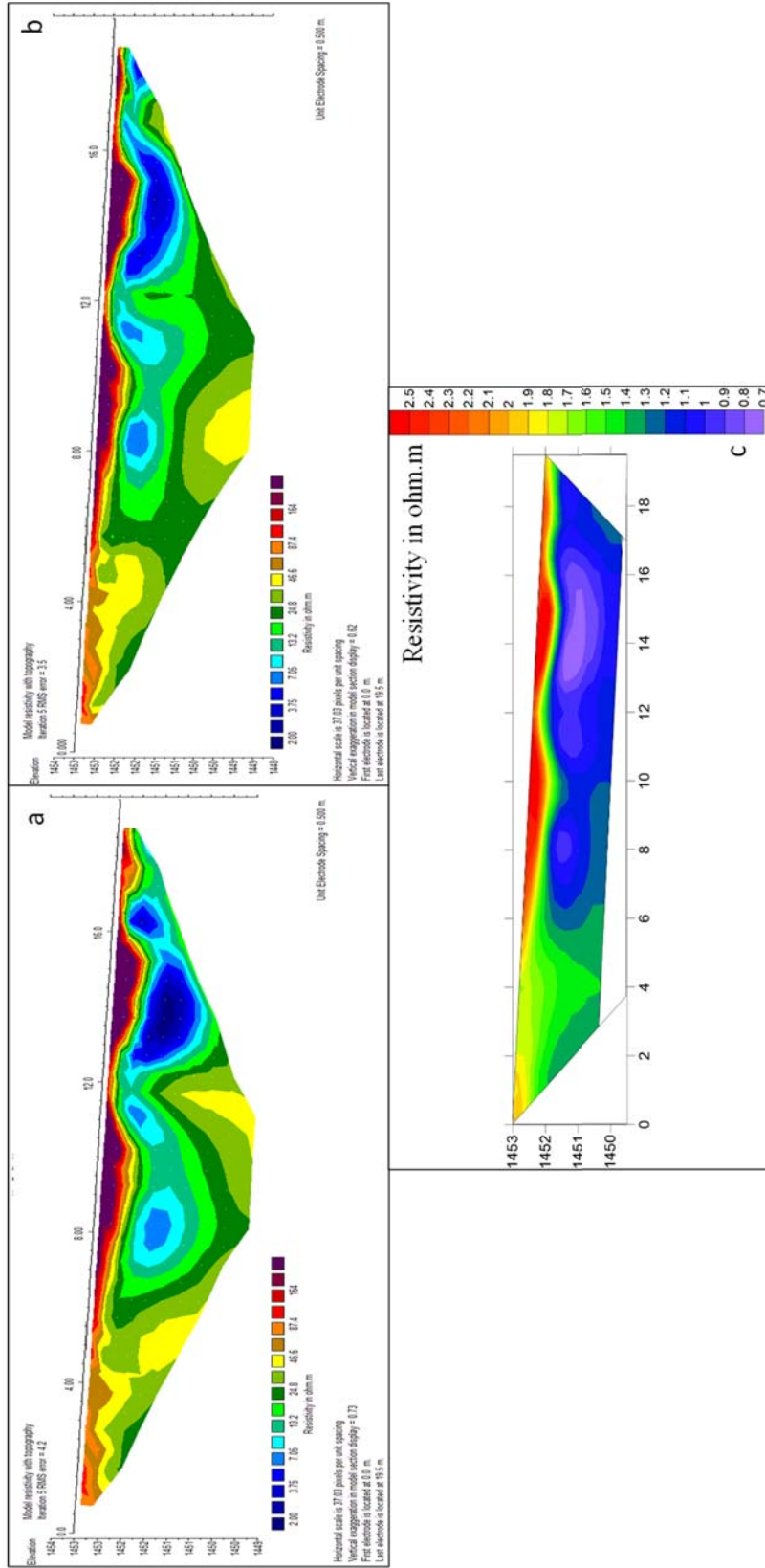


Figure B-6-3 ERI 3 (Aug 2017) inversion results; Wenner-alpha via Res2DInv (a), Schlumberger via Res2DInv (b), combined Wenner-alpha & Schlumberger geometry via ProfileR (c)

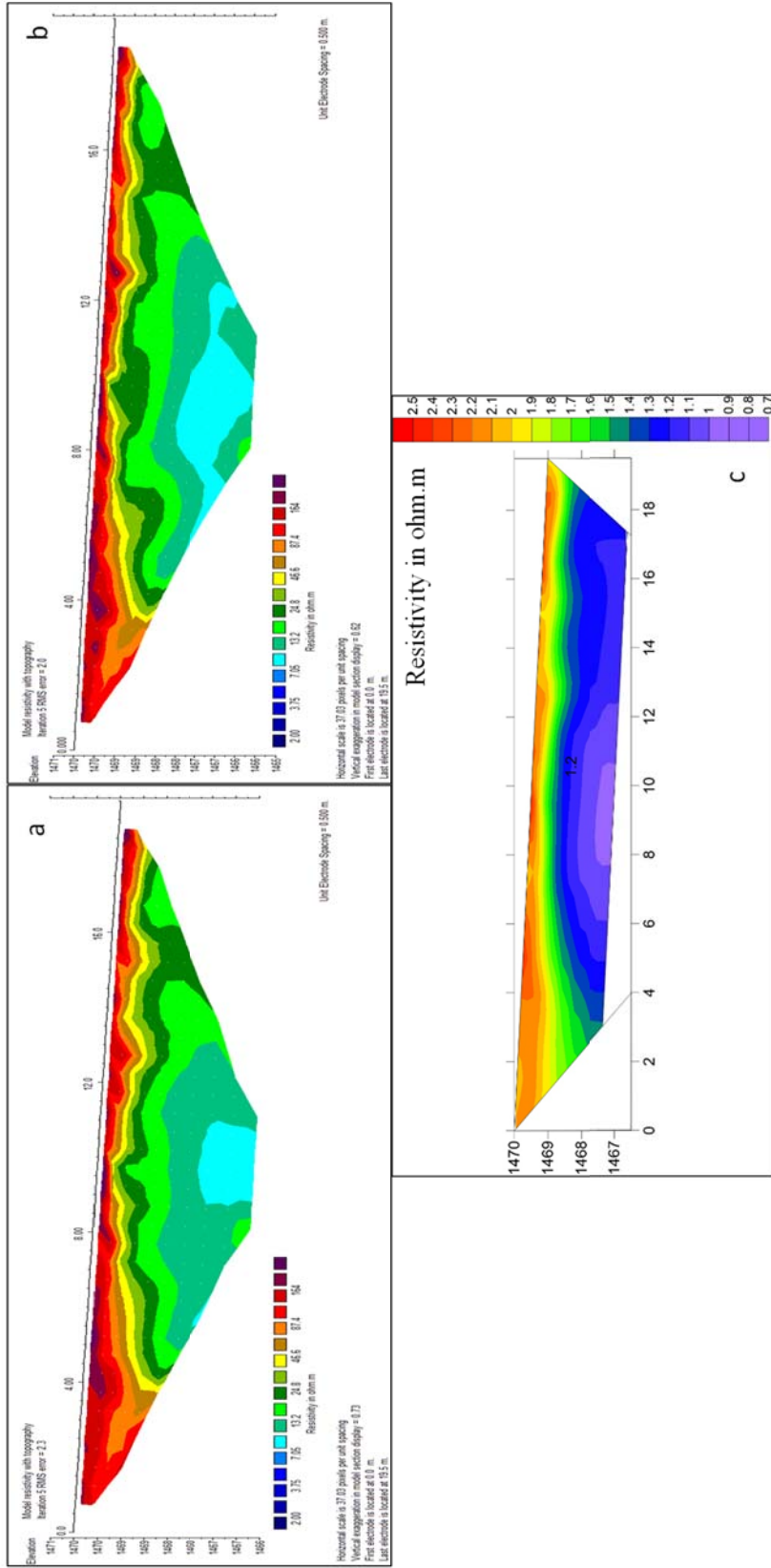


Figure B-6-4 ERI 4 (Aug 2017) inversion results; Wenner-alpha via Res2DInv (a), Schlumberger via Res2DInv (b), combined Wenner-alpha & Schlumberger geometry via ProfileR (c)

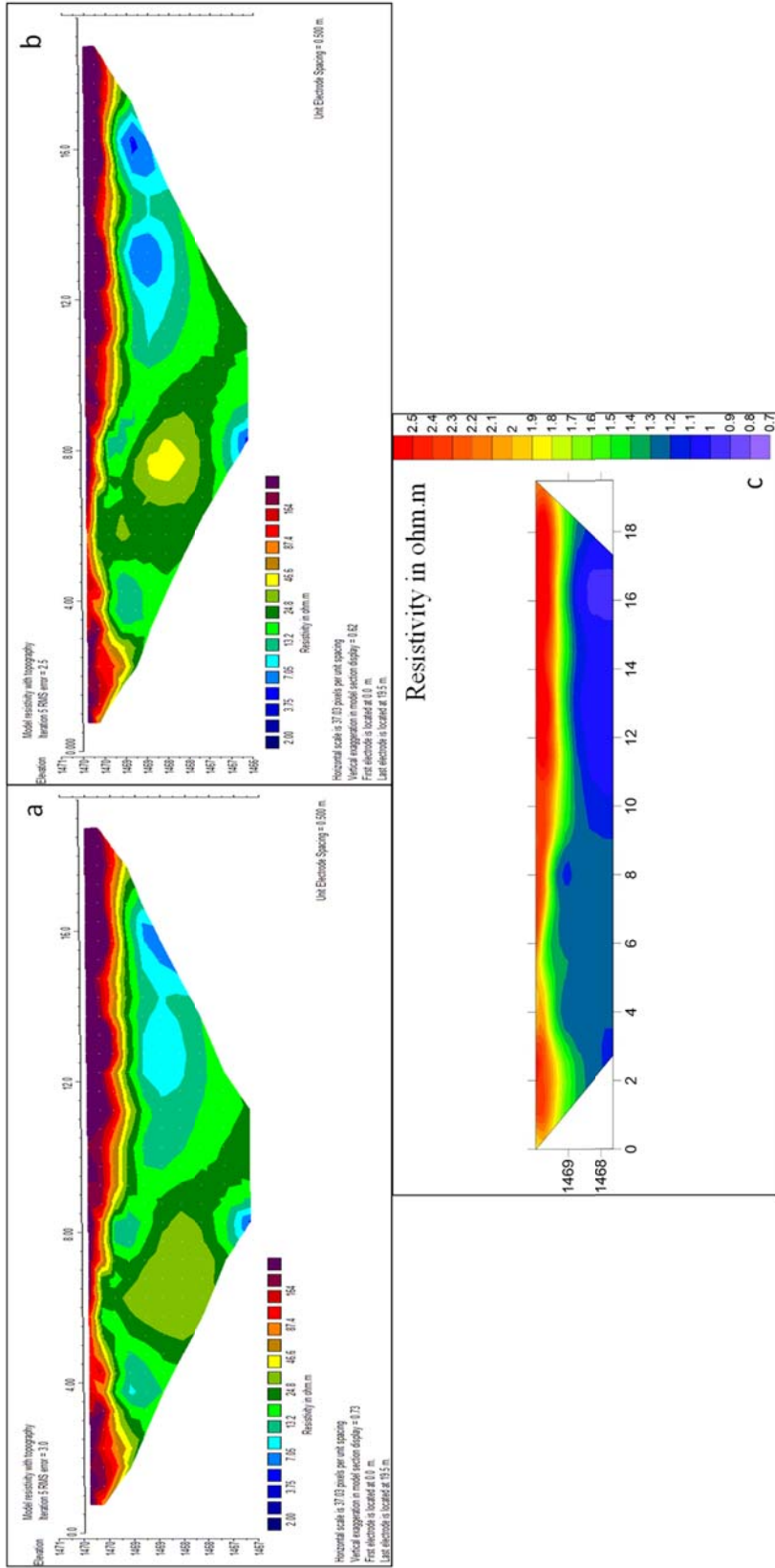


Figure B-6-5 ERI 5 (Aug 2017) inversion results; Wenner-alpha via Res2DInv (a), Schlumberger via Res2DInv (b), combined Wenner-alpha & Schlumberger geometry via ProfileR (c)

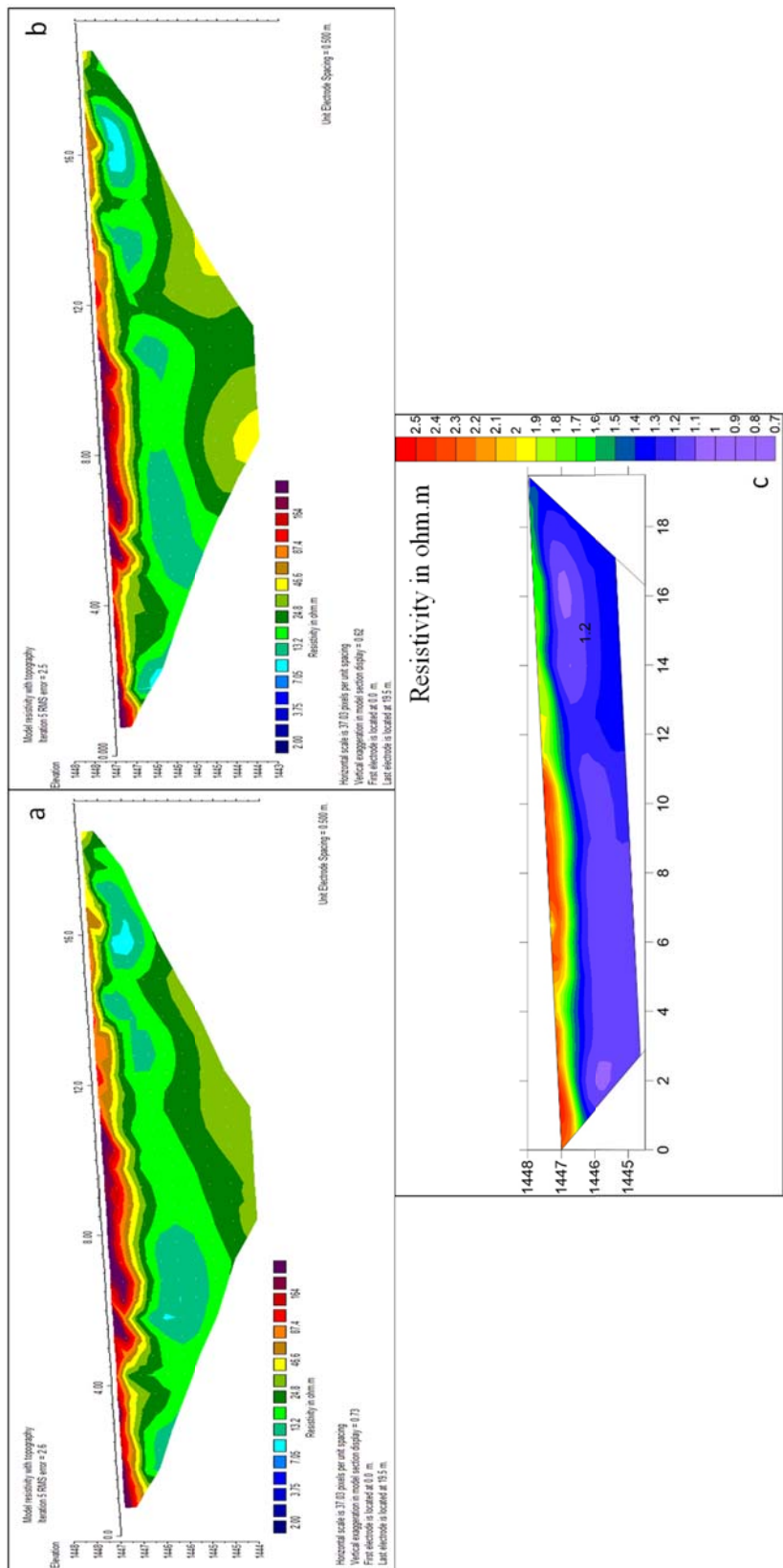


Figure B-6-6 ERI 6 (Aug 2017) inversion results; Wenner-alpha via Res2DInv (a), Schlumberger via Res2DInv (b), combined Wenner-alpha & Schlumberger geometry via ProfileR (c)

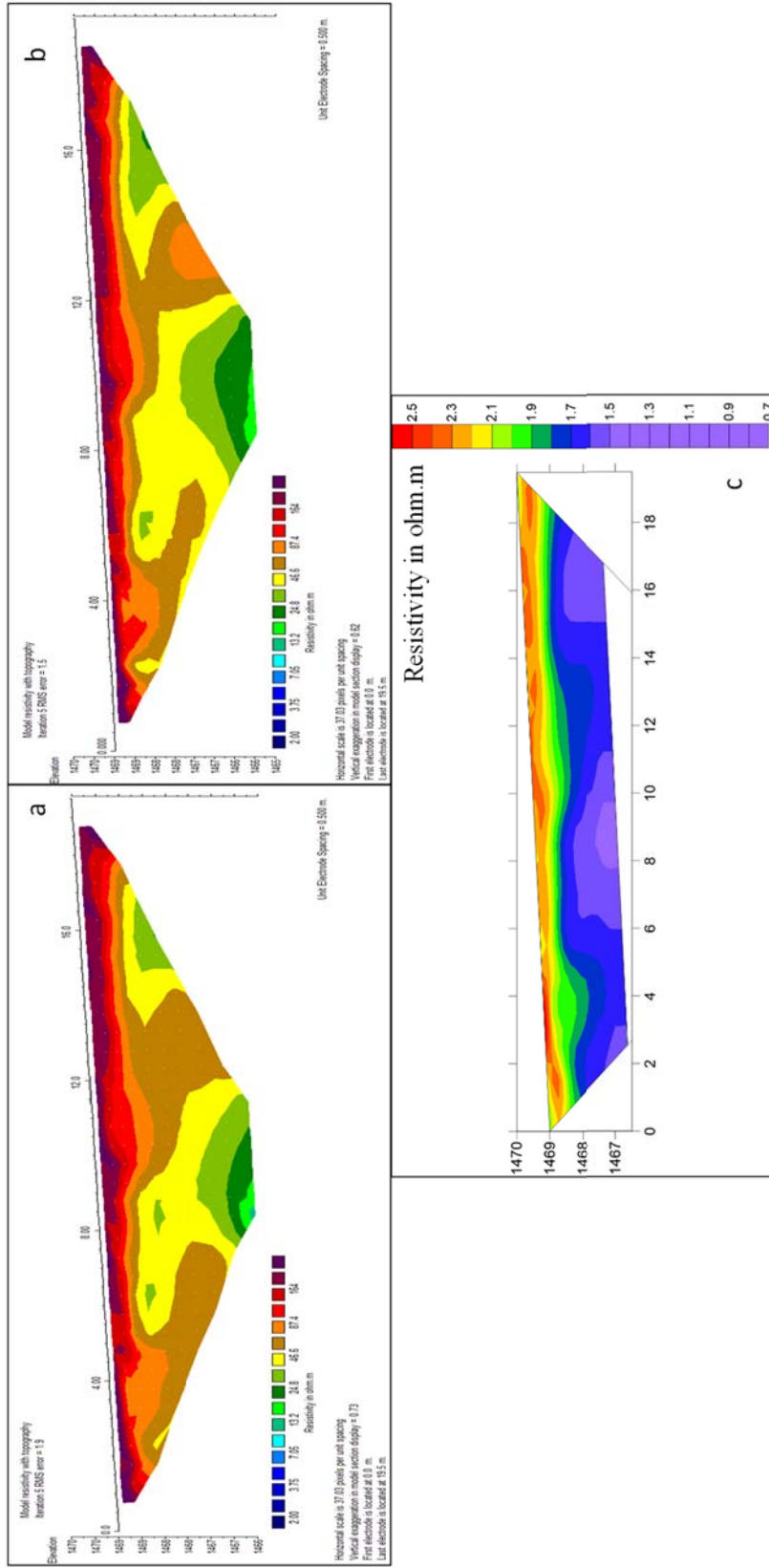


Figure B-6-7 ERI 7 (Aug 2017) inversion results; Wenner-alpha via Res2DInv (a), Schlumberger via Res2DInv (b), combined Wenner-alpha & Schlumberger geometry via ProfileR (c)

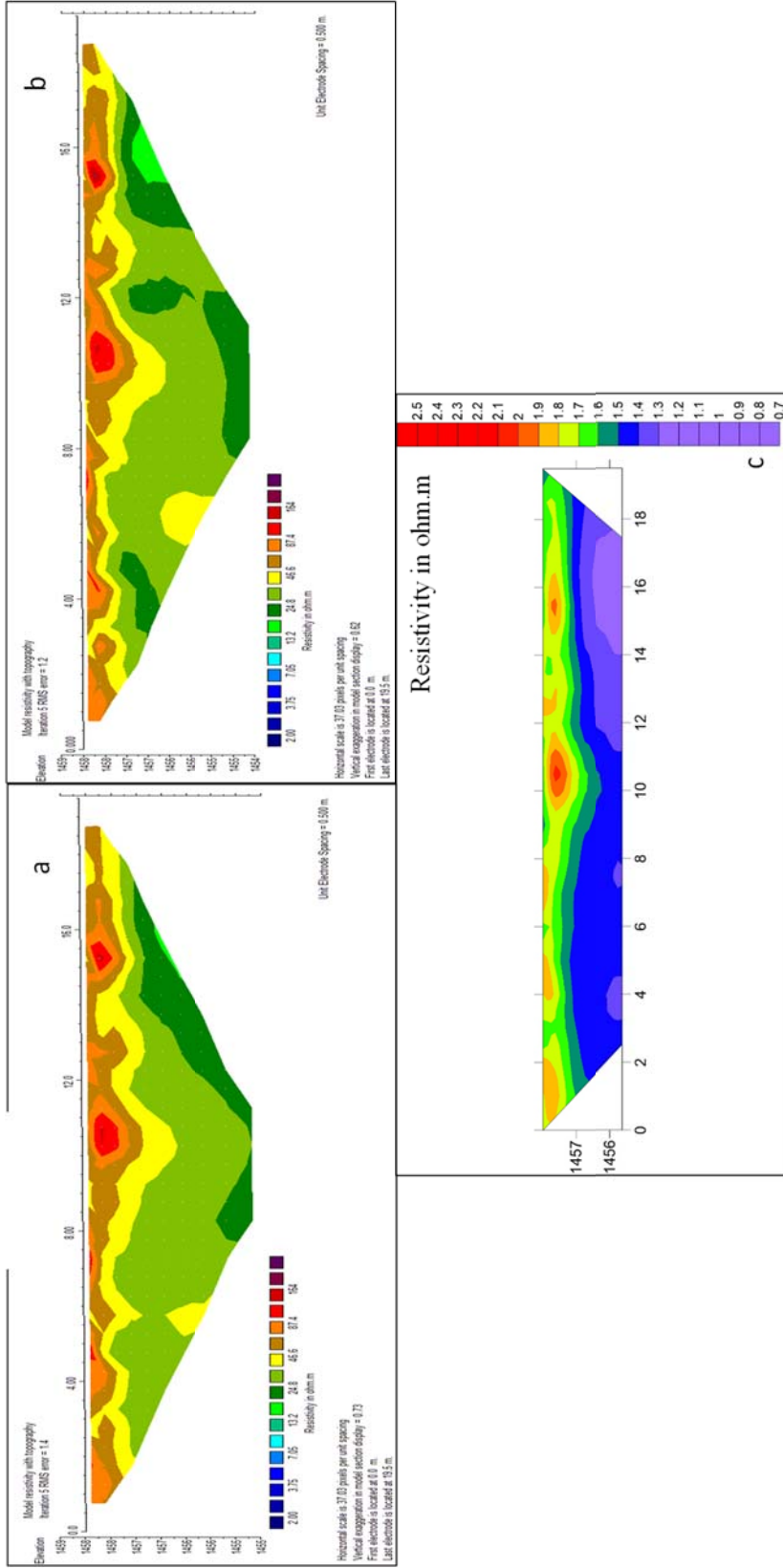


Figure B-6-8 ERI 8 (Aug 2017) inversion results; Wenner-alpha via Res2DInv (a), Schlumberger via Res2DInv (b), combined Wenner-alpha & Schlumberger geometry via ProfileR (c)

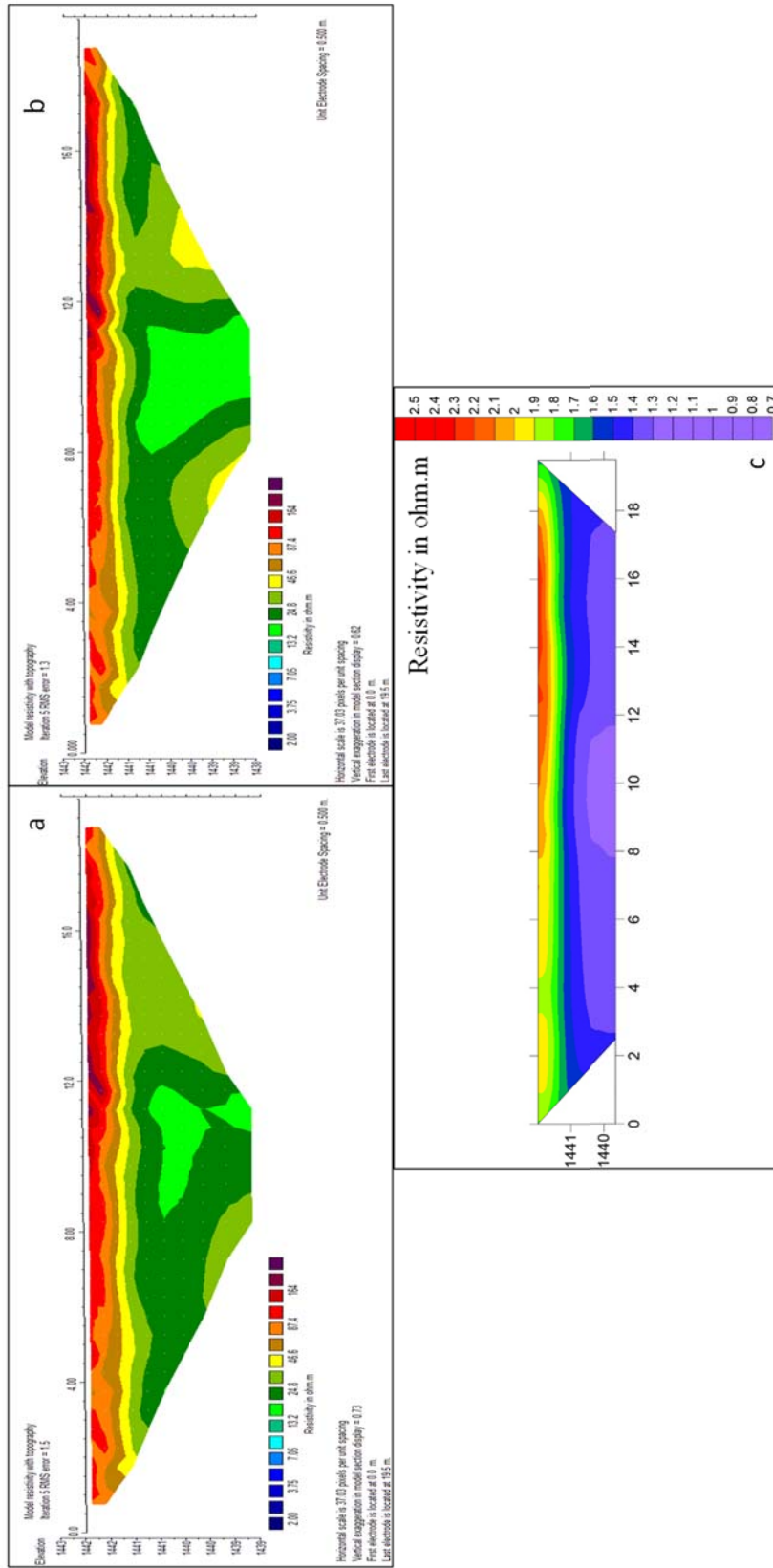


Figure B-6-9 ERI 9 (Aug 2017) inversion results; Wenner-alpha via Res2DInv (a), Schlumberger via Res2DInv (b), combined Wenner-alpha & Schlumberger geometry via ProfileR (c)

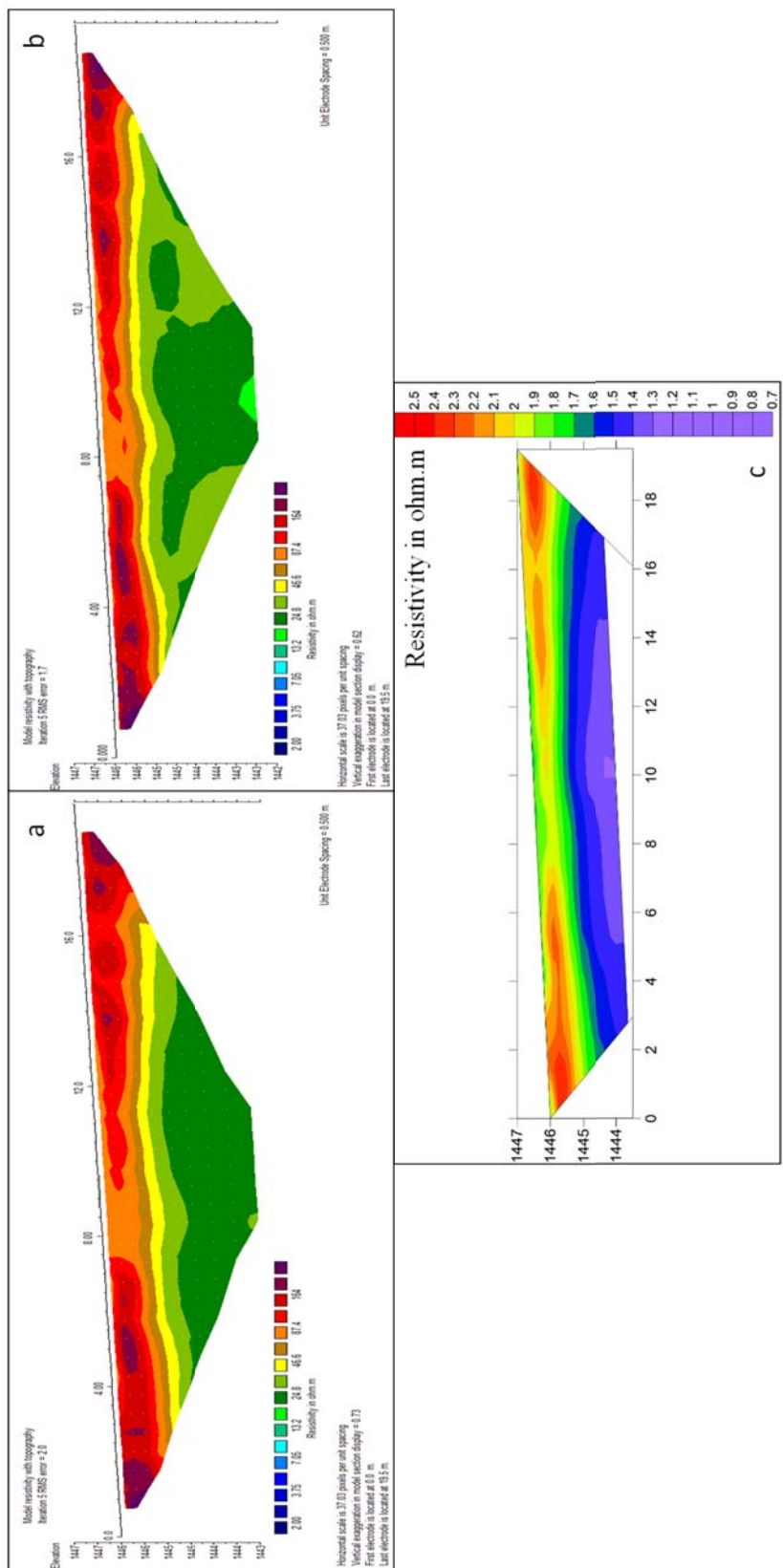


Figure B-6-10 ERI 10 (Aug 2017) inversion results; Wenner-alpha via Res2DInv (a), Schlumberger via Res2DInv (b), combined Wenner-alpha & Schlumberger geometry via ProfileR (c)

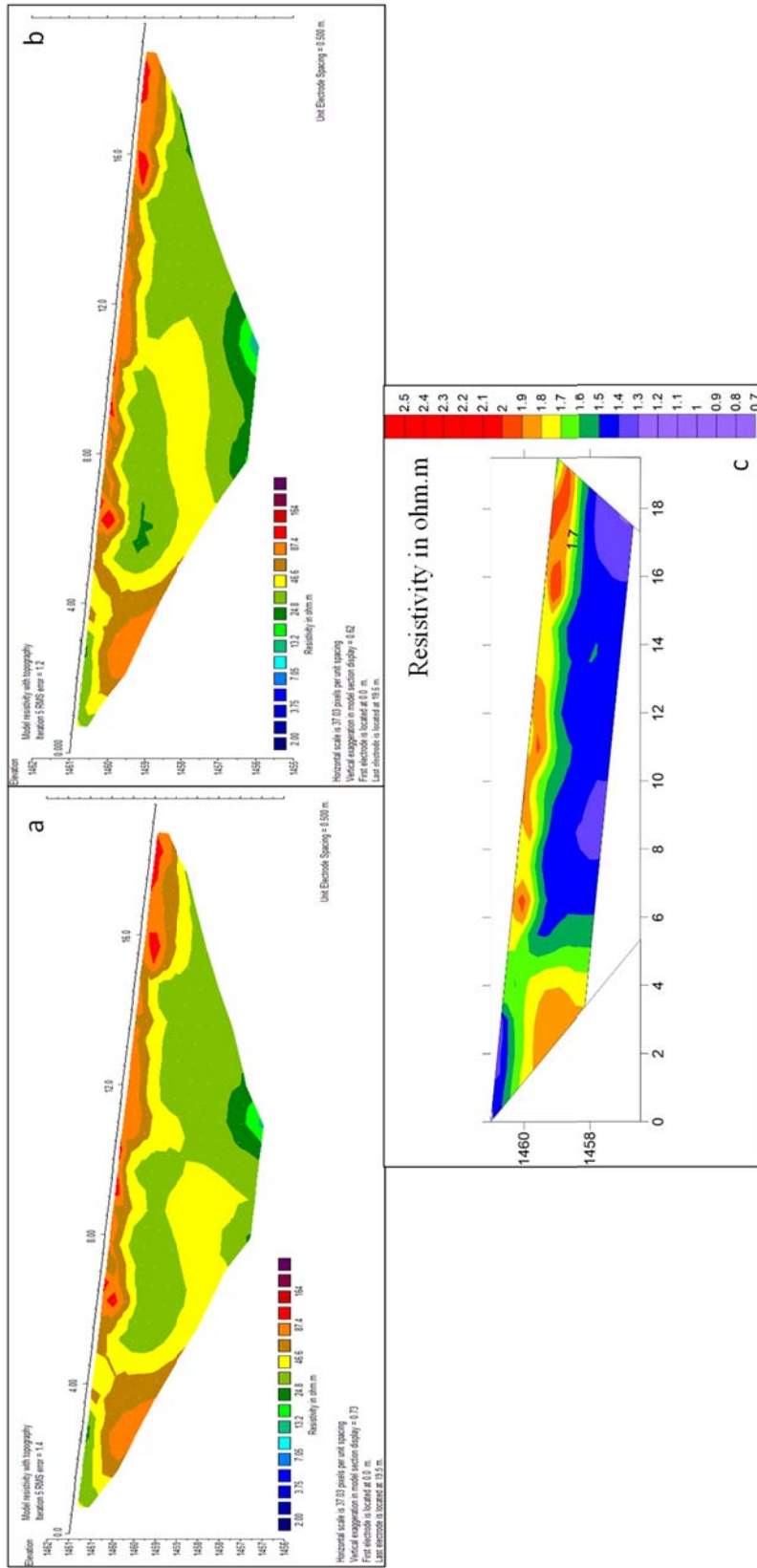


Figure B-6-11 ERI 11 (Aug 2017) inversion results; Wenner-alpha via Res2DInv (a), Schlumberger via Res2DInv (b), combined Wenner-alpha & Schlumberger geometry via ProfileR (c)

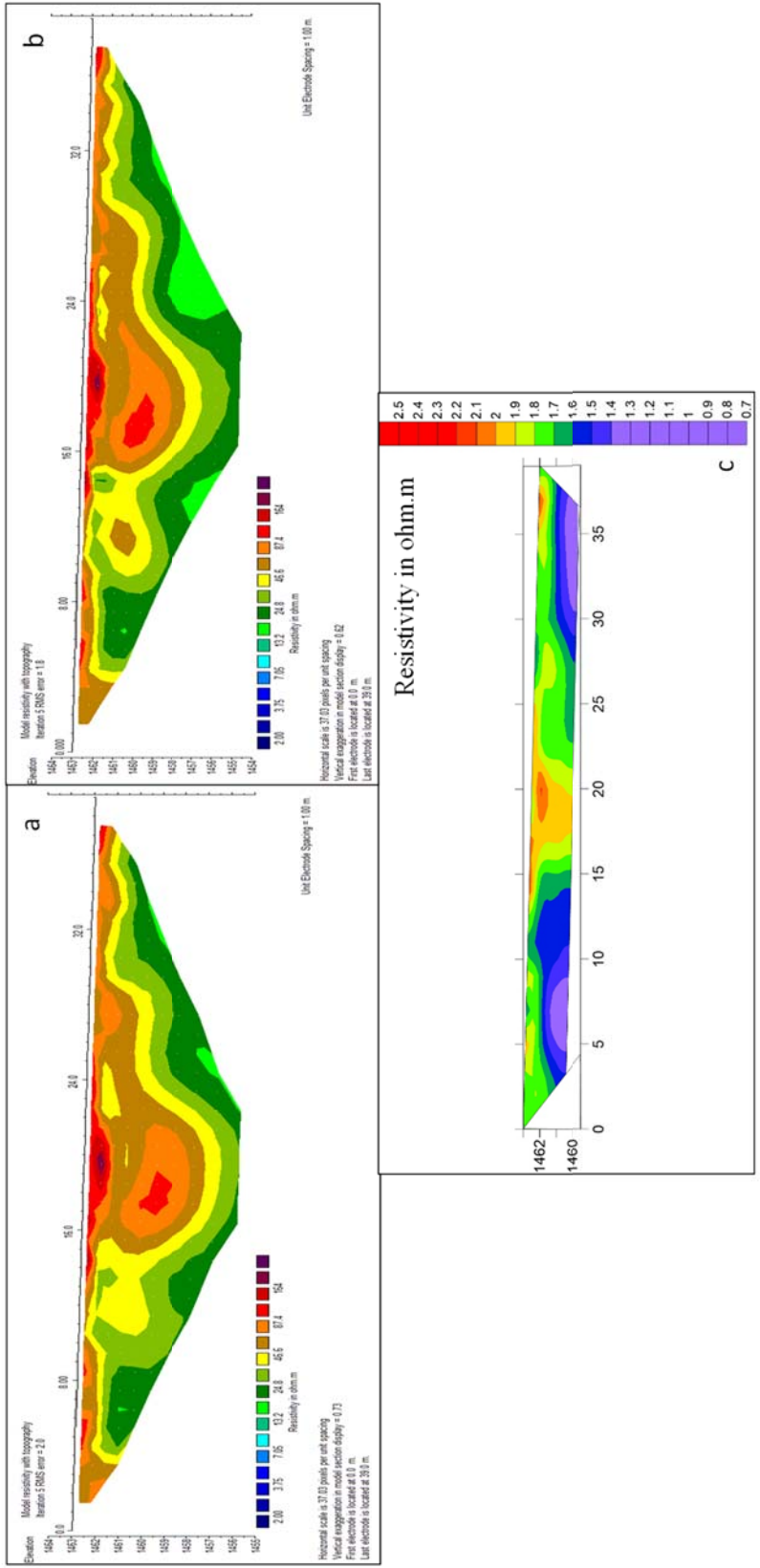


Figure B-6-12 ERI 12 (Aug 2017) inversion results; Wenner-alpha via Res2DInv (a), Schlumberger via Res2DInv (b), combined Wenner-alpha & Schlumberger geometry via ProfileR (c)

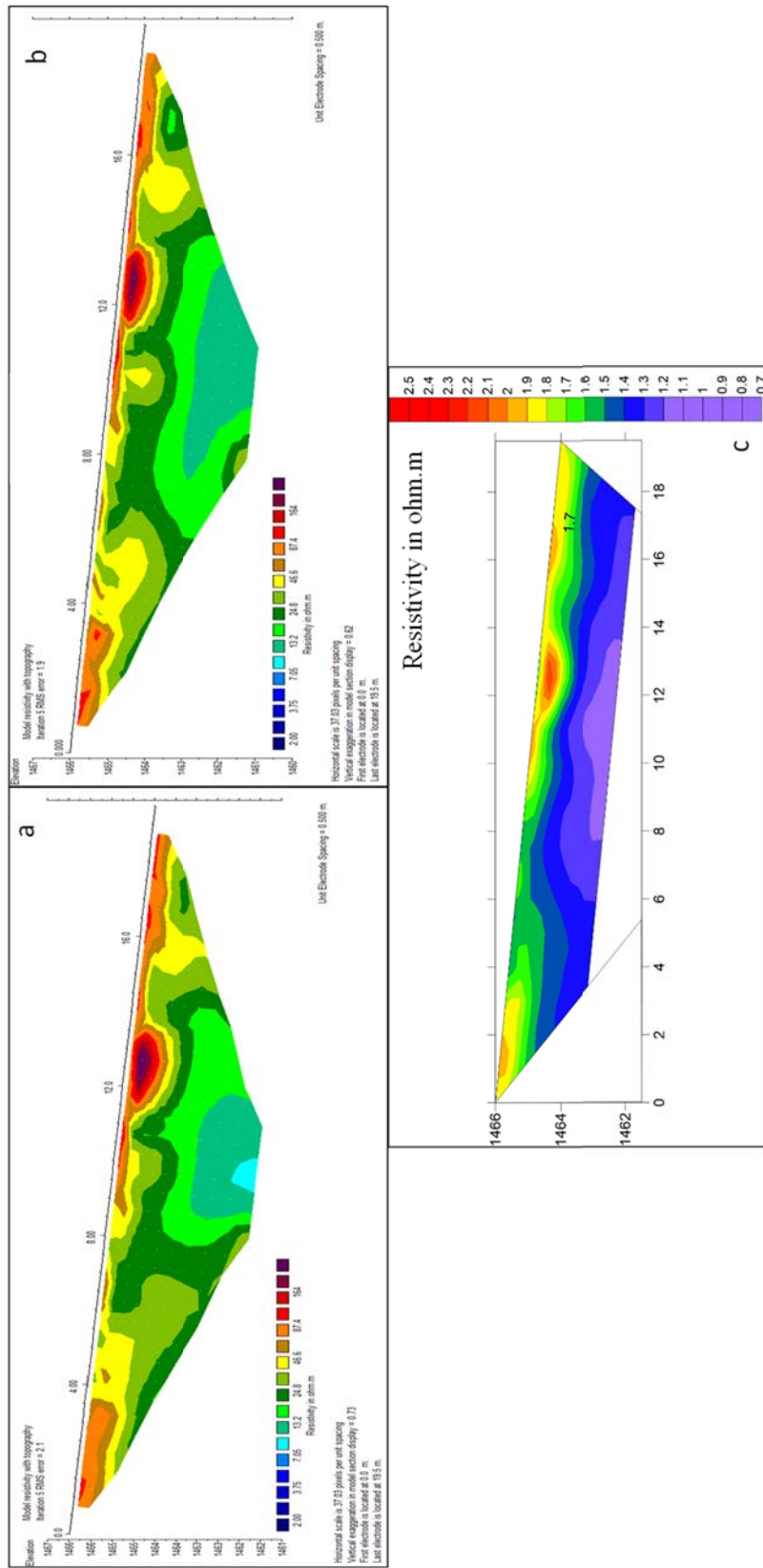


Figure B-6-13 ERI 13 (Aug 2017) inversion results; Wenner-alpha via Res2DInv (a), Schlumberger via Res2DInv (b), combined Wenner-alpha & Schlumberger geometry via ProfileR (c)

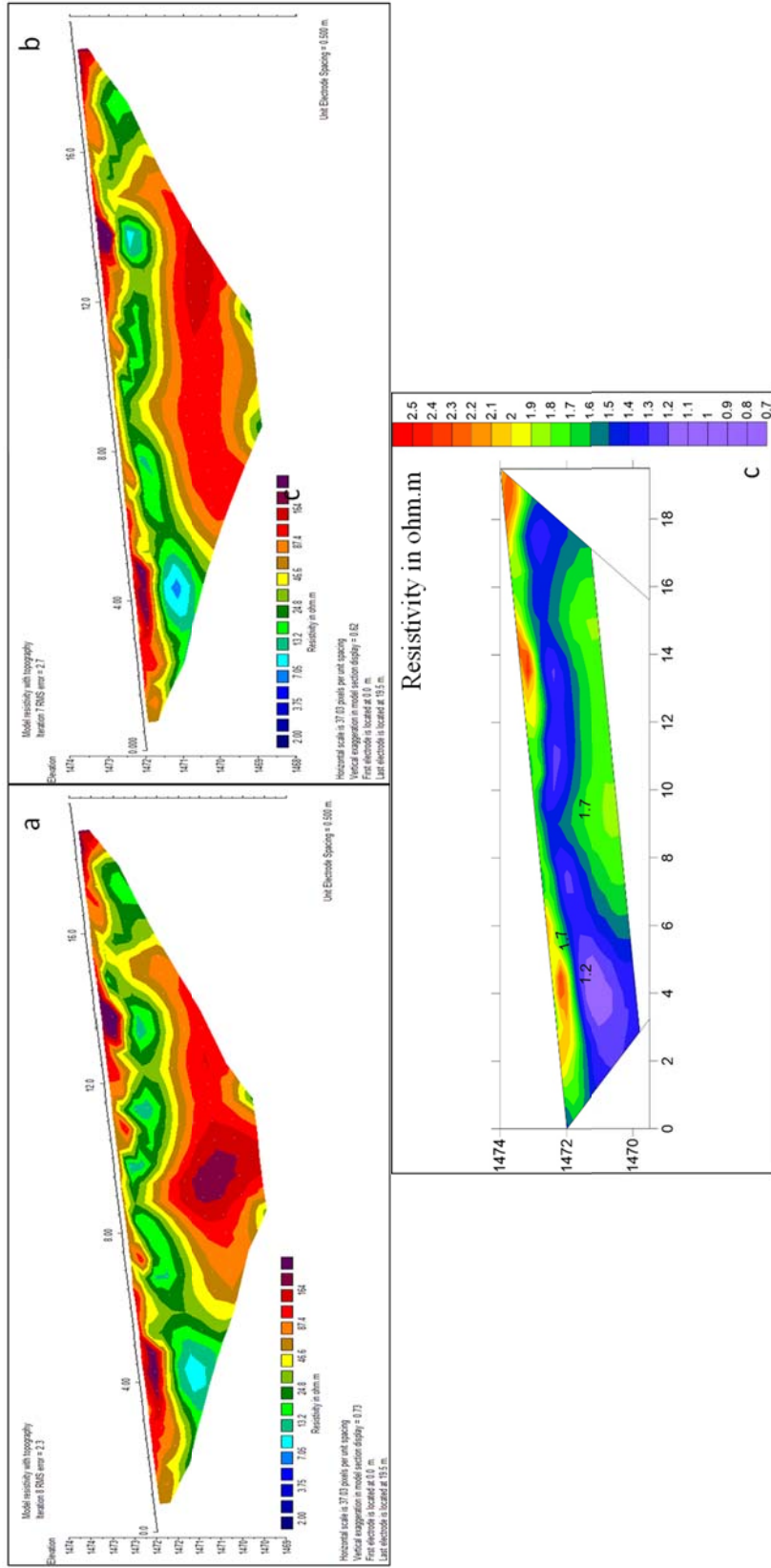


Figure B-6-14 ERI 14 (Aug 2017) inversion results; Wenner-alpha via Res2DInv (a), Schlumberger via Res2DInv (b), combined Wenner-alpha & Schlumberger geometry via ProfileR (c)

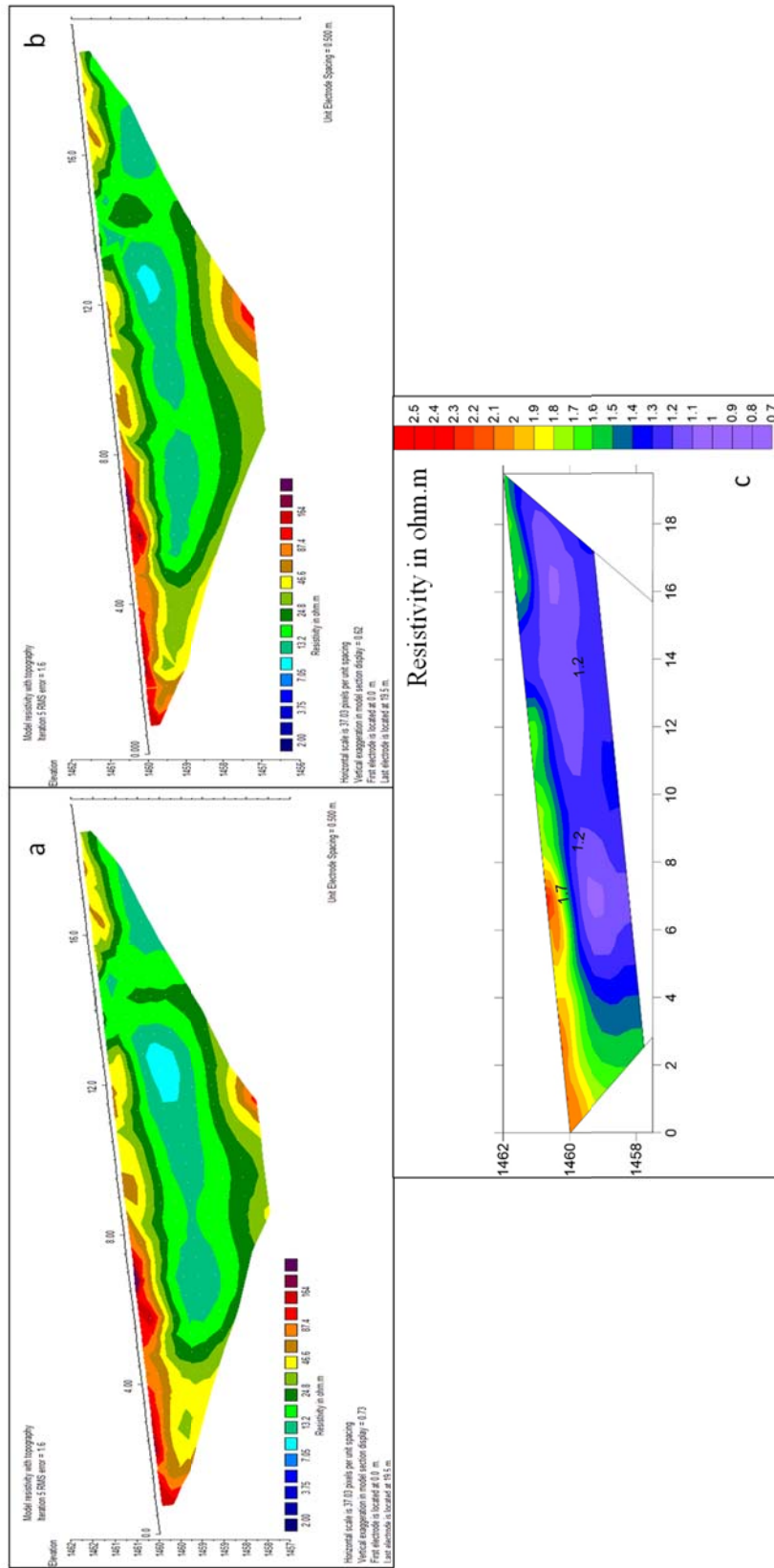


Figure B-6-15 ERI 15 (Aug 2017) inversion results; Wenner-alpha via Res2DInv (a), Schlumberger via Res2DInv (b), combined Wenner-alpha & Schlumberger geometry via ProfileR (c)

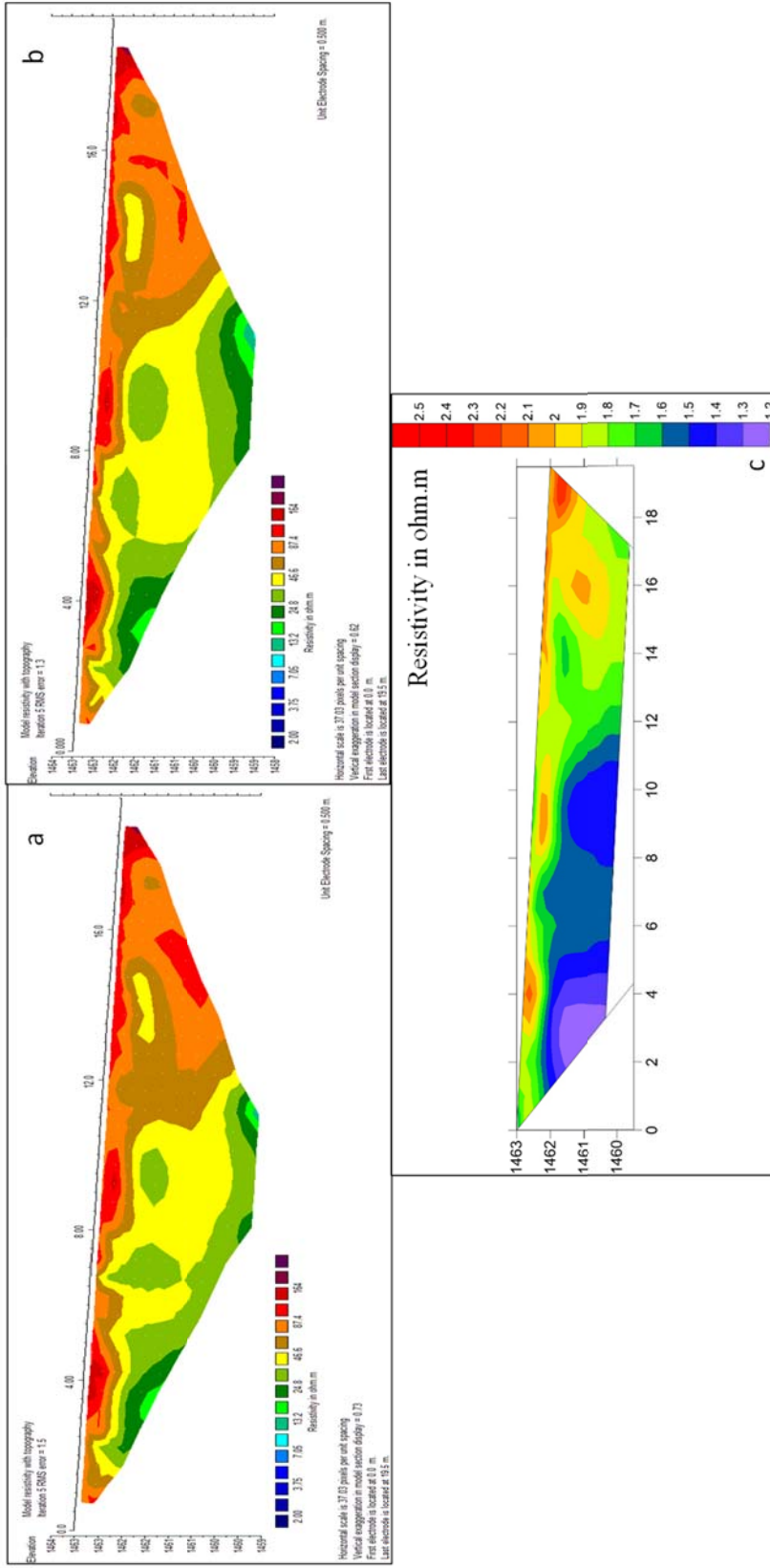


Figure B-6-16 ERI 16 (Aug 2017) inversion results; Wenner-alpha via Res2DInv (a), Schlumberger via Res2DInv (b), combined Wenner-alpha & Schlumberger geometry via ProfileR (c)